Theoretical Approaches for Studying Non-Valence Correlation-Bound and Correlation-Assisted Anion States of Molecules and Molecular Clusters

by

Arailym Kairalapova

B.S. Chemistry, Nazarbayev University, 2015

Submitted to the Graduate Faculty of

the Dietrich School of Arts and Sciences in partial fulfillment

of the requirements for the degree of

Doctor of Philosophy

University of Pittsburgh

2020

UNIVERSITY OF PITTSBURGH

DIETRICH SCHOOL OF ARTS AND SCIENCES

This dissertation was presented

by

Arailym Kairalapova

It was defended on

July 24, 2020

and approved by

Kenneth D. Jordan, Richard King Mellon Professor and Distinguished Professor of Computational Chemistry, Department of Chemistry

Peng Liu, Associate Professor, Department of Chemistry

Sean Garrett-Roe, Associate Professor, Department of Chemistry

David Yaron, Professor, Department of Chemistry, Carnegie Mellon University

Dissertation Director: Kenneth D. Jordan, Richard King Mellon Professor and Distinguished Professor of Computational Chemistry, Department of Chemistry

Theoretical Approaches for Studying Non-Valence Correlation-Bound and Correlation-Assisted Anion States of Molecules and Molecular Clusters

Arailym Kairalapova, PhD

University of Pittsburgh, 2020

Non-valence correlation-bound and correlation-assisted anion states of molecules and molecular clusters have been characterized using various electronic structure methods. In these species long-range dispersion type correlation interactions are responsible for binding of the excess electron in a spatially diffuse orbital. Therefore, the Hartree-Fock method and methods that depend on the Hartree-Fock wave function being a suitable reference fail to bind such anions or greatly underestimate the electron binding energy. The main approach used in the present studies is the equation of motion coupled-cluster method. Additional methods may also accurately describe these non-valence anions provided adequate orbital relaxation in response to long-range dispersion-like correlation effects is included. Non-valence correlation-bound anion states of a model $(H_2O)_4$ cluster, the bent CO_2, and tetracyanoethylene are characterized.

In addition to bound non-valence anions, some species may possess temporary anion states that lie energetically above the ground state of the neutral molecule and, thus, are subject to electron autodetachment. These temporary anion shape resonances are trapped by a potential barrier and are characterized by a complex energy. The temporary anion shape resonances of the model $(H_2O)_4$ cluster and rhombic $(NaCl)_2$ are described. In case of $(H_2O)_4$ cluster, the shape resonance corresponds to an asymmetric combination of the dipole-bound anion states of the subunit dimers. The resonance energy is determined as a function of the distance between the dimers of the $(H_2O)_4$ cluster. The temporary anion shape resonance of $(NaCl)_2$ corresponds to an antibonding combination of the hybridized orbitals associated with the two Na atoms. The resonance energy is determined as a function of distortion along the totally symmetric normal coordinate.

Finally, the molecular virial theorem is studied for a H atom interacting with a uniform electric field or with a point charge. Analytical expressions of the contributions to changes in average kinetic and potential energies due to these interactions are obtained by use of Dalgarno-Lewis perturbation theory.

Table of Contents

Preface . . . xiii

1.0 Introduction . . . 1

1.1 Non-Valence Anions . . . 1

1.2 Schrödinger Equation . . . 2

1.3 Hartree-Fock Theory . . . 3

1.4 Coupled-Cluster Theory . . . 4

1.5 Equation of Motion Theory . . . 6

1.6 Temporary Anion Shape Resonances . . . 6

1.7 Model Potential . . . 7

1.8 Discrete State and Discretized Continuum Wave Functions . . . 8

1.9 2x2 Model Problem . . . 9

1.10 Stabilization Method and Analytic Continuation . . . 10

2.0 Theoretical Approaches for Treating Non-Valence Correlation-Bound Anions . . . 13

2.1 Summary . . . 13

2.2 Introduction . . . 13

2.3 Theoretical Approaches . . . 15

2.4 $(H_2O)_4$ Cluster Model: Electrostatically Bound to Correlation-Bound Anion . . . 17

2.5 CO_2: Valence-Bound to Correlation-Bound Anion . . . 26

2.6 Non-Valence Correlation-Bound Anion of TCNE . . . 34

2.7 Conclusions . . . 37

2.8 Acknowledgments . . . 38

3.0 Prediction of a Non-Valence Temporary Anion Shape Resonance for a Model $(H_2O)_4$ System . . . 39

3.1 Summary . . . 39

3.2 Introduction . . . 40
3.3 $(H_2O)_4$ Model System and Computational Details . . . 41
3.4 Results . . . 44
3.5 Conclusions . . . 55
3.6 Acknowledgments . . . 56
4.0 Prediction of a Non-Valence Temporary Anion State of $(NaCl)_2$ . . . 58
4.1 Summary . . . 58
4.2 Introduction . . . 58
4.3 Computational Details . . . 61
4.4 Results and Discussion . . . 65
4.4.1 Stabilization Calculations . . . 65
4.4.2 Polarization and Effective Potentials for $e^- + (NaCl)_2$ . . . 70
4.4.3 Potential Energy Curves . . . 72
4.5 Conclusion . . . 75
4.6 Acknowledgements . . . 75
5.0 Analysis of the Contributions to the Kinetic and Potential Energies of an H Atom in the Presence of a Point Charge: The Molecular Virial Theorem Revisited . . . 76
5.1 Summary . . . 76
5.2 Introduction . . . 76
5.3 Theory . . . 79
5.4 Conclusions . . . 85
5.5 Acknowledgements . . . 87
5.6 Supporting Information . . . 87
5.6.1 Function g . . . 87
5.6.2 Function h . . . 88
6.0 Summary . . . 90
Bibliography . . . 92

List of Tables

2.1 Contributions to the EBE of the NVCB anion of the $(H_2O)_4$ model at $R = 4.2$ Å. 25

2.2 Contributions to $\Delta\langle T\rangle$ and $\Delta\langle V\rangle$ for a H atom perturbed by a point charge or a uniform efield evaluated in the complete basis set limit. 34

4.1 Electron binding energy (meV) of the A_g anion state of $(NaCl)_2$ calculated at various levels of theory in the frozen core and correlated core approximations. 74

5.1 Energies (au), virial ratios, $\langle V\rangle$, and $\langle T\rangle$ values (in au) of an H atom, both isolated and in the presence of a $-|e|$ point charge at $R = 10$ Bohr or a uniform electric field of strength 0.01 au. 80

5.2 Contributions to $\Delta\langle T\rangle$ and $\Delta\langle V\rangle$ for an H atom perturbed by a point charge or a uniform efield evaluated in the complete basis set limit. 83

5.3 Contributions to $\Delta\langle T\rangle$ and $\Delta\langle V\rangle$ for an H atom perturbed by a point charge or a uniform efield evaluated in the complete basis set limit with the diagonal and off-diagonal $\langle n\mathrm{p}|\hat{A}|m\mathrm{p}\rangle$ contributions split apart. 84

List of Figures

1.1 Diagrams for the model potential possessing resonance (left), the modified potential for the discrete state (DS) (middle), and the potential to generate discretized continuum (DC) levels 7

1.2 Stabilization graph of the model potential 10

2.1 Geometry of the $(H_2O)_4$ cluster model studied in this work. R ranges from 2.5 to 9.5 Å. 17

2.2 EBE of $(H_2O)_4$ calculated using various theoretical methods in conjunction with the aug-cc-pVDZ+7s7p basis set. (a) Results obtained using the KT, ΔHF, ΔMP2, ΔCCSD, ΔCCSD(T) methods, and (b) results obtained using the ADC(2), ΔOO-MP2, ΔBCCD(T), and various EOM methods. 19

2.3 Orbital plots of the LUMO from HF calculations of the neutral $(H_2O)_4$ cluster and the SONO from the EOM-CCSD calculations of the anion as a function of the distance from the center of the cluster along the direction perpendicular to the plane of the cluster. The aug-cc-pVDZ+7s7p basis set was used for these calculations. 21

2.4 EBE of $(H_2O)_4$ calculated using various theoretical methods in conjunction with the aug-cc-pVTZ basis set. The ΔMP2 and ΔCCSD curves, not depicted, essentially overlap with the ΔBCCD curve. Also, the ΔCCSD(T) and EOM-CCSD(T)(a)* curves, not depicted, essentially overlap with the ΔBCCD(T) curve, and the EOM-MP2 curve, not depicted, essentially overlaps with that from the EOM-CCSD calculations. 23

2.5 EBE of the NVCB anion of $(H_2O)_4$ for different R values calculated using the ADC(2), diagonal-ADC(2), and G_0W_0 methods. 24

2.6 EBE of the NVCB anion of $(H_2O)_4$ calculated with the ΔHF, ΔSD-BO, and ΔBCCD methods. All results are obtained using the aug-cc-pVDZ+7s7p basis set. 25

2.7 Bending potentials of CO_2 and CO_2^- for values of the OCO angle between 147° and 154°. Over this range of angles, two different HF solutions are obtained for CO_2^-: one valence-like and the other corresponding to the neutral molecule plus the excess electron in a discretized continuum orbital. The HF, CCSD, and CCSD(T) potentials for the valence-like anion are reported in (a), and the corresponding results for the discretized continuum solution are reported in (b). In both cases, the bending potential energy curves of the neutral molecule are also reported. The zero of energy is taken to be that of the linear neutral molecule. 27

2.8 Plots of the singly occupied orbital from HF calculations and of the singly occupied natural orbital from EOM-MP2 calculations on CO_2^-. (a) and (d) depict the discretized continuum orbital at 147° and 154°, respectively; (b) and (e) depict the valence-type HF orbital at those angles; and (c) and (f) report the SONOs from the EOM calculations at the two angles. 28

2.9 Potential energy curves of CO_2 and CO_2^-. The potential energy curve for the neutral molecule was calculated using the CCSD(T) method, and those for anion were generated by adding, at each geometry considered, the negative of the EBE calculated at that level of theory to the CCSD(T) energy of the neutral molecule. The zero of energy was taken to correspond to the neutral molecule with 180° OCO angle. The CO bond lengths were generated as described in the text. All calculations were performed using the ANOTZ+3s3p basis set. For the MP2 and CCSD(T) calculations on the anion, the valence-type HF solution was used as the reference for angles up to 154°. 29

2.10 Electron binding energy of CO_2^- calculated using various EOM methods as a function of a predominantly bending coordinate. The calculations were carried out using the ANOTZ+3s3p basis set. 31

2.11 The SONO of the non-valence correlation-bound anion of TCNE from EOM-MP2 calculations using the aug-cc-pVDZ+7s7p basis set. The isosurfaces enclose 70% of the excess electron charge. Two different orientations are shown. 35

2.12 Distribution of the excess electron of the non-valence $^2B_{3g}$ (orange) anion state and of the NVCB ^2A_g (green) anion state of TCNE. The two electron density distributions are plotted as functions of $r_{nearest}$. 36

3.1 $(H_2O)_4$ cluster model. R is fixed to 4.0 Å, while R' is varied. The black dots indicate the locations of the supplemental sets of diffuse basis functions, which are located at $\pm(R'/2 + 2.27)$ in Å. 43

3.2 Electron binding energies of the A_g (blue dots) and B_{2u} (red squares) anion states of the $(H_2O)_4$ cluster model as a function of the distance R' separating the two dimers. The EBEs are obtained from EOM-CCSD calculations using the aug-cc-pVTZ basis set augmented with two sets of 9s GTO basis functions located at $\pm(R'/2 + 2.27)$ in Å. The horizontal dashed line indicates the EBE of the dimer subunit. 45

3.3 NOs associated with the excess electron of the A_g (upper) and B_{2u} (lower) anions states of the $(H_2O)_4$ cluster model at $R' = 13.5$ Å and characterized by EOM-CCSD calculations using the aug-cc-pVTZ basis set augmented with two sets of 9s functions as described in the text. The contours shown enclose 90% charge of the charge density. 46

3.4 Stabilization graph for $(H_2O)_4$ with $R' = 4.46$ (top), 6.46 (middle), and 7.96 Å (bottom). The energies of the excess electron states from EOM-CCSD calculations are shown as blue dots, and the energies of the DC levels are shown as black squares. 48

3.5 Resonance energy, E_r, (blue dots) and half-width, $\Gamma/2$, (red triangles) from stabilization calculations using EOM-CCSD energies of the B_{2u} anion of the $(H_2O)_4$ model as a function of R'. The figure also includes the negative of the EBE for R' values for which the anion is bound. 51

3.6 Effective radial potential, V_{eff} (solid red line), vs r, the distance from the center of the cluster, for p-wave scattering from the $(H_2O)_4$ cluster model with $R' = 7.96$ Å. The electrostatic contribution (ES) is shown as the dashed black line, the polarization contribution (Pol) is shown as the blue dot-dashed line, and the angular momentum contribution (AM) is shown as the green dotted line. 53

3.7 NOs associated with the excess electron of the B2u anion states of the $(H_2O)_4$ cluster model at $R' = 9.46$, 8.96, and 7.96 Å. The anion is weakly bound at $R' = 9.46$ Å and is metastable at the two shorter R' values. The NOs are from EOM-CCSD calculations using the aug-cc-pVTZ basis set augmented with two sets of 9s functions, as described in the text. The contours shown enclose 90% of the charge density of the NOs. The black dots indicate the positions of the water molecules. 57

4.1 Lowest unoccupied molecular orbital from a Hartree-Fock calculation on neutral $(NaCl)_2$ using the aug-cc-pVTZ basis set on the atoms and two sets of 9s functions as described in the text and centered at the location of the two black spheres, on the same axis as the sodium atoms. The contour shown encloses 90% of the charge density. 61

4.2 (a) Stabilization graph for $(NaCl)_2$ obtained from EA-EOM-CCSD calculations at $q = 0$ and using the correlated core approximation. The energies of the excess electron states from EOM-CCSD calculations and of the DC levels are shown as blue dotted lines and black dashed lines, respectively. (b) The energies of the excess electron states from EOM-CCSD calculations are shown as blue dotted lines. The energies of the DC levels are shown as black dashed lines and the unmixed discrete level by the horizontal red line, while estimates of the energies of the second and third DC levels orthogonalized to the discrete level are indicated by the sloped red line. 66

4.3 Resonance energy, E_r and $\Gamma/2$, from EA-EOM-CCSD stabilization calculations on the B_{2u} anion of $(NaCl)_2$ as a function of q, the distortion along the symmetric breathing normal coordinate. Results obtained in the frozen core (shown in blue) and correlated core (shown in red) approximations are reported. The figure also includes the negative of the EBE for q values for which the anion is bound. 68

4.4 $\Gamma/2$ vs E_r from EA-EOM-CCSD/stabilization calculations on the B_{2u} anion of $(NaCl)_2$ with the results from the frozen core and correlated core approximations shown as blue triangles and red triangles, respectively. Also shown are fits based on eq 4.5, with the fit using the expression for a p-wave resonance shown as the black dotted line and that for an f-wave resonance shown as the solid green line. 69

4.5 Polarization potential for the correlated core (solid red line) and frozen core (dashed blue line) approximations as a function of distance along the Na-Na axis (r, in angstroms). 71

4.6 Effective radial potential, V_{eff} (solid black line), vs r, the distance from the center of the cluster, for p-wave scattering from the $(NaCl)_2$ cluster model with $q = 0$. The electrostatic contribution (ES) is shown as the dashed blue line, the polarization contribution (Pol) is shown as the red dash-dotted line, and the angular momentum contribution (AM) is shown as the green dotted line. . . 72

4.7 Relative energies of the A_g (dashed blue) and B_{2u} (dash-dotted red) anion states and of the ground state of the neutral $(NaCl)_2$ cluster (solid green) as a function of q, the fractional distortion along the symmetric breathing normal coordinate. The energy of the neutral ground state at its most stable geometry ($q = -0.06$) is taken as the zero of the energy scale. The energy of the neutral is from CCSD calculations and the energies of the anion states are from the EOM-CCSD calculations, all obtained using the correlated core approximation. . . 73

5.1 Change in $r^2\psi^2$ in going from the unperturbed 1s orbital to allowing for the field-induced admixture of excited ns orbitals, for an external uniform field of 0.01 au. 86

Preface

I thank my advisor, Ken Jordan, for teaching, mentoring, and supporting me throughout my studies, for providing me with countless opportunities to learn, for always being there for me whenever I needed his advice. I would like to thank my committee members, Peng Liu, Sean Garrett-Roe, and David Yaron, for their guidance. I would like to thank my collaborator, Mike Falcetta, for our teamwork on joint projects.

I would like to thank the Department of Chemistry faculty and staff for making this journey possible. I would like to thank the Center for Research Computing for providing me with all of the necessary computational resources. I would like to thank the Pittsburgh Quantum Institute for providing me with opportunities to present my work.

I would like to thank former group members who helped me integrate into the group and research, namely, Vamsee Voora, Xun Wang, Togo Odbadrakh, Kaye Archer, and Kevin Gasperich. I would also like to thank the current Jordan group members, Tae Hoon Choi, Elva Henderson, Amanda Dumi, Shiv Upadhyay, Devin Mulvey, Ryan Wheat, and Stephen Slimak, for healthy and friendly environment within our group.

I would like to thank my fellow graduate students, Shreya Ghosh and Xing Yee Gan, for their continuous support and friendship. I would like to thank my friends, Bibifatima Kaupbayeva, Moldir Ibraiymova, Nursulu Dildabekova, Ainur Mukhambetova, and Aizat Nurshatayeva, for reminding me of life outside of the department.

I would like to thank my family, Kenzhesh Kairalapova, Islam Kairalapov, Olzhas Kairalapov, Anna Kassymova, and Layla Kairalapova, for their love and support. Finally, I would like to thank Ayan Baltabaiuly for encouraging me at every step of the way.

1.0 Introduction

1.1 Non-Valence Anions

Theoretical and computational studies have become an essential part of research that explains and validates data obtained experimentally. Quantum chemistry provides us with opportunities to study various chemical and biological processes. Many such processes occur via charge transfer resulting in creation of anions when an atom, molecule, or molecular cluster binds an excess electron.

Anions can be viewed as valence-bound or non-valence-bound depending on the nature of the interaction between the excess electron and the molecule. The excess electron in a valence-bound anion is bound by relatively short-range interactions in a valence orbital. In a non-valence-bound anion, however, there are long-range electrostatic and/or correlation interactions and the electron occupies an orbital that is not valence-like in nature. An example of electrostatically-bound anions are dipole-bound anions. Such anions form when molecules with a dipole moment greater than 1.625 D within the Born-Oppenheimer approximation bind excess electrons in the dipole field.[1–5] Provided a sufficiently flexible basis set is used, the dipole-bound anions can be observed at the Hartree-Fock method.

In the absence of a dipole moment, a molecule may bind an excess electron via correlation interactions.[6,7] In my research I focus on non-valence anions for which inclusion of electron correlation is essential for binding of the excess electron or dominates the electron binding energy. Non-valence correlation-bound (NVCB) anions are unbound at the Hartree-Fock level and in such calculations the electron falls onto a discretized continuum orbital. Correlation is often incorporated through post-Hartree-Fock methods such as coupled-cluster theory. However, since coupled-cluster calculations starting from the Hartree-Fock wave function also fail to bind the excess electron of the NVCB anion. Methods such as equation of motion coupled-cluster method are needed to observe NVCB anions.[6,8]

The following sections focus on briefly discussing *ab initio* methods mentioned above that are used within this work to study non-valence anions.

1.2 Schrödinger Equation

We begin the discussion of various electronic structure methods from the non-relativistic time-independent Schrödinger equation

$$H\left|\Psi\right\rangle = E\left|\Psi\right\rangle \tag{1.1}$$

where H is the Hamiltonian operator of N electrons and M nuclei, Ψ is a wave function, and E is an energy eigenvalue. Because nuclei are significantly heavier than electrons, electrons can be considered to be moving in the field of nuclei with fixed positions. This approximation is known as the Born-Oppenheimer approximation.[9] The electronic Hamiltonian within the Born-Oppenheimer approximation in atomic units is

$$H = -\sum_{i=1}^{N}\frac{1}{2}\nabla_i^2 - \sum_{i=1}^{N}\sum_{A=1}^{M}\frac{Z_A}{\left|\vec{r}_i - \vec{R}_A\right|} + \sum_{i=1}^{N}\sum_{j>i}^{N}\frac{1}{|\vec{r}_i - \vec{r}_j|} \tag{1.2}$$

where $\vec{r}_i$ and $\vec{R}_A$ are positions of electron i and nucleus A, respectively, and Z_A is the atomic number of nucleus A. The first term on the right-hand side of eq 1.2 is the kinetic energy operator for the electrons, the second and third terms are electron-nucleus attraction and electron-electron repulsion potential terms, respectively. The wave function, Ψ, can be taken as a product of single-electron spin orbitals.

$$\left|\Psi\right\rangle = \psi_i(\vec{r}_1,\omega_1)\psi_j(\vec{r}_2,\omega_2)\cdots\psi_k(\vec{r}_N,\omega_N) \tag{1.3}$$

where ω is a spin coordinate of an electron. Since the electrons are indistinguishable from each other, the wave function must be antisymmetrized. An antisymmetric wave function changes sign upon interchange of any two electrons. This can be achieved by using a Slater determinant for the wave function

$$\left|\Psi_0\right\rangle = \frac{1}{\sqrt{N!}}\begin{vmatrix} \psi_i(\vec{r}_1,\omega_1) & \psi_j(\vec{r}_1,\omega_1) & \cdots & \psi_k(\vec{r}_1,\omega_1) \\ \psi_i(\vec{r}_2,\omega_2) & \psi_j(\vec{r}_2,\omega_2) & \cdots & \psi_k(\vec{r}_2,\omega_2) \\ \vdots & \vdots & \ddots & \vdots \\ \psi_i(\vec{r}_N,\omega_N) & \psi_j(\vec{r}_N,\omega_N) & \cdots & \psi_k(\vec{r}_N,\omega_N) \end{vmatrix} \tag{1.4}$$

where $(N!)^{-1/2}$ is a normalization factor. A more brief notation can be chosen for the wave function

$$|\Psi_0\rangle = |\psi_i\psi_j\cdots\psi_k\rangle = |ij\cdots k\rangle \tag{1.5}$$

According to variational principle, increasing the flexibility of a trial wave function lowers its energy

$$E = \int \Psi_0^* H \Psi_0 d\vec{r} d\omega = \langle\Psi_0|H|\Psi_0\rangle \tag{1.6}$$

Starting from Slater determinant of orbitals, the energy is minimized by optimizing the orbitals.

1.3 Hartree-Fock Theory

The electronic Hamiltonian in eq 1.2 has one-electron and two-electron terms. The one-electron terms can be combined into a core-Hamiltonian operator

$$h(i) = -\frac{1}{2}\nabla_i^2 - \sum_{A=1}^{M} \frac{Z_A}{\left|\vec{r}_i - \vec{R}_A\right|} \tag{1.7}$$

The Hartree-Fock (HF) method approximates the wave function as a single Slater determinant, which simplifies the calculation of the energy contribution from the two-electron operator.

$$\sum_{i=1}^{N}\sum_{j>i}^{N} \langle\Psi_0|\frac{1}{|\vec{r}_i - \vec{r}_j|}|\Psi_0\rangle = \sum_{i=1}^{N}\sum_{j>i}^{N}(\langle ij|ij\rangle - \langle ij|ji\rangle) \tag{1.8}$$

where the integrals on the right-hand side are Coulomb integrals, J_{ij}, and exchange integrals, K_{ij}, respectively

$$J_{ij} = \langle ij|ij\rangle = \int \psi_i^*(\vec{r}_1,\omega_1)\psi_j^*(\vec{r}_2,\omega_2)\frac{1}{|\vec{r}_1 - \vec{r}_2|}\psi_i(\vec{r}_1,\omega_1)\psi_j(\vec{r}_2,\omega_2)d\vec{r}_1 d\vec{r}_2 d\omega_1 d\omega_2 \tag{1.9a}$$

$$K_{ij} = \langle ij|ij\rangle = \int \psi_i^*(\vec{r}_1,\omega_1)\psi_j^*(\vec{r}_2,\omega_2)\frac{1}{|\vec{r}_1 - \vec{r}_2|}\psi_j(\vec{r}_1,\omega_1)\psi_i(\vec{r}_2,\omega_2)d\vec{r}_1 d\vec{r}_2 d\omega_1 d\omega_2 \tag{1.9b}$$

It is useful to derive the operator forms of the two-electron integrals to observe their effects on a particular single-electron spin orbital. The Coulomb and exchange operators acting on electron 1 are

$$J_j(1) = \int \psi_j^*(\vec{r}_2, \omega_2) \frac{1}{|\vec{r}_1 - \vec{r}_2|} \psi_j(\vec{r}_2, \omega_2) d\vec{r}_2 d\omega_2 \tag{1.10a}$$

$$K_j(1) = \int \psi_j^*(\vec{r}_2, \omega_2) \frac{1}{|\vec{r}_1 - \vec{r}_2|} \psi_i(\vec{r}_2, \omega_2) d\vec{r}_2 d\omega_2 \tag{1.10b}$$

These operators can be combined into a Hartree-Fock potential

$$v^{HF}(1) = \sum_j (J_j(1) - K_j(1)) \tag{1.11}$$

Combining the core-Hamiltonian with the Hartree-Fock potential we derive the Fock operator

$$f(1) = h(1) + v^{HF}(1) \tag{1.12}$$

Then the Hartree-Fock equation for a spin orbital ψ_i is

$$f \left|\psi_i\right\rangle = E_i \left|\psi_i\right\rangle \tag{1.13}$$

Since the Hartree-Fock potential in f depends on the form of ψ_i, eq 1.13 is nonlinear and is solved iteratively.

1.4 Coupled-Cluster Theory

In the Hartree-Fock method electrons "feel" the electron-electron repulsive potential as an averaged field. This means that the Hartree-Fock method does not account for electron correlation effects. In fact, the correlation energy is defined as the difference between the exact nonrelativistic energy and the Hartree-Fock energy. Post-Hartree-Fock methods such as coupled-cluster theory are used to approximate correlation energy. Before describing the coupled-cluster approximation,[10] it is useful to illustrate the second quantization formalism.

The creation operator, $a_i^\dagger$, adds an electron to a spin orbital ψ_i and the annihilation operator, a_i removes an electron from a spin orbital ψ_i

$$a_i^\dagger |\psi_j\rangle = |\psi_i \psi_j\rangle \tag{1.14a}$$

$$a_i |\psi_i \psi_j\rangle = |\psi_j\rangle \tag{1.14b}$$

If an electron already exists in ψ_i, then $a_i^\dagger |\psi_i \psi_j\rangle = 0$. Similarly, if an electron is not in ψ_i, then $a_i |\psi_j\rangle = 0$. The creation and annihilation operators are related by an anticommutation relation

$$a_i a_j^\dagger + a_j^\dagger a_i = \delta_{ij} \tag{1.15}$$

where δ_{ij} is the Kronecker delta.

The wave function for the coupled-cluster method[10] is

$$|\Psi_{\mathrm{CC}}\rangle = e^T |\Psi_0\rangle \tag{1.16}$$

where T is a cluster operator and $|\Psi_0\rangle$ is a single determinant reference wave function such as the ground state Hartree-Fock wave function. The operator T has single, double, etc. excitations depending on the coupled cluster method

$$T = T_1 + T_2 + \cdots = \sum_{ir} t_i^r a_r^\dagger a_i + \frac{1}{4} \sum_{ijrs} t_{ij}^{rs} a_r^\dagger a_s^\dagger a_j a_i + \ldots \tag{1.17}$$

where t are coefficients, i and j represent occupied orbitals, and r and s are excited states. e^T can be expanded in a Taylor series

$$e^T = \sum_{n=0}^{\infty} \frac{T^n}{n!} = 1 + T + \frac{T^2}{2!} + \ldots \tag{1.18}$$

In the coupled-cluster singles and doubles (CCSD) method,[11] the cluster operator is truncated at the second excitation, T_2. The CCSD energy is found by solving a system of equations resulting when equation

$$H e^{T_1 + T_2} |\Psi_0\rangle = E e^{T_1 + T_2} |\Psi_0\rangle \tag{1.19}$$

is multiplied by $\langle\Psi_0|$, $\langle\Psi_i^r|$, and $\left\langle\Psi_{ij}^{rs}\right|$ which appear when $\langle\Psi_0|$ is multiplied by 1, T_1, and T_2, respectively.

Coupled-cluster methods are size consistent, which means that the energy of a non-interacting system is equal to the sum of the energies of the constituents of the system at infinitely large separation.

1.5 Equation of Motion Theory

The equation of motion (EOM) method[12] has an excitation operator acting on the coupled cluster wave function

$$|\Psi\rangle = R\,|\Psi_{CC}\rangle = Re^{T}\,|\Psi_0\rangle \tag{1.20}$$

where the R operator can correspond to an excitation operator R_{EE}, electron attachment R_{EA}, or ionization potential R_{IP}. The R_{EA} and R_{IP} operators add and remove an electron, respectively.

$$R_{EE} = c_0 + \sum_{ir} c_i^r a_r^\dagger a_i + \frac{1}{4}\sum_{ijrs} c_{ij}^{rs} a_r^\dagger a_s^\dagger a_j a_i + \ldots \tag{1.21a}$$

$$R_{EA} = \sum_{r} c^r a_r^\dagger + \frac{1}{2}\sum_{irs} c_i^{rs} a_r^\dagger a_s^\dagger a_i + \ldots \tag{1.21b}$$

$$R_{IP} = \sum_{i} c_i a_i + \frac{1}{2}\sum_{ijr} c_{ij}^{r} a_r^\dagger a_j a_i + \ldots \tag{1.21c}$$

The EOM-CC energy is

$$E = \langle\Psi_0|Le^{-T}He^{T}R|\Psi_0\rangle \tag{1.22}$$

where L is the de-excitation operator.

1.6 Temporary Anion Shape Resonances

The EOM-CC methods can accurately describe non-valence correlation-bound anions. The species possessing NVCB states may additionally possess temporary anion states. Temporary anions are higher in energy than the corresponding neutral ground states. Temporary anion shape resonances of atoms and molecules are trapped by an angular momentum barrier.[13] Shape resonances are short-lived with the electron detaching by tunneling through the potential barrier.

The resonance energy is described by real and imaginary parts

$$E_{res} = E_r - \frac{i\Gamma}{2} \tag{1.23}$$

where E_r is the resonance position and Γ is the resonance width which is inversely proportional to the lifetime of the resonance.[14]

In the following sections we describe a model potential possessing a resonance and use the model to illustrate how to obtain resonance energy and position.

1.7 Model Potential

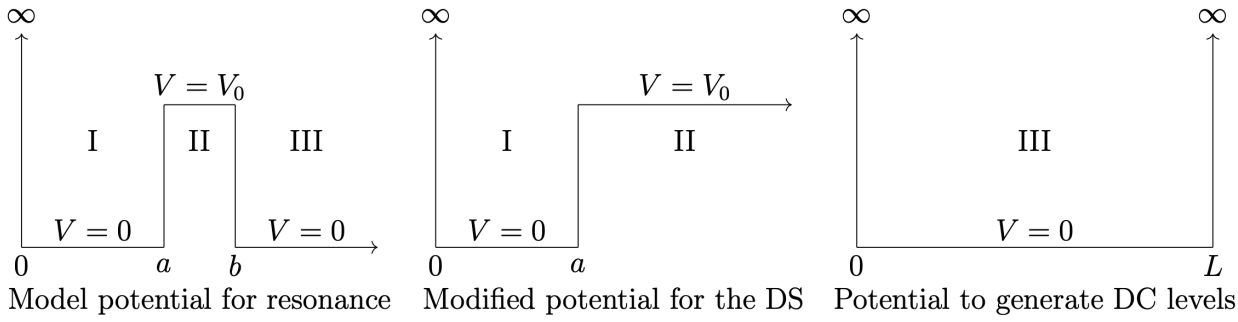

Figure 1.1: Diagrams for the model potential possessing resonance (left), the modified potential for the discrete state (DS) (middle), and the potential to generate discretized continuum (DC) levels

The model potential consists of an infinite potential wall at $x = 0$ and a potential barrier V_0 from $x = a$ to b as illustrated in the leftmost diagram of Figure 1.1. In order to study the resonance, we partition the problem into a discrete state (DS) and discretized continuum levels (DC) illustrated in Figure 1.1 middle and rightmost diagrams, respectively.

The model potential is described by the Hamiltonian in 1D given in atomic units as

$$H = -\frac{1}{2}\frac{d^2}{dx^2} + V(x) \tag{1.24}$$

where $V(x)$ is the potential described above.

1.8 Discrete State and Discretized Continuum Wave Functions

The discrete state has an infinite potential at $x = 0$, then a well of $V = 0$ until $x = a$, and a fixed potential $V = V_0$ as $x \to \infty$. The wave function is 0 when $x = 0$ and when $x \to \infty$. The wave function has two regions

$$\psi_1 = A \sin(k_1 x), \text{ for } 0 < x < a \tag{1.25a}$$

$$\psi_2 = B e^{-k_2(x-a)}, \text{ for } x > a \tag{1.25b}$$

k_1 and k_2 are defined as

$$k_1 = \sqrt{2E_{DS}} \tag{1.26a}$$

$$k_2 = \sqrt{2(V_0 - E_{DS})} \tag{1.26b}$$

where E_{DS} is the energy of the discrete state. The DS wave function and its derivative have to be continuous at $x = a$

$$A \sin(k_1 a) = B \tag{1.27a}$$

$$k_1 A \cos(k_1 a) = -k_2 B \tag{1.27b}$$

Thus, k_1 and k_2 are related by

$$k_1 + k_2 \tan(k_1 a) = 0 \tag{1.28a}$$

$$\sqrt{2E_{DS}} + \sqrt{2(V_0 - E_{DS})} \tan\sqrt{2E_{DS}}a = 0 \tag{1.28b}$$

where in eq 1.28b we used the expressions from eq 1.26 to estimate the energy of the discrete state for given values of V_0 and a

In order to find the coefficients A and B, the discrete wave function is normalized.

$$\int_0^a \psi_1^* \psi_1 dx = A^2 \left(\frac{a}{2} - \frac{\sin(2k_1 a)}{4k_1} \right) \tag{1.29a}$$

$$\int_a^\infty \psi_2^* \psi_2 dx = \frac{B^2}{2k_2} = \frac{A^2 (\sin(k_1 a))^2}{2k_2} \tag{1.29b}$$

$$A = \left(\frac{a}{2} - \frac{\sin(2k_1 a)}{4k_1} + \frac{(\sin(k_1 a))^2}{2k_2} \right)^{-1/2} \tag{1.29c}$$

where eq 1.27a relation between A and B was used.

The discretized continuum potential is simply a particle in a 1D box of size L. The normalized wave function of the n^{th} state is

$$\psi_3 = \sqrt{\frac{2}{L}} \sin\left(\frac{n\pi x}{L}\right) \tag{1.30}$$

1.9 2x2 Model Problem

We can apply the Hamiltonian from eq 1.24 on a 2x2 problem mixing the discrete state with one continuum state ($n = 1$).

$$\begin{vmatrix} H_{11} - E & H_{12} - S \\ H_{21} - S & H_{22} - E \end{vmatrix} = 0 \tag{1.31}$$

where $H_{11} = \langle \psi_1 + \psi_2 | H | \psi_1 + \psi_2 \rangle$ is the energy of the discrete state, $H_{22} = \langle \psi_3 | H | \psi_3 \rangle$ is the energy of the discretized continuum state, $H_{12} = \langle \psi_1 + \psi_2 | H | \psi_3 \rangle$ and $H_{21} = \langle \psi_3 | H | \psi_1 + \psi_2 \rangle$ are mixing of the two states, and $S = \langle \psi_1 | \psi_3 \rangle + \langle \psi_2 | \psi_3 \rangle$ is the overlap of the two states.

The energies of the discrete state and the discretized continuum state are

$$H_{11} = \frac{A^2 k_1^2}{2}\left(\frac{a}{2} - \frac{\sin(2k_1 a)}{4k_1}\right) - \frac{B^2 k_2}{4} - \frac{B^2 V_0 (e^{-2k_2(b-a)} - 1)}{2k_2} \tag{1.32a}$$

$$H_{22} = \frac{\pi^2}{2L^2} + \frac{V_0}{L}\left[(b-a) - \frac{L}{2\pi}\left(\sin\left(\frac{2\pi b}{L}\right) - \sin\left(\frac{2\pi a}{L}\right)\right)\right] \tag{1.32b}$$

Prior to discussing the mixing of the states, it is convenient to obtain the overlap integral S partitioning it into overlap S_{13} from 0 to a and S_{23} from a to L. In addition a potential energy contribution P_{23} is calculated from a to b

$$S_{13} = \frac{A\sqrt{2/L}}{-k_1^2 + \pi^2/L^2}\left(-\frac{\pi}{L}\sin(k_1 a)\cos\left(\frac{\pi a}{L}\right) + k_1 \cos(k_1 a)\sin\left(\frac{\pi a}{L}\right)\right) \tag{1.33a}$$

$$S_{23} = \frac{B\sqrt{2/L}}{k_2^2 + \pi^2/L^2}\left(\frac{\pi}{L}\cos\left(\frac{\pi a}{L}\right) + k_2 \sin\left(\frac{\pi a}{L}\right) + \frac{\pi}{L}e^{-k_2(L-a)}\right) \tag{1.33b}$$

$$P_{23} = \frac{B\sqrt{2/L}}{k_2^2 + \pi^2/L^2}\left[\frac{\pi}{L}\cos\left(\frac{\pi a}{L}\right) + k_2 \sin\left(\frac{\pi a}{L}\right) - e^{-k_2(b-a)}\left(\frac{\pi}{L}\cos\left(\frac{\pi b}{L}\right) + k_2 \sin\left(\frac{\pi b}{L}\right)\right)\right] \tag{1.33c}$$

The mixed states in terms of the S_{12}, S_{23}, and P_{23} integrals are

$$H_{12} = \frac{\pi^2}{2L^2} S_{13} + \frac{\pi^2}{2L^2} S_{23} + V_0 P_{23} \tag{1.34a}$$

$$H_{21} = \frac{k_1^2}{2} S_{13} - \frac{k_2^2}{2} S_{23} + V_0 P_{23} \tag{1.34b}$$

In order to simplify solving for eigenvalues of the H matrix, the basis set can be orthonormalized. For the model problem described here we choose the following parameters: $a = 10$ au, $b = 12$ au, and $V_0 = 0.3$ au. Using these parameters and the expression from eq 1.28b, we calculate the energy of the discrete state to be $E_{DS} = 0.03850797$ au. For values of $L > 20$ au, H_{12} and H_{21} are essentially equal.

1.10 Stabilization Method and Analytic Continuation

The stabilization method can be applied to calculate the resonance energies.[15] The stabilization graph is a plot of eigenvalues of the Hamiltonian as a function of a scaling parameter. In our model potential problem, we plot the eigenvalues as a function of $1/L^2$ to observe the avoided crossing.

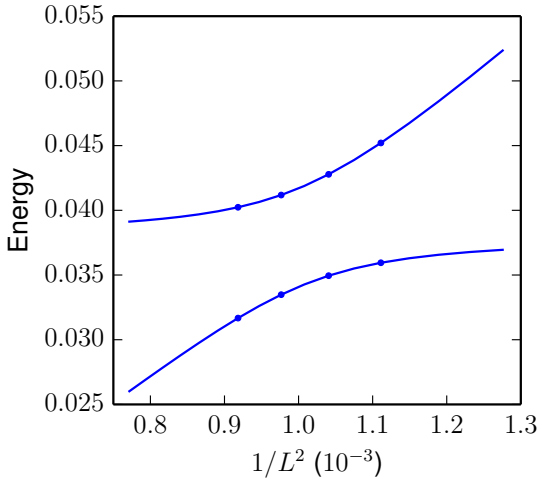

Figure 1.2: Stabilization graph of the model potential

Analytic continuation method can be used to obtain the resonance position and width from the data points close to the avoided crossing in the stabilization plot.[16] The energies from the plot can be fit to a quadratic equation

$$PE^2 + QE + R = 0 \tag{1.35}$$

where P, Q, and R are polynomials of the scaling parameter $\beta = 1/L^2$

$$P(\beta) = 1 + p_1\beta + p_2\beta^2 + \cdots \tag{1.36a}$$

$$Q(\beta) = q_0 + q_1\beta + q_2\beta^2 + \cdots \tag{1.36b}$$

$$R(\beta) = r_0 + r_1\beta + r_2\beta^2 + \cdots \tag{1.36c}$$

We choose eight points in the vicinity of the avoided crossing indicated in Figure 1.2 to determine the resonance energy. The polynomials $P(\beta)$, $Q(\beta)$, and $R(\beta)$ are of the 1$^{\text{st}}$, 2$^{\text{nd}}$, and 3$^{\text{rd}}$ orders in β, respectively. We solve a system of eight equations for eight parameters of the polynomials. Once the exact form of eq 1.35 is determined, we solve for the energy

$$E = \frac{-Q(\beta) \pm \sqrt{Q^2(\beta) - 4P(\beta)R(\beta)}}{2P(\beta)} \tag{1.37}$$

and search for a complex stationary point β^* for which

$$\frac{dE}{d\beta} = 0 \tag{1.38}$$

With the model potential parameters and eight data points, we get $\beta = 0.001136 \pm 0.001755i$. Plugging this value of β into eq 1.35 yields $E_{res} = 0.037932 \pm 0.000319i$ au. Thus, the resonance position is $E_r = 0.037932$ and the resonance width is $\Gamma = 0.000638$.

The model potential described in the last sections is a useful tool in understanding resonances. Stabilization graph allows one to qualitatively estimate the position of the resonance. Analytically continuing energies from the stabilization graph into a complex plane allows one to determine resonance position and width. These techniques can be applied to study resonances of atoms, molecules, and molecular clusters.[17,18]

Temporary anion shape resonances are relatively short-lived, i.e. they have large resonance widths. For broad resonances where E_r and Γ are in the same order of magnitude, analytic continuation involves higher powers of E.[17,18] Generally, more data points are chosen from the stabilization graph and they are fit using the least squares method. In later chapters we use stabilization method in combination with analytic continuation to characterize temporary anion shape resonances of $(H_2O)_4$ and $(NaCl)_2$.

2.0 Theoretical Approaches for Treating Non-Valence Correlation-Bound Anions

The text and figures in this chapter have been reprinted from Voora, V. K.; Kairalapova, A.; Sommerfeld, T.; Jordan, K. D. Theoretical approaches for treating non-valence correlation-bound anions. *J. Chem. Phys.* **2017**, *147*, 214114, DOI: 10.1063/1.4991497, with the permission of AIP Publishing. The author's contribution to the work included performing HF, MP2, CCSD, CCSD(T), EOM-CC, BCCD calculations, generating all figures, and revising the manuscript.

2.1 Summary

In this work, we use a model $(H_2O)_4$ cluster, the bent CO_2 molecule, and tetracyanoethylene as systems to explore the applicability of various electronic structure methods for characterizing non-valence correlation-bound anion states. The methods examined include the algebraic diagrammatic construction, various equation-of-motion coupled cluster methods, orbital-optimized MP2, and Brueckner coupled cluster doubles with perturbative triples. We demonstrate that the key to treating this challenging class of anions is the use of methods that include adequate orbital relaxation in response to long-range dispersion-like correlation effects.

2.2 Introduction

Bound anionic states of molecules can be classified as valence-bound or non-valence-bound depending on the nature of the interaction between the excess electron and the molecule. In valence-bound anion states, the excess electron is bound to the molecule by short-range interactions and occupies an orbital localized in the valence region. By contrast,

in non-valence-bound anion states, the binding of the excess electron is dominated by long-range electrostatics or dispersion-type correlation effects or a combination of these two effects, and the excess electron occupies an orbital that has relatively little weight in the valence region.[1,6,7,19–28] Dipole-bound anions are a well-known class of non-valence anions for which electrostatic interactions dominate the electron binding. Within the Born-Oppenheimer approximation, a molecule has to have a dipole moment in excess of 1.625 D to possess a dipole-bound anion, whereas the inclusion of non-Born-Oppenheimer corrections causes the critical moment to depend on the moment of inertia and to assume a value closer to 2.5 D.[1,19,26] Examples of systems for which long-range correlation effects dominate the binding of the excess electron are sufficiently large Xe_n clusters,[20] the s-type anion states of C_{60},[6] and large acenes.[25] In addition to these limiting cases, there are systems, e.g., succinonitrile[24] and certain structures of $(NaCl)_n$ clusters,[7] for which both electrostatics and long-range correlation effects play an important role in the binding of the excess electron. We refer to non-valence anions for which inclusion of long-range correlation effects is essential for electron binding as non-valence correlation-bound (NVCB) anions.

For non-valence anions for which the binding of the excess electron is dominated by long-range electrostatic interactions, both the Hartree-Fock (HF) and Koopmans' theorem (KT)[29] approximations give a bound anion, provided that sufficiently flexible basis sets are employed. For these species, quantum chemistry methods such as coupled-cluster singles and doubles plus perturbative triples [CCSD(T)][30] and, in some cases, even second-order Møller-Plesset perturbation theory (MP2)[31] can accurately predict the electron binding energies (EBEs) and other properties of the anions. By contrast, NVCB anions, by definition, are unbound at the HF level of theory. In fact, when flexible basis sets are employed for such systems, the HF wave function for the excess electron system actually describes the neutral system plus an electron in a discretized continuum orbital. As a result, electronic structure methods such as MP2 and CCSD(T) that start from the HF approximation are expected to fail to bind the excess electron when flexible basis sets are employed. Thus, it is of considerable interest to establish which electronic structure methods are suitable for describing NVCB anions. In this work, we consider a $(H_2O)_4$ cluster with zero net dipole moment and tetracyanoethylene (TCNE) as model systems for accessing the performance of various theoretical methods

for describing NVCB anions. We also consider the case of CO_2^- for which the inclusion of correlation effects is essential for the binding of the excess electron as the bending potential of the anion approaches that of the neutral. Although, the wave function of the ground electronic state of CO_2^- acquires considerable non-valence character at these geometries, the nature of the correlation contribution appears to be different from that of typical NVCB anions.

2.3 Theoretical Approaches

The theoretical methods considered include HF, MP2, second-order algebraic diagrammatic construction (ADC(2)),[32] CCSD, CCSD(T), various equation-of-motion (EOM) coupled cluster methods,[33–37] orbital-optimized MP2 (OO-MP2),[38,39] Brueckner coupled-cluster doubles with perturbative triples (BCCD(T)),[40] and the G_0W_0 Green's function method.[41] In the EOM, ADC(2), and G_0W_0 methods, the electron binding energy (EBE) is calculated directly. For the remaining methods, the energies of the neutral and anionic systems are calculated separately, with spin-unrestricted methods being employed for the anions, and the EBEs are obtained from the difference of the energies of the neutral and anionic species. These are referred to as delta (Δ) methods.

The ADC(2) and G_0W_0 methods are Green's function methods, with the former employing a second-order approximation to the self-energy. Unlike the CCSD(T) and MP2 methods, the BCCD(T) and OO-MP2 methods employ orbitals that are optimized in the presence of correlation effects. The BCCD(T) method optimizes the orbitals so as to eliminate single excitations to all orders in the inter-electron interaction, while the OO-MP2 method optimizes the orbitals in the presence of the second-order correlation effects. The EOM approximations considered are EOM-CCSD(2) (here referred to as EOM-MP2),[33,34] EOM-CCSD,[35] EOM-CCSDT,[36] and EOM-CCSD(T)(a)*.[37] In the EOM-MP2, EOM-CCSD, and EOM-CCSDT methods, the energy of the neutral system is calculated using the MP2, CCSD, and CCSDT[42] methods, respectively, and the resulting excitation amplitudes (doubles for EOM-MP2, singles and doubles for EOM-CCSD, and doubles, singles, and triples for EOM-

CCSDT) are used to perform a similarity transform of the Hamiltonian which is then used to carry out a CI calculation on the anion. In the EOM-MP2 and EOM-CCSD methods, the CI calculations include all symmetry-allowed one-particle (1p) and two-particle-one-hole (2p1h) configurations, and in the EOM-CCSDT method, the 3p2h configurations are included as well. The EOM-CCSD(T)(a)* method includes the effects of triple excitations in a non-iterative manner and, thus, is computationally considerably less demanding than full EOM-CCSDT calculations.

Both the EOM and ADC(2) methods are free of the "collapse" to the continuum problem for which the HF method and the MP2 and coupled cluster methods employing HF orbitals are susceptible. The OO-MP2 and BCCD(T) methods can also avoid the collapse onto the continuum in calculations on the anion, provided suitable initial guess orbitals are employed. For the BCCD(T) calculations, orbitals from a HF calculation on the cation were used for the starting guess for the anion. Thus, when employing a large basis set with very diffuse functions, the singly occupied orbital of the initial guess wave function for the anion actually corresponds to a Rydberg orbital, which is more localized in the molecular region than is a discretized continuum orbital. For the OO-MP2 calculations, orbitals from a B3LYP[43–45] density functional theory calculation were used as the initial guess orbitals.

The EOM, MP2, BCCD(T), and CCSD(T) calculations were carried out using the CFOUR code,[46] the ADC(2) and OO-MP2 calculations were carried out using the Psi4 code,[47] and the G_0W_0 calculations were performed using Turbomole.[48] The ADC(2) algorithm, as implemented in Psi4, actually calculates excitation energies rather than EBEs. However, this was "tricked" into calculating EBEs by choosing as the ground state a "dianion" with two electrons occupying a very diffuse "continuum" orbital. The electron binding energy of the NVCB anion state is then recovered as an excitation energy (which is of negative sign) in the ADC(2) calculations. The EOM-CCSDT and EOM-CCSD(T)(a)* calculations were also carried out using the electronic excitation implementations of the algorithms together with the "continuum" orbital trick. The basis sets employed in the various calculations are described in Secs. 2.4-2.5.

2.4 $(H_2O)_4$ Cluster Model: Electrostatically Bound to Correlation-Bound Anion

The $(H_2O)_4$ model cluster employed in this work was taken from Ref. 49 and is depicted in Figure 2.1. By design, it has a zero net dipole moment, with the water molecules arranged so that each monomer points an OH group toward the cluster interior, which results in a favorable electrostatic interaction for the excess electron near the cluster center. The cluster is treated as two rigid dimers with OO separations of 3.461 Å, the distance (R) between which is varied. This arrangement is not intended to correspond to an experimentally observable structure for $(H_2O)_4$, but rather is designed as a model for which one can vary the relative importance of correlation and non-correlation contributions to the EBE. In particular, starting at large R and progressing to shorter R, we expect correlation effects to grow in importance relative to the sum of the other contributions to the EBE. Calculations using the various theoretical methods considered are carried out for R values ranging from 2.5 to 9.5 Å.

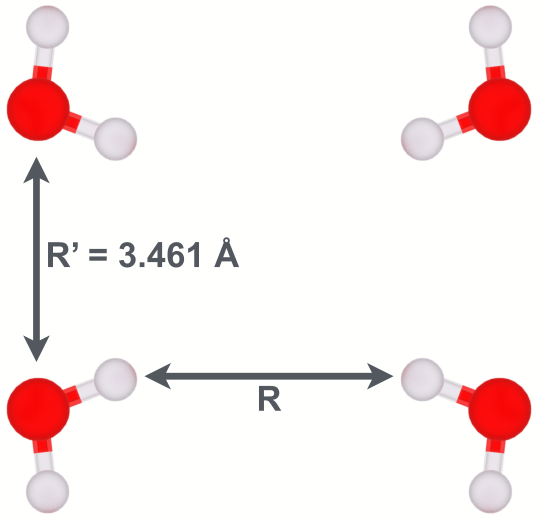

Figure 2.1: Geometry of the $(H_2O)_4$ cluster model studied in this work. R ranges from 2.5 to 9.5 Å.

The majority of the calculations on the $(H_2O)_4$ cluster were carried out using an aug-cc-pVDZ+7s7p Gaussian-type orbital basis formed by supplementing the standard aug-cc-pVDZ basis set[50,51] with a set of seven diffuse s and seven diffuse p primitive Gaussian functions located at the center of mass of the cluster. The exponents of the supplemental Gaussians were chosen to be in geometric ratios with values ranging from 0.025 to 0.000025 and 0.022 to 0.000022 for s and p, respectively. To help elucidate the role of these diffuse functions in describing the NVCB anion, calculations were also carried out with the aug-cc-pVTZ basis set,[50,51] which lacks supplemental diffuse functions. Also, in order to establish the sensitivity of the EBE to the basis set employed, EOM-CCSD(T)(a)* calculations were also carried out for the $(H_2O)_4$ model with $R = 4.2$ Å and using an aug-cc-pVTZ+6s6p6d basis set, with the supplemental functions again being centered at the center-of-mass of the cluster.

We first consider the results obtained with the aug-cc-pVDZ+7s7p basis set. Figure 2.2(a) reports the EBEs from the KT, ΔHF, ΔMP2, ΔCCSD, and ΔCCSD(T) calculations, and Figure 2.2(b) reports the EBEs from the ADC(2), ΔOO-MP2, ΔBCCD(T), and various EOM methods using this basis set. At the largest separation considered, $R = 9.5$ Å, the anion is calculated to be bound by ∼35 and 40 meV in the KT and ΔHF approximations, respectively. Here, and elsewhere in this paper, we use the convention that bound anions correspond to positive EBE values. As R decreases, the KT and ΔHF EBEs decrease, going to zero at $R \sim 4.2$ Å. For $R \lesssim 4.2$ Å, the LUMO from the HF calculation on the neutral molecule has collapsed onto an approximate continuum orbital and the HF wave function of the excess electron system has collapsed onto an approximate continuum state. In contrast to the KT and HF results, the EBEs obtained from the various methods that recover correlation effects (with the exception of MP2 which will be discussed below) increase as R decreases from 9.5 to 4.2 Å. However, while the ADC(2), OO-MP2, EOM, and BCCD(T) methods continue to bind the excess electron for R values $\lesssim 4.2$ Å, the EBEs calculated using the CCSD and CCSD(T) methods collapse to zero once the HF method ceases to bind the electron.

The MP2/aug-cc-pVDZ+7s7p calculations considerably underbind the excess electron for the $(H_2O)_4$ model at all R values considered. Also, the MP2 method, unlike the CCSD

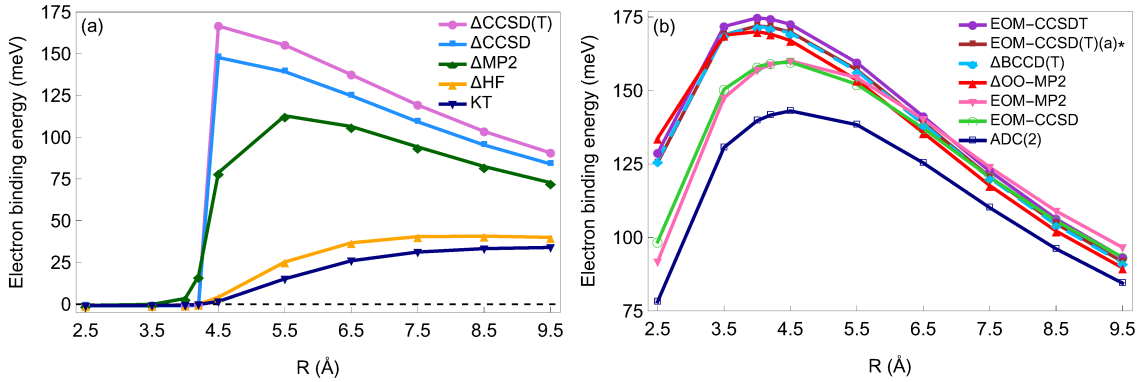

Figure 2.2: EBE of $(H_2O)_4$ calculated using various theoretical methods in conjunction with the aug-cc-pVDZ+7s7p basis set. (a) Results obtained using the KT, ΔHF, ΔMP2, ΔCCSD, ΔCCSD(T) methods, and (b) results obtained using the ADC(2), ΔOO-MP2, ΔBCCD(T), and various EOM methods.

and CCSD(T) methods, weakly binds the excess electron for R values between about 3.6 and 4.2 Å. The binding by the MP2 calculations of the excess electron over this distance range is fortuitous and is a consequence of the fact that although the singly occupied orbital of the HF wave function has collapsed onto a discretized continuum solution, it does have some weight in the molecular region. As a result, the MP2 method gives a slightly larger correlation correction for the excess electron system than for the neutral cluster, leading to very weak binding of the excess electron. Coupled cluster doubles calculations (without singles corrections) also weakly bind the excess electron for R values slightly less than 4.2 Å, leading us to conclude that for these geometries, the single excitations in the CCSD and CCSD(T) calculations stabilize the neutral molecule more than the excess electron system.

For large R values, the OO-MP2, BCCD(T), CCSD(T), and various EOM methods give similar EBE values, while the ADC(2) and CCSD methods give weaker binding due to their less complete treatment of relaxation in response to cor- relation effects. In progressing from large R to $R = 4.2$ Å, there is a growing discrepancy between both the EOM-MP2 and EOM-CCSD values of the EBEs and the EOM-CCSDT and EOM-CCSD(T)(a)* values of the EBEs, with the latter two methods giving larger values of the EBE (by about 10% at

$R = 4.5$ Å). As R approaches 4.2 Å, the EBEs calculated using the OO-MP2, BCCD(T), and CCSD(T) methods all remain close to the EOM-CCSDT results, which we take as the benchmark values. By contrast, as noted above, the CCSD and CCSD(T) calculations collapse onto the neutral plus an approximate continuum orbital for R values less than 4.2 Å.

For $R \lesssim 4.2$ Å, the ADC(2) method continues to give weaker binding than do the OO-MP2, EOM, and BCCD(T) methods. In addition, at these short R values, the EOM-MP2 and EOM-CCSD methods bind the excess electron more strongly than does the ADC(2) method but less strongly than do the EOM-CCSDT, EOM-CCSD(T)(a)*, BCCD(T), and OO- MP2 methods, all of which give EBEs in close agreement with one another. At $R = 3.5$ Å, the EBEs from the EOM-MP2 and EOM-CCSD methods are about 15% smaller than the EOM-CCSD(T)(a)* and EOM-CCSDT values. These results lead us to conclude that for the $(H_2O)_4$ model at geometries at which the HF method fails to bind the excess electron, the OO-MP2 and BCCD(T) methods are more successful at describing relaxation in response to correlation effects than are the EOM-MP2 and EOM-CCSD methods.

It is instructive to compare, at different R values, the LUMO from the HF calculations on the neutral cluster and the singly occupied natural orbital (SONO) from the EOM-CCSD calculations on the anion, both calculated using the aug-cc-pVDZ+7s7p basis set. Figure 2.3 plots these two orbitals along the axis perpendicular to the cluster center for $R = 2.5$, 3.5, 4.5, and 8.5 Å. For each of these R values, the charge distribution associated with the SONO from the EOM-CCSD calculations is largely localized in a region within 10 Å of the center of the cluster, with the extent of localization increasing slightly as R decreases. For $R = 8.5$ Å, the LUMO from the HF calculations is qualitatively similar to the SONO from the EOM-CCSD calculations, but as R decreases, the LUMO from the HF calculations becomes progressively more diffuse than the EOM-CCSD SONO. For $R = 4.5$ Å, the LUMO, while still bound, is far more radially extended than the EOM-CCSD SONO, and for $R = 2.5$ and 3.5 Å, the LUMO has little weight in the vicinity of the cluster, consistent with its collapse onto an approximate continuum function. In fact, at $R = 3.5$ Å, it is the sixth lowest unoccupied orbital from the HF calculations of the neutral cluster that most closely resembles the SONO from the EOM-CCSD calculations.

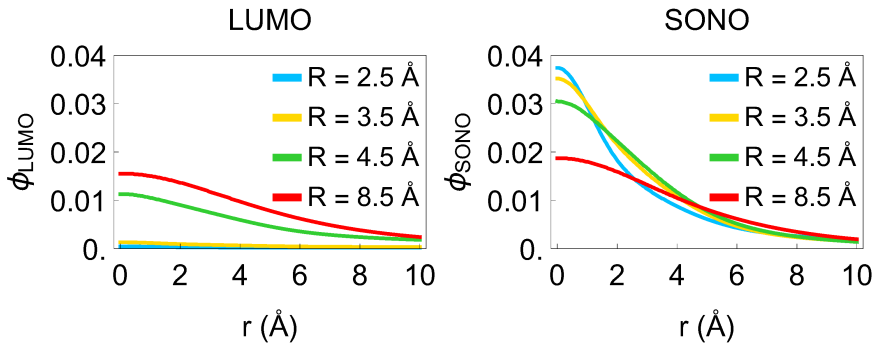

Figure 2.3: Orbital plots of the LUMO from HF calculations of the neutral $(H_2O)_4$ cluster and the SONO from the EOM-CCSD calculations of the anion as a function of the distance from the center of the cluster along the direction perpendicular to the plane of the cluster. The aug-cc-pVDZ+7s7p basis set was used for these calculations.

The results presented above were obtained using the aug-cc-pVDZ+7s7p basis set. We now examine the sensitivity of the EBE of the $(H_2O)_4$ model to further expansion of the basis set. This analysis is done at $R = 4.2$ Å using the EOM-CCSD(T)(a)* method. The resulting EBE obtained using the aug-cc-pVTZ+6s6p6d basis set is 208 meV, which is about 20% greater than that obtained using the aug-cc-pVDZ+7s7p basis set. We also carried out EOM-CCSD(T)(a)* calculations using the aug-cc-pVDZ+6s6p6d and aug-cc-pVTZ+7s7p basis sets, and, based on the results of these calculations, we conclude that roughly half of the 20% increase in EBE noted above comes from the improvement of the description of the charge distribution of the excess electron upon inclusion of the diffuse d functions and about half is due to the improved description of the response of the valence electrons of the water molecules in going from the aug-cc-pVDZ+7s7p to the aug-cc-pVTZ+6s6p6d basis set. This is consistent with the dominant correlation effects being long-range dispersion-like interactions between the excess electron and the valence electrons of the water molecules. The value of the EBE obtained from the EOM-CCSD(T)(a)*/aug-cc-pVTZ+6s6p6d calculations is expected to be close to the exact value, i.e., that which would be obtained from a full

CI calculation in the complete-basis-set limit. In particular, we note that in an earlier publication, where we considered the $(H_2O)_4$ model at a single geometry (R = 5.3 Å), we found that the EBE increased by only 5 meV in going from the aug-cc-pVTZ+6s6p6d to the aug-cc-pVQZ+6s6p6d.[52]

We now turn our attention to the calculations using the aug-cc-pVTZ basis set, with the main results being reported in Figure 2.4. For this basis set, the anion is calculated to be unbound by 200 to 550 meV in the KT and Hartree-Fock approximations over the entire range of R values considered. The failure of the KT and ΔHF calculations using the aug-cc-pVTZ basis set to bind the excess electron to the $(H_2O)_4$ cluster at large R values is a consequence of the artificial confinement (due to the lack of very diffuse functions in the basis set) of the orbital occupied by the excess electron, which, in turn, causes the kinetic energy contribution to be too high. For R values ranging from 2.5 to about 5.5 Å, all of the methods that include correlation corrections bind the excess electron when employing the aug-cc-pVTZ basis set. However, this binding is fortuitous as it is a consequence of the unrealistically large correlation contributions to the EBE that result from the artificial confinement of the singly occupied orbital in the vicinity of the water monomers. Thus, it is not surprising that the R dependence of the binding energy is not properly reproduced in the calculations with the aug-cc-pVTZ basis set. In fact, none of the methods considered give a bound anion for $R >$ 5.5 Å, in contrast to the calculations carried out with the aug-cc-pVDZ+7s7p basis set.

The most important take-away message from the calculations on the NVCB anion of the $(H_2O)_4$ cluster model is that in order to properly describe this system, it is essential to employ a theoretical method that adequately accounts for the coupling of orbital relaxation and dispersion-like correlation effects and to use a basis set that includes s and p basis functions considerably more diffuse than those in the standard aug-cc-pVXZ basis sets. The fact that the EBEs from the OO-MP2 calculations are nearly identical to those from the EOM-CCSDT calculations indicates that for this cluster, even a second-order treatment of the dispersion-like correlation effects suffices for describing the NVCB anion, provided that orbitals optimized in the presence of these correlation effects are employed. In the case of the ADC(2) method, this relaxation is accomplished through the off-diagonal terms

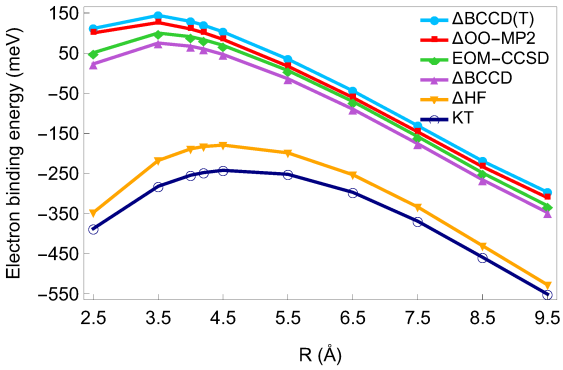

Figure 2.4: EBE of $(H_2O)_4$ calculated using various theoretical methods in conjunction with the aug-cc-pVTZ basis set. The ΔMP2 and ΔCCSD curves, not depicted, essentially overlap with the ΔBCCD curve. Also, the ΔCCSD(T) and EOM-CCSD(T)(a)* curves, not depicted, essentially overlap with the ΔBCCD(T) curve, and the EOM-MP2 curve, not depicted, essentially overlaps with that from the EOM-CCSD calculations.

in the self-energy. When the off-diagonal coupling is neglected, the EBE from the ADC(2) calculations using the aug-cc-pVDZ+7s7p basis set goes to zero with decreasing R even more rapidly than the MP2 value of the EBE, and the diagonal ADC(2) method fails to bind the excess electron for R values less than 4.2 Å. The non-self-consistent G_0W_0 method, which also neglects off-diagonal self-energy terms, is found to give results similar to those obtained using the diagonal ADC(2) method. The EBEs obtained with the ADC(2), diagonal-ADC(2), and G_0W_0 methods are compared with the corresponding EOM-CCSDT results in Figure 2.5.

The success of the BCCD(T) method, in contrast to the CCSD(T) method for R values for which the HF method does not bind the excess electron, is particularly noteworthy. Because a Slater determinant of Brueckner orbitals is that with the maximum overlap with the true wave function, the Brueckner procedure results in a singly occupied orbital for the anion with a charge distribution close to that of the SONO from the EOM calculations. Figure 2.6 compares the EBEs obtained using the difference of the energy of the anion and the neutral cluster both calculated using Slater determinants of Brueckner orbitals (and here referred to as ΔSD-BO) with the corresponding ΔHF results. For large R, the ΔSD-BO

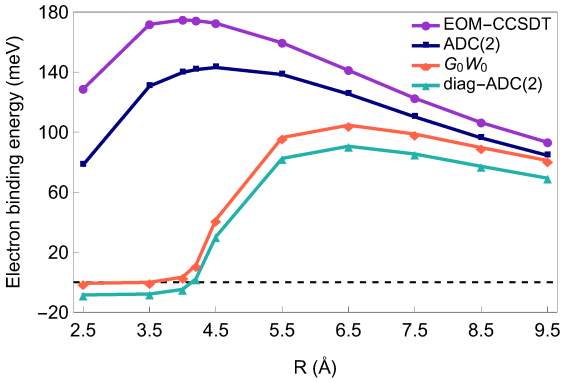

Figure 2.5: EBE of the NVCB anion of $(H_2O)_4$ for different R values calculated using the ADC(2), diagonal-ADC(2), and G_0W_0 methods.

calculations bind the excess electron albeit less strongly than the ΔHF method, but for R values $\lesssim 6$ Å, they give a negative EBE. At $R = 2.5$ Å, the shortest distance considered, the anion is predicted to be unbound by 220 meV in the ΔSD-BO method. These results are consistent with the singly occupied orbital from the BCCD calculations on the anion being slightly more localized than the HF LUMO at large R and with the former becoming more localized and the latter more delocalized as R decreases. We also see from Figure 2.6 that the difference between the ΔBCCD(T) and ΔSD-BO values of the binding energy grows in magnitude from 69 meV at $R = 9.5$ Å to 350 meV at $R = 2.5$ Å,consistent with the growing importance of the correlation contribution to the EBE as R decreases.

We also applied the self-consistent polarization model of Ref. 49 to calculate the electron binding energy of the $(H_2O)_4$ cluster at $R = 4.2$ Å. With the model potential approach, the net EBE can be decomposed into kinetic energy, electrostatics, repulsion, and polarization contributions, where the kinetic energy contribution results from localization of the excess electron, the electrostatics contribution results from the interaction of the electron with the three point charges employed on each water monomer, the repulsion contribution results from the pseudopotential used to prevent overattraction to the positively charged H atoms and to effectively account for charge penetration and exchange effects, and the polarization contribution describes the correlation effects between the excess electron and the valence

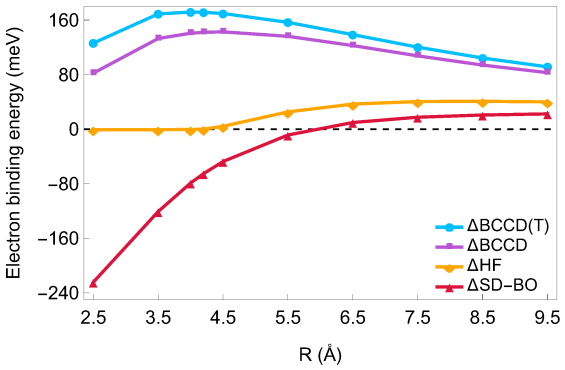

Figure 2.6: EBE of the NVCB anion of $(H_2O)_4$ calculated with the ΔHF, ΔSD-BO, and ΔBCCD methods. All results are obtained using the aug-cc-pVDZ+7s7p basis set.

electrons. The results of the energy decomposition are summarized in Table 2.1. At $R = 4.2$ Å, the model potential gives an electrostatic contribution to the binding energy of 709 meV. However, the sum of the kinetic energy and repulsive contributions is even greater in magnitude, with the sum of these three contributions being −104 meV, roughly comparable to the ΔSD-BO value of the EBE at $R = 4.2$ Å. The polarization contribution to the EBE is 312 meV, giving a net binding of 208 meV, which is in close agreement with the EOM-CCSDT and ΔBCCD(T) results.

Table 2.1: Contributions to the EBE of the NVCB anion of the $(H_2O)_4$ model at $R = 4.2$ Å.

Contribution	Energy (meV)
Electrostatic	709
Kinetic energy	−655
Repulsion	−157
Polarization	302
Total EBE	208

It is important to note that both the BCCD(T) and polarization potential approaches use orbitals that have been optimized in the presence of correlation effects. It is more traditional to define correlation corrections with reference to the HF energy, in which orbitals are calculated using orbitals determined in the absence of correlation effects. However, for

NVCB anions, the HF wave function collapses onto a discretized continuum solution, and we believe it is more instructive to perform the energy decomposition using orbitals optimized in the presence of correlation effects.

2.5 CO_2: Valence-Bound to Correlation-Bound Anion

As our second test case, we consider the bending potential of the ground state anion of CO_2. It is known from electron scattering measurements that vertical electron capture into the valence π^* orbital of CO_2 results in a temporary anion located energetically about 3.7 eV above the neutral molecule.[53] It is also known that CO_2^- has a valence-like $^2A_1$ anion state with a minimum energy structure with an OCO angle of about 138° at which it lies energetically about 1.5 eV below the neutral molecule at the same geometry and about 0.5 eV above the neutral molecule at its minimum energy linear structure.[54–57] The temporary anion of CO_2^- formed by vertical electron capture splits into $^2B_1$ and $^2A_1$ components as the molecule is bent, and, in the standard textbook explanation, the $^2A_1$ component of the π^* temporary anion state correlates with the bound valence-type $^2A_1$ anion state with OCO angle $\sim$ 138°.[54–57] In this picture, the bending potential of the lowest energy anion state of CO_2^- would be expected to be similar to that of the isoelectronic $^2A_1$ state of NO_2. However, theoretical studies of Vanrose and co-workers,[58] Sommerfeld,[54] and Sommerfeld et al.[57] have shown that this textbook picture of CO_2 is not correct. In particular, as shown by Sommerfeld, EOM-CCSD calculations employing a large basis set with several sets of diffuse functions predict that as the OCO angle increases from ∼138°, the potential energy curve of the anion first rises slightly in energy, having a maximum near 150°, and then descends in energy, approaching the potential energy curve of the neutral molecule, ceasing to be bound near an OCO angle of 154°. Moreover, as the potential energy curve of the anion approaches that of the neutral, the wave function of the anion becomes much more diffuse than that associated with a typical valence state.

In Sommerfeld's study of CO_2^-, the CCSD(T), EOM-CCSD, ADC(2), and ADC(3)[59] methods were considered. In the present investigation, we extend this work to examine

also the performance of the OO-MP2, EOM-CCSD(T)(a)*, EOM-CCSDT, and BCCD(T) methods for this challenging system. We employ an ANOTZ+3s3p basis set formed by augmenting the ANOTZ basis set[60] on each atom with three diffuse s and three diffuse p functions, the exponents of which were taken from Ref. 54. The CO distance is allowed to vary with the OCO angle, as was done in Ref. 54. In particular, CO_2^- in its bent structure and CO_2 in its linear structure were optimized using the CCSD method, and a linear interpolation of these two geometries was used to determine the CO distances at other values of the OCO angle.

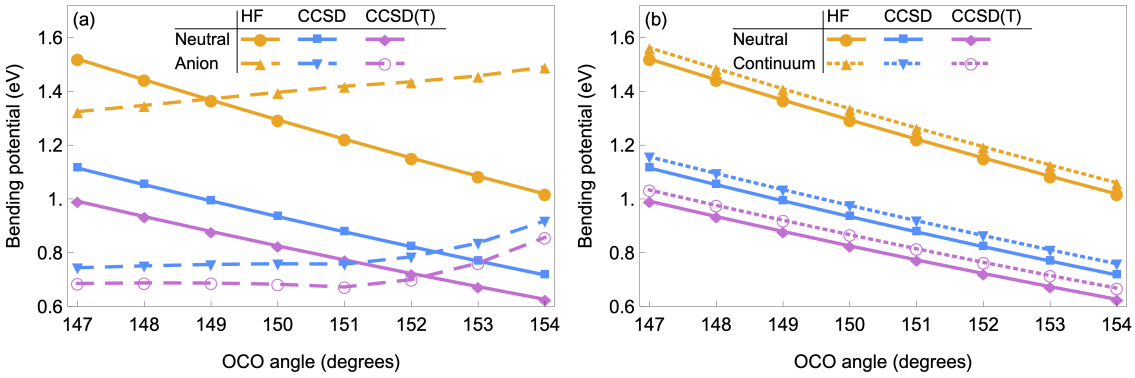

Figure 2.7: Bending potentials of CO_2 and CO_2^- for values of the OCO angle between 147° and 154°. Over this range of angles, two different HF solutions are obtained for CO_2^-: one valence-like and the other corresponding to the neutral molecule plus the excess electron in a discretized continuum orbital. The HF, CCSD, and CCSD(T) potentials for the valence-like anion are reported in (a), and the corresponding results for the discretized continuum solution are reported in (b). In both cases, the bending potential energy curves of the neutral molecule are also reported. The zero of energy is taken to be that of the linear neutral molecule.

In our calculations on CO_2^-, we discovered that for OCO angles between 147° and 154°, it was possible to obtain two different HF solutions: one corresponds to the valence state and the other to the neutral molecule plus an electron in a discretized continuum orbital. One HF solution was obtained by using orbitals from calculations at smaller angles as the initial guess for calculations at larger angles, and the other by using orbitals from calculations at

larger OCO angles as the initial guess for the calculations at smaller angles. Figure 2.7(a) depicts for the 147°–154° range of angles the anion potentials obtained using the valence-like HF orbitals, while Figure 2.7(b) shows the corresponding potentials obtained using orbitals from the HF solution that collapsed onto the discretized continuum. The potential for the neutral molecule calculated using the various theoretical methods is also reported. From Figure 2.7(a) it is seen that the HF solution that corresponds to the valence state rises in energy with increasing bending angle up to 154° (beyond that it collapses onto the neutral plus discretized continuum orbital). By contrast, the HF potential corresponding to the discretized continuum solution is essentially parallel to the potential for the neutral, lying about 0.04 eV above it. (The reason it lies slightly above the neutral in energy rather than on top of it is a consequence of the basis set employing only three sets of supplemental diffuse functions on each atom.)

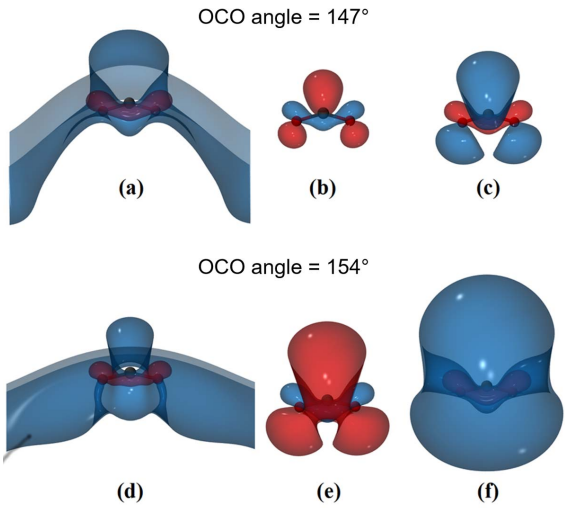

Figure 2.8: Plots of the singly occupied orbital from HF calculations and of the singly occupied natural orbital from EOM-MP2 calculations on CO_2^-. (a) and (d) depict the discretized continuum orbital at 147° and 154°, respectively; (b) and (e) depict the valence-type HF orbital at those angles; and (c) and (f) report the SONOs from the EOM calculations at the two angles.

The singly occupied orbital for the two HF solutions of the anion at OCO angles of 147° and 154° is shown in Figure 2.8 as is the SONO from the EOM-MP2 calculations. The

valence-type HOMO of the anion becomes more extended as the OCO angle increases from 147° to 154°, but the increase is relatively modest. Interestingly, the SONO from the EOM calculations is somewhat more extended than the HOMO from the HF calculations on the valence-type state, and it grows in extent with the increase in the OCO angle from 147° to 154° more than the HF HOMO. Over the 147°–154° range, the bending potentials of CO_2^- obtained from the two sets of CCSD calculations are fundamentally different. In particular, over this range of angles, the CCSD calculations starting from the valence-like HF orbitals do not collapse onto the "continuum" solution even when the continuum solution lies lower in energy and the CCSD calculations starting from the "collapsed" HF wave function do not give the valence-like solution even when the valence-like solution lies lower in energy. In other words, there is a range of angles for which the single excitations in the CCSD wave function are not sufficient for overcoming the limitations of the HF starting point.

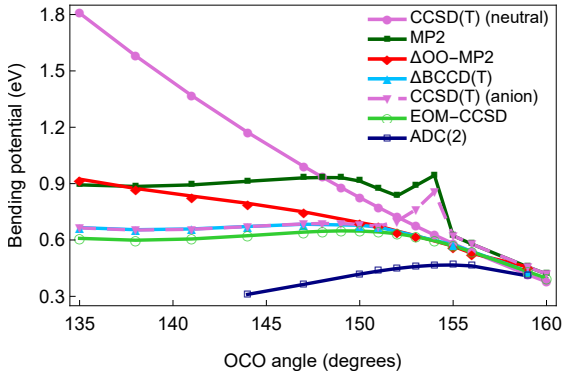

Figure 2.9: Potential energy curves of CO_2 and CO_2^-. The potential energy curve for the neutral molecule was calculated using the CCSD(T) method, and those for anion were generated by adding, at each geometry considered, the negative of the EBE calculated at that level of theory to the CCSD(T) energy of the neutral molecule. The zero of energy was taken to correspond to the neutral molecule with 180° OCO angle. The CO bond lengths were generated as described in the text. All calculations were performed using the ANOTZ+3s3p basis set. For the MP2 and CCSD(T) calculations on the anion, the valence-type HF solution was used as the reference for angles up to 154°.

Figure 2.9 reports the calculated bending potentials of CO_2 and CO_2^- for the entire range of angles considered. The bending potential for the neutral CO_2 molecule was generated at the CCSD(T) level of theory, and for the anion, results are reported for the MP2, CCSD(T), EOM-CCSD, ADC(2), OO-MP2, and BCCD(T) methods, with the anion potentials being generated by subtracting the EBE calculated with each method from the CCSD(T) value of the energy of the neutral at the same geometry. (Results obtained using higher-order EOM methods will be presented below.) In the case of the MP2 and CCSD(T) calculations, the results shown are based on orbitals from the valence-like HF solution. The EOM-CCSD and BCCD(T) methods give similar bending potentials for the anion. In both cases, the anion bending potential is very flat over the 135°–148° range, with a small barrier near 150°, and then descends slightly in energy, intercepting the neutral potential near an OCO angle of 156°. The bending potentials of CO_2^- from the CCSD and CCSD(T) calculations based on the HF valence-type wave function for the anion agree closely with those from the EOM-CCSD and BCCD(T) calculations up to an angle of about 151° but then rise in energy rather than descending as found in the EOM-CCSD and BCCD(T) calculations as the OCO angle is further increased, collapsing onto the neutral plus continuum for angles greater than ∼154°. The MP2 potential, on the other hand, lies about 0.3 eV above the EOM-CCSD potential for the whole range of angles for which the former is bound.

We note that for OCO angles greater than about 154°, the CCSD(T) potential reported by Sommerfeld[54] descends in energy rather than rising as found in the present study. This difference in behavior is due to the different basis sets used in the two studies: whereas Sommerfeld started with a valence-type basis set of Dunning[61] contracted to 5s3p1d, the more flexible augmented ANOTZ basis set contracted to 5s4p3d2f was used in this work.

The OO-MP2 potential starts out about 0.3 eV too high in energy at an OCO angle of 135° and "rapidly" descends in energy crossing the neutral potential at essentially the same angle as that found with the EOM-CCSD and BCCD(T) methods. The ADC(2) bending potential lies too low in energy at all angles and crosses the neutral potential near an OCO angle of 159°. Although the MP2, OO-MP2, and ADC(2) methods all fail to adequately describe correlation effects important for the binding of the excess electron to CO_2 at angles for which the anion is bound, the latter two methods do predict a rapid energy descent as

the anion potential approaches that of the neutral. This is a consequence of their including orbital relaxation in response to correlation effects. The theoretical characterization of CO_2^- is complicated by the fact that the anion has significant multiconfigurational character at small OCO angles where the anion is valence-like and by the rapid growth of non-valence character as the anion potential approaches that of the neutral. The former is primarily responsible for the inadequacy of the MP2, OO-MP2, and ADC(2) methods for describing the bending potential of the anion at small OCO angles.

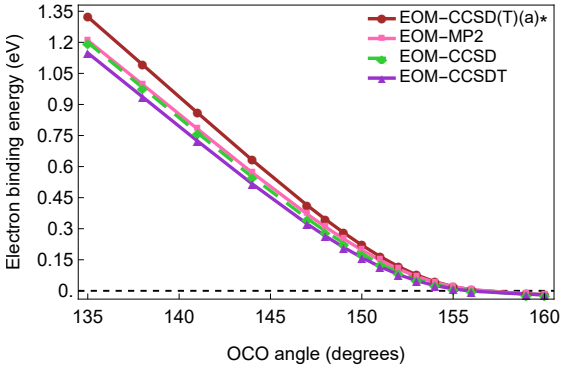

Figure 2.10: Electron binding energy of CO_2^- calculated using various EOM methods as a function of a predominantly bending coordinate. The calculations were carried out using the ANOTZ+3s3p basis set.

Figure 2.10 reports as a function of the bending angle the EBE of CO_2 calculated using the EOM-MP2, EOM-CCSD(T)(a)*, and EOM-CCSDT methods as well the EOM-CCSD method, already considered above. It is seen from this figure that for OCO angles between 135° and 154°, the EOM-MP2, EOM-CCSD and EOM-CCSDT methods give essentially the same EBE values, while the EOM-CCSD(T)(a)* method slightly overbinds the excess electron for small values of the OCO angle.

The results presented above indicate that there is a fundamental difference in the nature of the $(H_2O)_4$ and CO_2 anions near the crossing points of the anion and neutral potential energy surfaces. In the case of the (H2O)4 cluster, the singly occupied orbital of the HF wave function of the anion rapidly expands in radial extent as the crossing point is approached from the large R side. By contrast, for CO_2, two different HF solutions can be found for

OCO angles ranging from 147° to 154°. One of these is valence-like and the other corresponds to the neutral molecule plus an excess electron in an approximate continuum orbital. The HF bending potential of the valence-like anion state crosses the potential of the neutral near an OCO angle of 149° and continues to rise up to an angle of about 154°, after which it collapses to the lower-energy "continuum solution." Most importantly, the wave function of the valence-like HF solution for CO_2^- undergoes only a moderate growth in its extent as the crossing point is approached (from the bound state side). Moreover, while the SONO from the EOM calculations on $(H_2O)_4^-$ does not change significantly in its extent as R passes through the HF crossing point, the SONO from the EOM calculations on CO_2^- (shown in Figure 2.8) evolves from being relatively compact (valence-like) at an OCO angle of 135°, to being much more extended for values of the OCO angle greater than 149°. For the $(H_2O)_4$ model system, the anion evolves from being largely electrostatically bound at large separation between the two $(H_2O)_2$ dimers to being correlation bound at short separation between the dimers, with correlation effects causing the anion wave function to contract at R values where the anion is only weakly bound in the HF approximation. By contrast, the CO_2^- ion evolves from being valence-like for values of the OCO near 135°, but with correlation effects being responsible for the more diffuse character of the anion function near the crossing point of the anion and neutral bending potentials.

The change in the charge distribution of the CO_2^- with bending angle appears to result from an avoided crossing between the valence-like state and a non-valence anion state. Three candidates for the non-valence state (or states) can be envisioned: (1) a NVCB anion, which, over a range of OCO angles near 149° and in the absence of mixing with the valence state, would lie slightly below the neutral in energy; (2) a virtual state,[58,62] and (3) the manifold of continuum levels. We note that an avoided crossing between valence states and a NVCB anion state has been demonstrated in a theoretical study of $C_6F_6^-$.[8] NVCB anion states and virtual states are closely related in that a virtual state turns into a NVCB anion state if the potential experienced by the electron is made slightly more attractive. With respect to the possibility of a NVCB anion of CO_2, we note that for an OCO angle of 149°, the calculated (HF level) dipole moment and average dipole polarizability of the neutral molecule are 1.05

D and 14.3 a.u.,[20] respectively. Based on our experience with a wide range of NVCB anions, we would not expect a molecule with a polarizability this small, even with a dipole moment of 1.05 D, to support a NVCB anion in which long-range dispersion interactions are primarily responsible for the binding of the excess electron. Rather, we favor the third possibility, namely, that near OCO angles of 149°, the bound anion state from strong mixing of the valence state and the continuum. We suggest, therefore, that it may be useful to broaden the definition of NVCB anions to include such species.

Although our focus in this section has been on the performance of various theoretical methods for describing the anion of CO_2 near the crossing point of the anion and neutral bending potentials, it is interesting to reflect on the implications of the current results for the interpretation of experiment. In this context, we note that CO_2^- has been observed mass spectroscopically upon collision of high energy alkali atoms with CO_2.[63] This study gave, for CO_2, an adiabatic electron affinity of -0.60 ± 0.2 eV, which is consistent with the results of the present EOM and coupled cluster calculations. However, there is the issue that the calculated bending potential has only a very small ($\sim$0.036 eV or 290 cm^{-1}) barrier before it bends downward near an OCO angle of $\sim$150°, and with such a small barrier, the bent valence-type anion would be expected to autoionize in a short time compared to the experiment if the zero-point level were above or near the top of the barrier. We have calculated, using the Gaussian 09 program,[64] anharmonic vibrational frequencies of bent CO_2^- using the second-order vibrational perturbation theory (VPT2)[65] approach with the MP2 electronic structure method in conjunction with the ANOTZ+3s3p basis set. These calculations give an anharmonic frequency of 600 cm^{-1} for the bending vibration, which places the zero-point vibrational level slightly above the barrier. However, we note that the bending potential of CO_2^- is very flat, and it is likely that the VPT2 calculations considerably overestimate the value of the frequency of the bending mode, and it seems highly likely that the zero-point level is below the barrier.

2.6 Non-Valence Correlation-Bound Anion of TCNE

In the two examples considered above, there are no valence anion states energetically below the NVCB anion state. However, as we demonstrated for C_{60}, molecules with bound, valence anion states can also possess NVCB anion states.[6] Accurately describing the NVCB anion states of such systems can be especially challenging since high-order correlation effects can be important. To illustrate this, we consider TCNE which has a valence anion state bound by 3.2 eV[66] as well as several low-lying valence-like temporary anion states.[67] Calculations to search for a possible ^2A_g NVCB anion of TCNE were performed using the aug-cc-pVDZ and aug-cc-pVTZ basis sets augmented with 3s, 3s3p, and 3s3p3d sets of supplemental diffuse functions centered at the midpoint of the central CC bond. The calculations indicate that TCNE does have a NVCB anion, with the EBEs obtained using the various theoretical methods summarized in Table 2.2. The SONO from the EOM-MP2/aug-cc-pvDZ+7s7p calculations on the ^2A_g NVCB anion state of TCNE is depicted in Figure 2.11.

Table 2.2: Contributions to $\Delta\langle T\rangle$ and $\Delta\langle V\rangle$ for a H atom perturbed by a point charge or a uniform efield evaluated in the complete basis set limit.

	AVDZ+3s	AVDZ+3s3p	AVDZ+3s3p3d	AVTZ+3s3p
EOM-MP2	82	87	94	130
EOM-CCSD	67	71	79	104
EOM-CCSD(T)(a)*	56	63	69	100
BCCD	−8	−4		
BCCD(T)	59	63		
OO-MP2		176 [b]		
ADC(2)		293 [b]		

[a] The calculations were carried out at the MP2/cc-pVTZ optimized geometry of the neutral molecule.

[b] These results were obtained using the aug-cc-pVDZ basis set supplemented with a 7s7p set of diffuse functions. EOM calculations with the aug-cc-pVDZ+3s3p aug-cc-pVDZ+7s7p basis sets give nearly the same EBE values.

For each basis set considered, the EOM-CCSD(T)(a)* and EOM-CCSD values of the EBE are in close agreement, and in the assessment of the performance of the various approaches, the results of the EOM-CCSD(T)(a)* calculations will be used as the benchmark

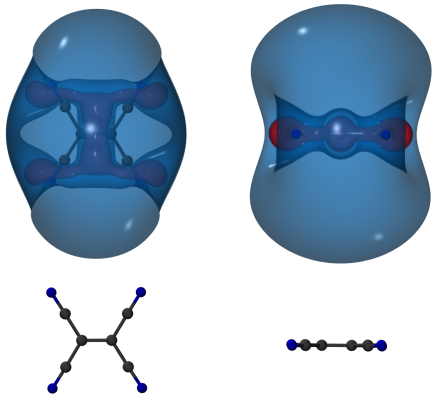

Figure 2.11: The SONO of the non-valence correlation-bound anion of TCNE from EOM-MP2 calculations using the aug-cc-pVDZ+7s7p basis set. The isosurfaces enclose 70% of the excess electron charge. Two different orientations are shown.

reference. The EOM-CCSD(T)(a)* EBEs obtained with the aug-cc-pvDZ+3s3p and aug-cc-pvTZ+3s3p basis sets are 63 and 101 meV, respectively. The BCCD(T) calculations give EBE values for the NVCB anion of TCNE very close to the corresponding EOM-CCSD(T)(a)* results when the same basis set is employed for the two methods. By contrast, the EOM-MP2 OO-MP2 and ADC(2) methods all give EBE values much larger than the EOM-CCSD(T)(a)* values, with the EOM-MP2 method overestimating the EBE by 20%-30% and the OO-MP2 and ADC(2) methods by factors of 2.7 and 4.7, respectively. These results indicate that the inclusion of high-order correlation effects is essential for obtaining an accurate estimate of the EBE of the NVCB anion of TCNE. We have calculated the dipole polarizability of TCNE using the Perdew-Burke-Ernzerhof (PBE) density functional method[68] in conjunction with the aug-cc-pVTZ basis set. The resulting average polarizabilities in the uncoupled and coupled Kohn-Sham approximations are 229 and 99 a.u.,[20] respectively. The large reduction of the polarizability due to the coupling of excitations is consistent with screening effects playing an important role in the interaction of the excess electron with TCNE, which, in turn, could explain the large overestimation of the EBE as calculated with the OO-MP2 and ADC(2) methods.

One surprising result of our calculations on the NVCB anion of TCNE is that the mid-bond supplemental diffuse p functions play a negligible role in the electron binding. This indicates that the excitations of the excess electron contributing to the dispersion interaction between it and the valence electrons of the molecule are dominated by excitations into virtual orbitals with a large component of the diffuse aug-functions in the basis sets.

As TCNE supports both a valence-bound ($^2B_{3g}$) anion and a NVCB (^2A_g) anion, it provides an opportunity for a direct comparison of the properties of these two types of anion states. We note that EOM-CCSD/aug-cc-pVDZ+3s3p3d calculations predict the valence-type anion to be bound by 2.91 eV, as compared to the 79 meV EBE for the NVCB anion. For both states, the natural orbital occupied by the excess electron has an occupation number close to 0.985. (All other natural orbitals have occupation numbers greater than 1.9 or less than 0.1). Figure 2.12 reports the densities of these natural orbitals as a function of $r_{nearest}$ which is defined as

$$r_{nearest}(\vec{r}) \stackrel{\text{def}}{=} \min_{\alpha}(|\vec{r} - \vec{R}_\alpha|) \tag{2.1}$$

where $\vec{r}$ is the position of the excess electron and $\vec{R}_\alpha$ is the position of nucleus α. The corresponding expectation value $\langle r_{nearest} \rangle$ provides a measure of the extent of the orbital.[27]

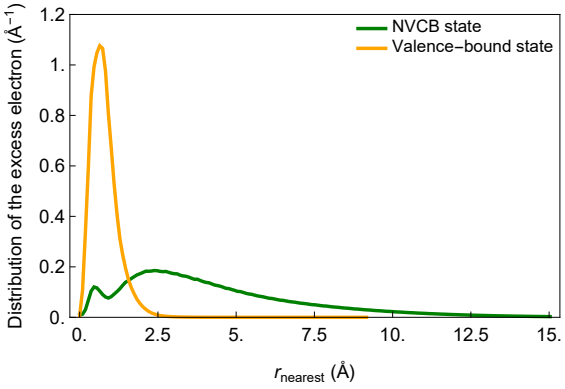

Figure 2.12: Distribution of the excess electron of the non-valence $^2B_{3g}$ (orange) anion state and of the NVCB ^2A_g (green) anion state of TCNE. The two electron density distributions are plotted as functions of $r_{nearest}$.

The densities of the EOM-CCSD natural orbitals associated with the excess electron of the ground state valence-bound anion and of the NVCB anion of TCNE are shown in

Figure 2.12, and, as expected, the difference is striking. In the valence-bound state, the excess electron is localized close to the molecular framework, with the maximum of the density distribution function occurring at 0.70 Å and $\langle r_{nearest} \rangle$ being only slightly larger at 0.83 Å. By contrast, the excess electron of the NVCB state extends much further out and shows a broad distribution with a long-range tail. The maximum of its distribution occurs at 2.4 Å, while unction occurring at 0.70 Å and is 4.4 Å, emphasizing the smeared-out character of a NVCB electron.

2.7 Conclusions

In contrast to valence and dipole-bound anions, non-valence correlation bound anions have been much less studied. Theoretical studies from our group and others have predicted the existence of NVCB anions for several clusters and molecules.[6–8,24,25,49,69] The picture that has emerged from the theoretical studies is that any system for which the electrostatics are not sufficiently attractive to give electron binding but which has a sufficiently high polarizability will possess one or more NVCB anion states. Although there is a paucity of experimental data on NVCB anions of gas-phase molecules and clusters, we note that NVCB anions are the finite system analogs of image potential states of metallic and graphitic surfaces, which have been characterized experimentally and theoretically.[70–72] In both the finite and extended systems, the binding of the excess electron results from long-range dispersion interactions between the excess electron and the other electrons of the system.

Theoretical characterization of NVCB anions requires the use of methods that allow for orbital relaxation effects in response to the dispersion-like correlation effects. We have demonstrated that equation-of-motion coupled cluster and algebraic diagrammatic Green's function direct methods and also the orbital-optimized MP2 and Brueckner coupled cluster delta methods are all able to treat such anion states. However, depending on the nature of the neutral molecule or cluster, lower-order methods such as OO-MP2, ADC(2), and even EOM-MP2 may have significant errors in the EBEs. The need to include higher-order correlation effects is especially important when considering NVCB anions of systems

with small HOMO/LUMO gaps and/or for which screening effects are important. This is evident from the results presented here for the NVCB anion of TCNE and from the previously reported results for the NVCB anion of C_{60}. While methods such as BCCD(T) and EOM-CCSD, particularly when used with the large, flexible basis sets required for adequate characterization of NVCB anions, are computationally prohibitive for large molecules and clusters, it is possible to design one-electron models that can accurately describe these species at low computational cost.[49,69,73]

2.8 Acknowledgments

K.D.J. acknowledges support from NSF Grant No. CHE1362334, and T.S. acknowledges support from NSF Grant No. CHE1565495. The calculations were carried out on computers in the University of Pittsburgh's Center for Research Computing. We thank Professor D. Sherrill for helpful discussions concerning orbital optimized methods and Professor John Stanton for helpful discussions about EOM-CCSD(T)(a)* calculations.

3.0 Prediction of a Non-Valence Temporary Anion Shape Resonance for a Model $(H_2O)_4$ System

The text and figures in this chapter have been reprinted with permission from Kairalapova, A.; Jordan, K. D.; Maienshein, D. N.; Fair, M. C.; Falcetta, M. F. Prediction of a Non-valence Temporary Anion Shape Resonance for a Model $(H_2O)_4$ System. *J. Phys. Chem. A* **2019**, *123*, 2719–2726, DOI: 10.1021/acs.jpca.8b11881. The author's contribution to the work included performing DC and EOM-CCSD calculations, generating figures, and editing/revising the manuscript.

3.1 Summary

Ab initio calculations are used to demonstrate the existence of a nonvalence temporary anion shape resonance for a model $(H_2O)_4$ cluster system with no net dipole moment. The cluster is composed of two water dimers, the distance between which is varied. Each dimer possesses a weakly bound nonvalence anion state. For large separations of the dimer subunits, there are two bound nonvalence anion states (of A_g and B_{2u} symmetry) corresponding to the symmetric and asymmetric combinations of the nonvalence anion states of the two dimer subunits. As the separation between the dimer subunits is decreased, the B_{2u} anion increases in energy and becomes a temporary anion shape resonance. The real part of the resonance energy is determined as a function of the distance between the dimers and is found to increase monotonically from just above threshold to 28 meV for the range of geometries considered. Over this same range of geometries, the resonance half-width varies from 0 to 21 meV. The B_{2u} anion, both when bound and when temporary, has a very diffuse charge distribution. The effective radial potential for the interaction of the excess electron with the cluster has a barrier at large distance arising from the electron-quadrupole interaction in combination with the repulsive angular momentum ($l = 1$) contribution. This barrier impacts both the resonance energy and its lifetime.

3.2 Introduction

Anion states formed by electron capture into normally unfilled valence orbitals are of importance in a wide range of chemical and biological processes. Less well-known in the chemistry community at large are anions that result from electron capture into diffuse nonvalence orbitals, with a combination of long-range electrostatic and correlation effects being responsible for the electron binding. The most widely studied class of nonvalence anions are dipole-bound anions in which the electrostatic attraction to the molecular dipole potential alone can bind the excess electron, although correlation effects can cause a significant increase in the electron binding energy (EBE).[1,19,74] (Here we adopt the sign convention of a positive EBE when the anion is bound, i.e., energetically below the electronic ground state of the neutral.) Recently, several examples of another class of nonvalence anions, which we refer to as nonvalence correlation-bound (NVCB) anions, have also been demonstrated.[6,8,24,25,69,75–77] For these, long-range correlation effects are essential for the binding of the excess electron. Although the excess electron in dipole-bound and NVCB anions occupies a very diffuse orbital, such anion states can be important in chemical processes, e.g., acting as doorway states for formation of valence anions.[8,76,78] Specifically, geometrical distortion can lead to mixing (via the electronic Hamiltonian) of nonvalence and valence anion states, which may be of different symmetry in the undistorted molecule.[79] Additionally, molecular anions in which the electrostatic attraction of the excess electron to the quadrupole moment plays a role in the binding of the excess electron have been investigated,[7,24,80,81] as have model systems in which the electron-quadrupole interaction makes a significant contribution to the EBE.[75,82,83] We note that there are several studies that interpret experiments in terms of "quadrupole-bound" anions.[81,84–86] However, for many of these systems (e.g., *trans*-succinonitrile[80]), the anion is not bound in the Koopmans' theorem (KT) approximation,[29] which means that the quadrupole moment alone is not large enough to bind the excess electron. Rather, it is the combination of electron correlation effects and the electrostatic potential associated with the quadrupole moment that gives rise to the electron binding. We believe that such anions are better classified as NVCB. In the case of CS_2, which has been proposed to have a quadrupole-bound anion,[84] it appears that the state involved is actually valence-like.[87]

In addition to bound anions, atoms and molecules can possess anion states that lie energetically above the ground state of the neutral species. These anions are termed temporary as they are subject to decay by electron autodetachment, and they appear as resonances in electron scattering cross sections.[13,88] Temporary anions (TAs) are involved in a range of processes including chemical bond breaking and vibrational and electronic excitation. Generally, low-energy TAs are associated with electron capture into unfilled valence orbitals, with the trapping mechanism being due to an angular momentum barrier in the effective radial potential.[13,88] TAs are also referred to as shape resonances because the trapping is due to the shape of the electron-atom or electron-molecule potential. Another type of TA involves trapping of an excess electron in the potential of an electronically excited state,[13] but these will not be considered further here.

In the present study, we examine the possibility of the existence of nonvalence correlation-assisted TA shape resonances for a cluster with no dipole moment but with a sizable quadrupole moment. We use the label "correlation-assisted" to indicate that electron correlation effects play a major role in establishing the energy and lifetime of the anion. In our search for a nonvalence TA, we consider a model $(H_2O)_4$ system that, for a range of geometries, possesses a NVCB anion with a p-like, i.e., $l = 1$, leading partial wave but that can be distorted to geometries for which this anion is "pushed" into the continuum of the neutral species plus a free electron. We note that nonvalence TA resonances have been reported for molecules with sizable dipole moments.[89–91]

3.3 $(H_2O)_4$ Model System and Computational Details

The $(H_2O)_4$ cluster model, which was employed in our earlier study of NVCB anions,[75] is shown in Figure 3.1. By design, the monomers in this model are arranged so that there is no net dipole and the leading permanent moment is a quadrupole. The absence of a dipole is essential for the existence of a low-energy resonance with a leading $l = 1$ partial wave. Although this arrangement of monomers would not be observed experimentally, our earlier work demonstrated that this is a useful model for exploring the interplay of electrostatics and

electron correlation in nonvalence anion states. In the present study, we fix the distance R and vary the distance R' defined in Figure 3.1. Thus, we are varying the separation between two water dimers (albeit with geometrical structures far from equilibrium). The individual dimers have a dipole moment of 2.1 D (MP2[31] level with the aug-cc-pVTZ[50,51] Gaussian-type orbital basis set). As a result, in isolation and assuming the validity of the Born-Oppenheimer approximation, each dimer subunit has a dipole-bound anion. In the KT approximation, the EBE is approximated by the negative of the energy of the appropriate virtual orbital from a Hartree-Fock (HF) calculation on the neutral species (although care has to be exercised when applying the KT approximation to unbound virtual orbitals). In the KT approximation, the dimer is calculated to have a miniscule EBE of 0.9 meV. There is only a small increase of the EBE to 1.0 meV when allowing for relaxation effects by calculating the difference in the HF energies of the anion and neutral (the so-called ΔSCF approximation). Thus, at large R' values, the $(H_2O)_4$ cluster model has two, nearly degenerate, bound anion states, one of A_g and the other of B_{2u} symmetry, resulting from the symmetric and asymmetric linear combinations of the bound states of the two dimer subunits in the tetramer. At the KT level, these become unbound for R' values less than about 40 Å (A_g) and 70 Å (B_{2u}). Similar crossing points are found in the ΔSCF approximation. However, we know from our earlier study of this model system that inclusion of electron correlation effects leads to a large increase in the EBE of the A_g anion state, in fact, resulting in a stable anion even at geometries at which the HF method fails to bind the excess electron. We anticipate, therefore, that inclusion of correlation effects will prove important in determining whether the B_{2u} anion is bound or metastable at different R' values.

In order to include electron correlation effects in the calculation of the energies of the A_g and B_{2u} nonvalence anion states of the $(H_2O)_4$ model as a function of R', we use the electron attachment equation-of-motion coupled-cluster singles and doubles (EOM-CCSD) method[34] as implemented in the CFOUR program[46] together with flexible Gaussian-type orbital (GTO) basis sets and the frozen core approximation. The EOM-CCSD method has been found to provide accurate characterization of both valence and nonvalence bound anion states as well as of valence-type TA states provided that sufficiently flexible basis sets are employed.[17,75,92] In the present study, we use the aug-cc-pVTZ basis set for the atoms

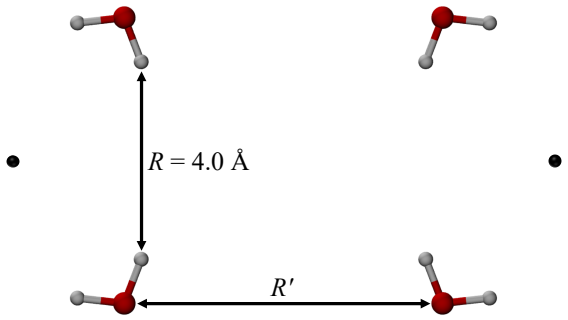

Figure 3.1: $(H_2O)_4$ cluster model. R is fixed to 4.0 Å, while R' is varied. The black dots indicate the locations of the supplemental sets of diffuse basis functions, which are located at $\pm(R'/2 + 2.27)$ in Å.

augmented with nonatom-centered sets of diffuse s (or s and p) Gaussian-type functions located on the positive dipole side of each dimer, as shown in Figure 3.1. Well-converged EBEs for the bound anions were obtained from calculations employing supplemental sets consisting of seven s or seven s plus seven p functions, with the largest exponent being 0.025 and with successive exponents reduced by a factor of 10. The location of the supplemental basis functions relative to the O atoms was determined by maximizing the EOM-CCSD value of the EBE of the A_g anion at $R' = 13.5$ Å. This optimization located the centers for the supplemental basis sets 2.27 Å farther from the origin along the R' coordinate than the oxygen atoms. In calculations at other R' values, the locations of the centers of the supplemental diffuse functions, relative to the dimers, were held fixed at this value. EOM-CCSD calculations also showed that omission of the p functions from the supplemental sets made little impact on the EBEs, and as a result, supplemental sets with only s functions were used for the majority of the calculations. For the TA, it was necessary to add two additional s functions with exponents of 0.250 and 0.079 to the supplemental sets, as will be described below. For consistency, these extra functions are retained in the calculations of the bound anion states when using supplemental sets with only s functions, although they do not make an important contribution to the EBEs. We note that in designing the basis sets for characterizing the anion states of the $(H_2O)_4$ model we first considered using only a

single set of supplemental diffuse functions located at the center of mass but found that to achieve well-converged results with such basis sets it was necessary to employ a basis as large as aug-cc-pV5Z[50,51] on the atoms and to include functions through f in the supplemental set. By using the two-center expansion for the supplemental functions described above, we were able to achieve well-converged EBEs with far fewer basis functions.

3.4 Results

For the $(H_2O)_2$ dimer with the geometry of our model, the EOM-CCSD calculations carried out using the aug-cc-pVTZ basis set plus a single 7s7p set of supplemental functions gave a binding energy of 38 meV for the A_g anion, in contrast to the 0.9 meV value obtained at the KT level of theory. The KT calculations failed to bind the excess electron with the supplemental set containing only s functions, but the EBE obtained using the EOM method was changed little upon omission of the diffuse p functions. Although the large percentage increase in the EBE of the dimer in going from the KT or ΔSCF levels of theory to the EOM-CCSD method would seem to indicate that electron correlation effects are far more important than electrostatic interactions for the binding of the excess electron, it is instructive to consider the results of one-electron model Hamiltonian[93] calculations on the dimer as this approach allows us to evaluate the various contributions to the EBE. These calculations give attractive electrostatic and polarization contributions to the EBE of 267 and 134 meV, respectively, while the repulsive kinetic energy and pseudopotential contributions are -305 and -66 meV, respectively. In interpreting these results, it is important to recognize that the polarization potential in the one-electron model Hamiltonian recovers correlation effects between the excess electron and the electrons of the cluster that are present in a many-electron treatment. Thus, analysis of the various contributions to the EBE in the model Hamiltonian calculation is based on an orbital whose binding energy and charge distribution were determined in the presence of correlation effects. This analysis reveals that when correlation effects are included the electrostatic contribution to the EBE is found to be substantial.

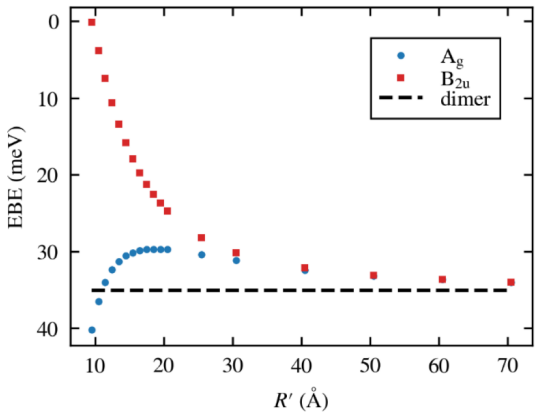

Figure 3.2: Electron binding energies of the A_g (blue dots) and B_{2u} (red squares) anion states of the $(H_2O)_4$ cluster model as a function of the distance R' separating the two dimers. The EBEs are obtained from EOM-CCSD calculations using the aug-cc-pVTZ basis set augmented with two sets of 9s GTO basis functions located at $\pm(R'/2 + 2.27)$ in Å. The horizontal dashed line indicates the EBE of the dimer subunit.

Figure 3.2 reports for R' values ranging from 9.5 to 70.0 Å the EOM-CCSD EBEs of the A_g and B_{2u} anion states of the $(H_2O)_4$ model. As expected, for large values of R', the two anion states are essentially degenerate, with EBEs being close to that of an individual dimer. The EBE of the A_g anion state decreases slightly as R' is reduced from 40.0 to about 18.5 Å due to a weakening of the electrostatic potential as R' is reduced and then increases as R' is further decreased to 9.5 Å due to a growing correlation contribution. In contrast, the EBE of the B_{2u} anion is found to decrease monotonically as R' decreases, with the anion ceasing to be bound for $R' \lesssim 9.5$ Å. However, we expect that the B_{2u} anion will continue to exist as a TA for R' values less than ~ 9.5 Å. On the basis of the analytic structure of the S matrix,[94] one also expects a virtual state at negative energy when the anion is weakly bound. (However, the virtual state cannot be identified from the stabilization/analytic continuation method that we employ.) At the R' value at which the anion just ceases to bind, the poles in the S matrix associated with the bound and virtual states coincide at zero energy. As R' is further decreased, the poles move into the complex energy plane corresponding to the resonance on the physical and unphysical energy sheets.

In order to characterize the charge distributions of the two anion states at a geometry ($R' = 13.5$ Å) at which both anions are bound, we have calculated the natural orbitals (NOs) associated with "singly occupied" orbitals of the A_g and B_{2u} anion states as described by the EOM-CCSD method. These NOs are shown in Figure 3.3, from which it is seen that both anion states are highly extended spatially and are decidedly nonvalence-like.

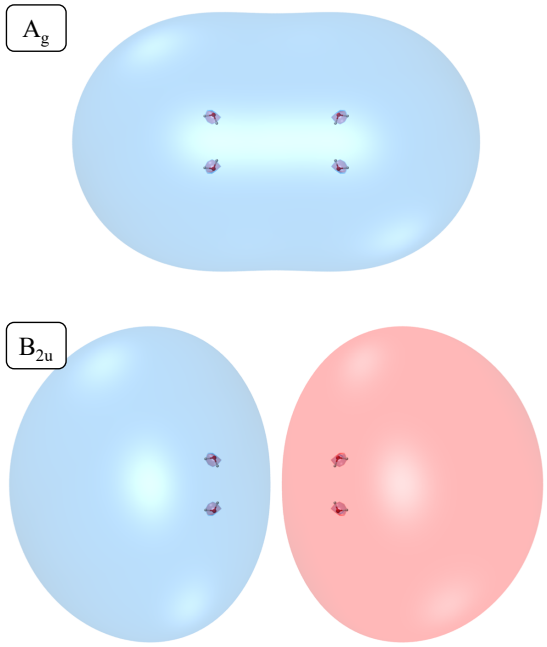

Figure 3.3: NOs associated with the excess electron of the A_g (upper) and B_{2u} (lower) anions states of the $(H_2O)_4$ cluster model at $R' = 13.5$ Å and characterized by EOM-CCSD calculations using the aug-cc-pVTZ basis set augmented with two sets of 9s functions as described in the text. The contours shown enclose 90% charge of the charge density.

In searching for a B_{2u} TA state for the $(H_2O)_4$ model with $R' \leq 9.0$ Å, we make use of the stabilization method.[15,18,95,96] The basic idea of the stabilization method is that a shape resonance can be viewed as a discrete state coupled to the continuum associated with the neutral molecule plus a free electron. In a diabatic picture, in which the coupling between the discrete state and continuum is suppressed, large basis set calculations on the excess electron system give eigenvalues corresponding to the discrete state as well as a series of discretized continuum (DC) levels. If one then scales a parameter that controls the radial extent of the

basis set, the energy of the discrete state stays nearly constant, while the energies of the DC levels drop rapidly in energy with increasing extent of the basis set. In an adiabatic picture, the discrete state and the DC states mix, leading to a series of avoided crossings as the scaling parameter is varied.

In the Siegert picture, a resonance is characterized by the complex energy, $E_r - i\Gamma/2$, where E_r is the real part of the resonance energy and Γ, the width, is the reciprocal of the lifetime in atomic units. By use of analytic continuation methods, one can use data from the avoided crossing regions of the stabilization graph (i.e., the plot of the energies vs the scale parameter) to obtain the real energies and the widths of the resonances.[18,95,96] In our application of the stabilization method to the $(H_2O)_4$ model, we use the EOM-CCSD method together with the aug-cc-pVTZ atomic basis set augmented with two sets of diffuse s functions located as described in section 3.3. A scale parameter, β, is included in the exponents of the supplemental diffuse basis functions, and to generate the stabilization graphs, β values ranging from 0.2 to 1.7 are used. The two tightest functions in the supplemental 7s set with exponents of 0.025 and 0.0079 make a sizable contribution to the anion wave functions. As a result, the use of scale factors as small as 0.2 necessitated the addition of s GTOs with exponents of 0.0790 and 0.250 to the 7s set described above.

The stabilization graphs for B_{2u} symmetry excess electron states of the $(H_2O)_4$ model at $R' = 7.96$, 6.46, and 4.46 Å are depicted in Figure 3.4. The figure also includes the energies of the DC levels calculated using Gaussian 16[97] by setting the nuclear charges equal to zero and solving for the eigenvalues of the single-electron system using the same basis set as used for the EOM-CCSD calculations. Over the energy range considered in stabilization graph for $R' = 7.96$ Å, the EOM calculations give four eigenvalues while there are only three DC levels. The appearance of an additional eigenvalue in the EOM calculations compared to the number of DC levels indicates the presence of a metastable anion state. It is also seen from this figure that the energy of the lowest eigenvalue from the EOM calculations corresponds closely to that of the lowest DC level. For small values of β, the second DC level also corresponds closely with the second eigenvalue from the EOM calculations. However, for β values larger than about 0.6, the energy of the second eigenvalue from the EOM calculations starts to level off to a value of $\sim$6 meV, while the energy of the DC level continues to increase linearly. This

indicates that for this R' value the resonance occurs near 6 meV. A similar analysis of the stabilization graph for $R' = 6.46$ Å shows that the resonance in that case occurs between 10 and 15 meV. The stabilization graph for $R' = 4.46$ Å shows a much broader crossing, with the lowest two eigenvalues from the EOM calculation closely paralleling the DC solutions and the third eigenvalue from the EOM calculation falling slightly below the DC solution for larger-scale factors. The fourth eigenvalue from the EOM calculations corresponds to the DC solution only for the smallest scale factors, with a decrease in the slope beginning at around $\beta = 0.5$. However, the energy does not plateau, as was the case for $R' = 6.46$ and 7.96 Å. Thus, for small values of R', it becomes increasingly difficult to ascertain the real part of the resonance energy by simple inspection of the stabilization graph.

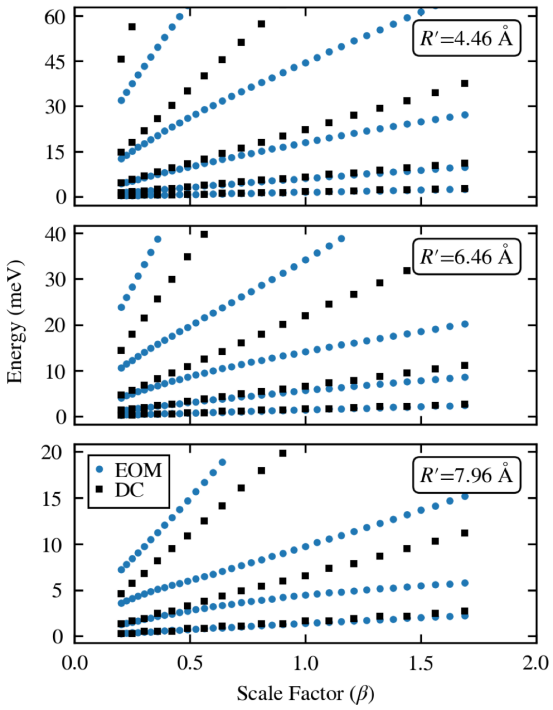

Figure 3.4: Stabilization graph for $(H_2O)_4$ with $R' = 4.46$ (top), 6.46 (middle), and 7.96 Å (bottom). The energies of the excess electron states from EOM-CCSD calculations are shown as blue dots, and the energies of the DC levels are shown as black squares.

In order to extract accurate values for the resonance position (i.e., E_r) and width, we used an analytic continuation method, originally introduced by one of the authors,[16] which, in the limit of a well-isolated avoided crossing between two eigenvalues, fits the energy to

$$PE^2 + QE + R = 0 \tag{3.1}$$

where P, Q, and R are polynomials in the scale parameter β, i.e.

$$P(\beta) = 1 + p_1\beta + p_2\beta^2 + \ldots \tag{3.2a}$$

$$Q(\beta) = q_0 + q_1\beta + q_2\beta^2 + \ldots \tag{3.2b}$$

$$R(\beta) = r_0 + r_1\beta + r_2\beta^2 + \ldots \tag{3.2c}$$

For systems with narrow resonances, i.e., with $\Gamma/2 \ll E_r$, stabilization graphs generally display well-defined avoided crossings between the diabatic discrete state and the DC solutions as the scale parameter is varied. However, when $\Gamma/2$ is not much less than E_r, the avoided crossings become less pronounced. This is the case for the stabilization graphs for the B_{2u} anion of the $(H_2O)_4$ cluster model, particularly at small R' values, necessitating a generalization of eq 3.1 to include terms of higher order in E. In this work, terms through E^5 were used in the analytic continuation for R' values less than 7 Å, while terms through E^3 or E^4 were used for larger R' values. The complex energy associated with the resonance is located by solving for the stationary point at which $dE/d\beta = 0$. The resulting complex value of β is substituted into eq 3.1 or its extension including higher powers of E to determine the real and imaginary parts of the resonance energy. The imaginary part corresponds to $-\Gamma/2$. In our application of this approach to extract resonance parameters of the B_{2u} anion, we employed fits where the polynomials were of order n minus the power of E in the prefactor. To obtain well-converged results, we found it necessary to use $n = 4$ or 5 and to use data from all of the interacting roots over the β range considered. Typically, more data points were used than parameters in combination with least-squares fitting. In addition, for each value of R', several independent analytic continuation calculations using different sets of data points were performed, each giving slightly different complex resonance energies, allowing us to assign error bars to the resulting values of E_r and Γ. In general, the uncertainties in the resonance parameters increase with growing width. For $R' = 7.96$ Å, the stabilization

calculations using energies from the EOM-CCSD calculations give resonance parameters of $E_r = 5.36\,(\pm 0.06)$ meV and $\Gamma = 2.2\,(\pm 0.1)$ meV, while at $R' = 6.46$ Å, the resonance parameters are $E_r = 11.0\,(\pm 0.3)$ meV and $\Gamma = 8.0\,(\pm 0.7)$ meV (the standard deviations from the analytic continuation procedure are given in parentheses as a measure of the uncertainty arising from that procedure but do not reflect errors arising from use of a finite basis set or incomplete recovery of electron correlation).

Valence-type TAs can usually be located by application of the stabilization method at the KT level, i.e., using virtual orbitals from Hartree-Fock calculations on the neutral molecule. This approach, sometimes referred to as the stabilized Koopmans' theory (SKT) approximation,[98] gives resonance positions and widths appreciably larger than the corresponding quantities obtained from methods such as EOM-CCSD that treat electron correlation effects in a balanced manner. Due to the importance of electron correlation effects for the EBE of the B_{2u} anion at R' values for which it is bound, we expected that it would not be possible to locate the corresponding TA in SKT calculations. In fact, at least for R' values for which the EOM-CCSD calculations give a value of Γ considerably smaller than E_r, we find that SKT calculations indicate the presence of a very broad resonance much higher in energy than that found in the EOM-CCSD calculations. For $R' = 7.96$ Å, the SKT calculations give $E_r \approx 230$ meV and $\Gamma \approx 220$ meV, as compared to the corresponding EOM-CCSD values of 5.4 and 2.2 meV. The identification of the resonance at the SKT level has implications for the trapping mechanism, which will be discussed below.

Figure 3.5 presents the real and imaginary parts of the resonance energy for values of R' ranging from 3.46 to 8.96 Å. In addition, the energy of the B_{2u} state is shown for larger R' values for which the state is bound and has a real-valued energy. The resonance is seen as a continuation of the bound state to positive attachment energies. For most R' values considered, the analytic continuation calculations using different sets of data points gave very similar values of the resonance parameters. However, for some of the R' values at which Γ is comparable to E_r, the analytic continuation calculations using different data points gave significantly different values for the stationary point and, hence, for the resonance parameters. While the averaged values of E_r and Γ from these calculations are in line with those from neighboring R' values, the large spread in the resonance parameters from the

different fits of the data leads to large standard deviations. For the smallest values of R' considered, the imaginary part is more than half of the real part of the resonance energy, which means that the resonance would extend to threshold.

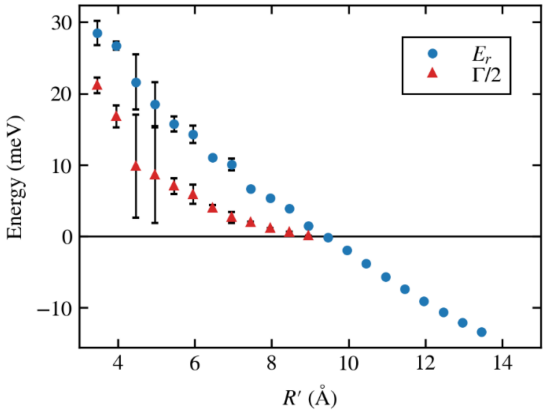

Figure 3.5: Resonance energy, E_r, (blue dots) and half-width, $\Gamma/2$, (red triangles) from stabilization calculations using EOM-CCSD energies of the B_{2u} anion of the $(H_2O)_4$ model as a function of R'. The figure also includes the negative of the EBE for R' values for which the anion is bound.

In order to understand the formation of the B_{2u} state in terms of the various contributions to the electron-molecule interaction potential, it is useful to convert the three-dimensional potential for the interaction of a negative point charge with the cluster to an effective radial potential, depending only on the distance, r, between the electron and the center of mass of the cluster. Neglecting the electrostatic contribution and assuming a spherically symmetric polarization potential, the effective long-range electron-molecule interaction potential is of the form

$$V_{\mathrm{eff}}(r) = -\frac{\alpha}{2r^4} + \frac{l(l+1)}{2r^2} \tag{3.3}$$

where α is the polarizability and l is the angular momentum quantum number. The r value of the maximum, r_{max}, of the confining potential occurs at

$$r_{\mathrm{max}} = \sqrt{\frac{2\alpha}{l(l+1)}} \tag{3.4}$$

The existence of a nonvalence resonance in a particular angular momentum channel requires that the confining barrier be peaked at a radial distance that is large compared to the molecule or cluster of interest. In the case of the $(H_2O)_4$ cluster model with $R' = 7.96$ Å and $l = 1$, r_{max} occurs near 3.5 Å, which is far too small to be consistent with a nonvalence shape resonance.

We now consider the impact of including the nonspherical electrostatic contribution to the interaction potential using the protocol of Boardman et al.[99] in which the interaction potential is decomposed into contributions from different spherical harmonics. Assuming that the resonance is purely p-wave in nature, only V_0 and V_2 components can contribute to the effective radial potential. The interaction potential was derived by calculating at the MP2 level the interaction energies of a negative point charge at various in-plane locations relative to the cluster using the same basis set as that used for the stabilization calculations. The electrostatic contribution to the effective potential was calculated separately, and the polarization potential was obtained by subtracting the electrostatic potential from the net potential at each location considered for the point charge. Figure 3.6 plots the resulting approximate effective radial potential (retaining only the V_0 and V_2 terms in the expansion) for p-wave electron scattering from the $(H_2O)_4$ cluster model with $R' = 7.96$ Å. From this figure, it is seen that with the inclusion of the electrostatic contribution V_{eff} crosses zero near $R' = 15$ Å and the maximum in the barrier (≈ 4.8 meV) in the effective potential occurs near 24 Å. We note also that if the effect of the V_4 term in the expansion on V_0 and V_2 terms is included, the barrier in the effective radial potential is further increased to 7 meV. These results are consistent with the prediction of the EOM-CCSD calculations of a B_{2u} resonance near 5 meV having a highly diffuse charge distribution. We have solved the Schrödinger equation associated with V_{eff} shown in Figure 6 and find that it predicts the anion to be weakly bound rather than metastable, but this is not surprising as V_{eff}, generated as described above, ignores exchange between the excess electron and the electrons of the water molecules as well as orthogonalization effects (but neither of these effects is important for the long-range behavior of the potential). From Figure 3.6, it is also seen that both electrostatics and polarization effects are important for generating the attractive well, but that polarization is inconsequential in the region of the barrier. The position of the TA as

located in the SKT calculations is about 225 meV above the barrier in V_{eff}. A resonance with the E_{r} and $\Gamma/2$ values predicted by the SKT calculations would be difficult to detect experimentally as the phase shift change would be gradual and would be far less than π as one sweeps through the resonance. Electron correlation effects lower the resonance position by about 225 meV, which places it just below the barrier in the effective potential as estimated above, leading to a significant decrease in the width.

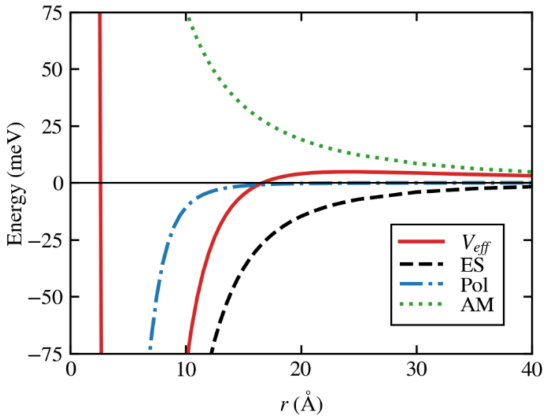

Figure 3.6: Effective radial potential, V_{eff} (solid red line), vs r, the distance from the center of the cluster, for p-wave scattering from the $(H_2O)_4$ cluster model with $R' = 7.96$ Å. The electrostatic contribution (ES) is shown as the dashed black line, the polarization contribution (Pol) is shown as the blue dot-dashed line, and the angular momentum contribution (AM) is shown as the green dotted line.

Having examined the effective radial potential for the electron-cluster interaction, it is instructive to consider the charge distribution of the TA. Figure 3.7 displays the singly occupied NO from EOM-CCSD calculations on the B2u anion state of the $(H_2O)_4$ cluster model at three different R' values. For $R' = 9.46$ Å, at which the anion is bound, and for $R' = 8.96$ Å, at which it is metastable, the NO displayed is for the first root of the EOM calculations, while at $R' = 7.96$ Å, at which it is also metastable, the NO plotted is that associated with the second root of the EOM calculations. For the two R' values at which the anion is metastable, the results shown were obtained at $\beta = 1.7$, at which the appropriate root is in the "plateau" region of the stabilization graph (see Figure 3.4 for $R' = 7.96$ Å). In

a diabatic picture, one can construct a discrete state that is uncoupled from the continuum. The finite lifetime then results from the coupling of this discrete state to the continuum. To a good approximation, the plateau regions of a stabilization graph correspond to the discrete state. Hence, what is actually depicted for $R' = 7.96$ and 8.96 Å in Figure 3.7 is the NO associated with the approximate discrete state (in a diabatic picture) rather than the NO actually associated with the TA. The latter is necessarily complex. Recently, methods for obtaining and plotting complex orbitals for resonance states have been developed, though these require the use of a complex Hamiltonian.[100–102] As seen from Figure 3.7, the anion charge distribution is highly extended both when it is weakly bound and when it is temporary. For $R' = 7.96$ Å, the NO associated with the discrete state has a nodal surface about 70 Å from the center of the cluster, which enforces orthogonality to the lower-lying DC level. A plot along the R' axis of the charge density associated with the singly occupied NO of the discrete state for $R' = 7.96$ Å is peaked near $r = 8$ Å, consistent with the effective potential shown in Figure 3.6.

Although the $(H_2O)_4$ model considered here has a geometry that is unrealizable experimentally, molecules such as $(NaCl)_2$, C_6F_6, tetracyanoethylene, and C_{60} have been predicted to have NVCB anions belonging to the totally symmetric representation at their equilibrium geometries.[6–8,75] Thus, these species are candidates for systems with nonvalence shape resonances. Exploratory calculations on $(NaCl)_2$ indeed indicate that this system has a nonvalence TA state of B_{2u} symmetry. For highly polarizable molecules such as C_{60}, there is also the possibility of d-like nonvalence TA states. Nonvalence shape resonances could be detected in an electron scattering experiment. However, this would be challenging given how close such resonances are expected to be to threshold, both because of the finite resolution of electron scattering experiments and because of the impact of the virtual state. A more viable route to their detection would be as resonances in the cross section for photodetachment from the bound ground state anion. At the shortest R' value considered for the $(H_2O)_4$ model, the A_g anion is bound by about 130 meV, and at this R' value, the resonance in the photodetachment cross section would appear near 160 meV or about 1300 cm^{-1}, which would be accessible with a tunable IR laser. For molecules or clusters with a bound valence-type ground state anion, the photodetachment resonances due to nonvalence TAs are likely to fall

in the visible or UV. We note also that there is the possibility that a nonvalence TA could be converted into a long-lived nuclear Feshbach resonance[79] in which the excess energy is distributed into vibrational degrees of freedom.

Fossez et al. have considered bound and resonance states of an electron interacting with a linear three-point-charge quadrupole.[103] However, the resonances demonstrated for this point-charge model appear to be fundamentally different from those of the $(H_2O)_4$ cluster model considered here. In particular, the resonances demonstrated in ref 103 have lifetimes orders of magnitude longer than that of the p-wave resonance of the $(H_2O)_4$ cluster model. In addition, electron correlation effects play an important role in establishing the energy and lifetime of the p-wave resonance considered here but are not included in the model Hamiltonian used in ref 103.

3.5 Conclusions

In recent years, several studies have appeared demonstrating the existence of nonvalence correlation bound anions of molecules and clusters with no net dipole moment.[6–8,75] Nonvalence anion states, whether bound or temporary in nature, have very diffuse charge distributions. For the $(H_2O)_4$ cluster model considered here, both the electrostatic potential (dominated by the quadrupole term) and electron correlation effects are important in establishing the energy position and width of the TA.

We anticipate that nonvalence TAs will exist slightly above threshold for many molecules and clusters that possess NVCB anions. The lowest-energy NVCB anion of a molecule or cluster necessarily belongs to the totally symmetric representation, but the excited nonvalence anion states will necessarily have sizable p or d character, being manifested as TA shape resonances if the electron-molecule potential is not attractive enough to cause these to be bound. Nonvalence TA shape resonances should be detectable as resonances in the photodetachment cross sections from a stable ground state anion, either valence or nonvalence in nature.

3.6 Acknowledgments

This research was carried out with the support of a grant from the National Science Foundation under Grant CHE1762337. Additional funding was provided by the Grove City College Swezey Fund. The calculations were carried out on computers in the University of Pittsburgh's Center for Research Computing and at Grove City College. We acknowledge helpful discussions with Shiv Upadhyay.

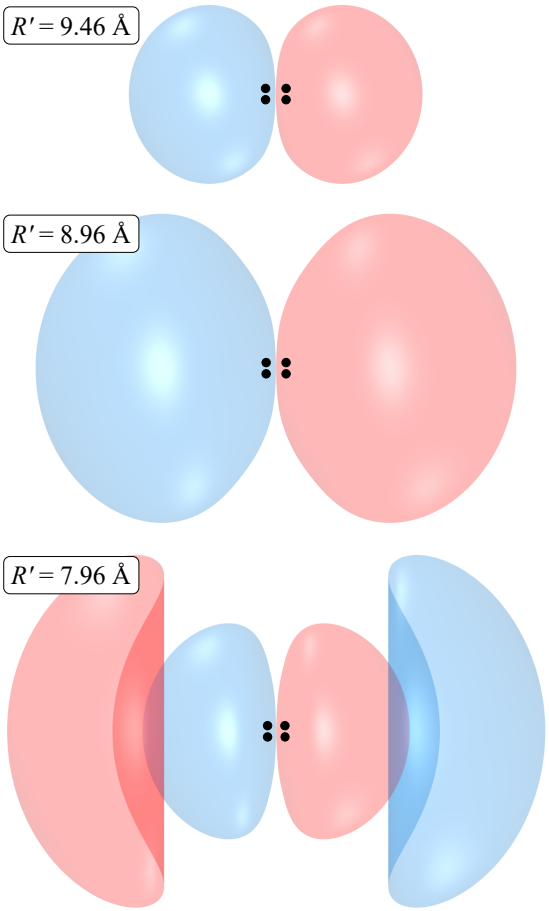

Figure 3.7: NOs associated with the excess electron of the B2u anion states of the $(H_2O)_4$ cluster model at R' = 9.46, 8.96, and 7.96 Å. The anion is weakly bound at R' = 9.46 Å and is metastable at the two shorter R' values. The NOs are from EOM-CCSD calculations using the aug-cc-pVTZ basis set augmented with two sets of 9s functions, as described in the text. The contours shown enclose 90% of the charge density of the NOs. The black dots indicate the positions of the water molecules.

4.0 Prediction of a Non-Valence Temporary Anion State of $(NaCl)_2$

The text and figures in this chapter have been reprinted with permission from Kairalapova, A.; Jordan, K. D.; Falcetta, M. F.; Steiner, D. K.; Sutter, B. L.; Gowen, J. S. Prediction of a Non-Valence Temporary Anion State of $(NaCl)_2$. *J. Phys. Chem. B* **2019**, *123*, 9198–9205, DOI: 10.1021/acs.jpcb.9b07782. The author's contribution to the work included performing DC, CCSD, CCSD(T), EOM-CCSD, and EOM-CCSD(T)(a)* calculations, generating all figures, and editing/revising the manuscript.

4.1 Summary

The equation-of-motion coupled cluster method is used to characterize the low-lying anion states of $(NaCl)_2$ in its rhombic structure. This species is known to possess a non-valence bound anion of A_g symmetry. Our calculations also demonstrate that it has a non-valence temporary anion of B_{2u} symmetry, about 14 meV above threshold. The potential energy curves of the two anion states and of the ground state of the neutral molecule are reported as a function of distortion along the symmetric stretch normal coordinate. Implications for experimental detection of the temporary anion state are discussed. The sensitivity of the results to the inclusion of high-order correlation effects and of core correlation is examined.

4.2 Introduction

Anionic states of molecules and clusters play important roles in many chemical processes. Anions can be characterized as valence or non-valence, depending on the nature of the electron-molecule interaction potential, with short-range interactions proving most important for valence anions and long-range electrostatics and/or correlation effects being

responsible for the existence of non-valence anions. Anions can also be classified as bound or unbound, depending on their energy relative to that of the ground state neutral system, with bound anions being energetically more stable than the electronic ground state of the neutral system and unbound anions being less stable, and hence subject to electron autodetachment. The relative energy of the anion and neutral may also change upon distortion of the molecular geometry, and care must be taken to clearly indicate the geometry under consideration. In some non-valence bound anions, the electrostatic attraction alone is sufficient to bind the electron, which means that the electron is bound in the Koopmans' theorem (KT) approximation[29] when employing sufficiently flexible basis sets. (Here we are assuming that electron correlation effects do not lead to a significant change in the electrostatic potential.) The best known non-valence bound anions are dipole-bound anions.[1,19,74] There are also reports of non-valence quadrupole-bound anions,[24,81] although we note that some anions that have been reported as quadrupole-bound actually fail to bind the excess electron in the KT and Hartree–Fock (HF) approximations, indicating that correlation effects are necessary for binding. We classify anions in which correlation and relaxation effects in response to correlation play a determinative role in the binding of the excess electron as non-valence correlation-bound (NVCB),[6,8,20,75] even though electrostatics may also play an important role in the binding.

While bound anions are most familiar to chemists, unbound anions, also referred to as temporary anions (TAs), play a vital role in a range of processes including vibrational and electronic excitation and chemical bond cleavage.[13,88,104] In addition to the valence vs non-valence classification, TAs can be further classified in terms of the mechanism giving rise to the trapping of the excess electron. In this study, we are interested in non-valence TAs for which the trapping is primarily due to an angular momentum barrier. Such anions are also referred to as shape resonances.[13]

Recently, we introduced a model $(H_2O)_4$ cluster for analyzing the relative importance of electrostatics and correlation effects in the binding of an excess electron in a non-valence anion.[75] The water molecules in the cluster were arranged so as to give D_{2h} symmetry, and, thus, to have no net dipole. By decreasing the separation between the two dimer subunits, the A_g ground state anion changes from bound to unbound at the KT level, although when

electron correlation effects are included by means of the electron attachment equation-of-motion coupled cluster singles plus doubles (EA-EOM-CCSD) method,[34] the anion is found to be bound for the entire range of geometries considered. In a subsequent paper, we showed that for a range of geometries the $(H_2O)_4$ model also possesses a non-valence temporary anion state.[105] Though there are reports of non-valence TAs of molecules with sizable dipole moments,[89,90] nonpolar systems are of interest because the long-range electrostatic attraction falls off more rapidly than r^{-2} (where r is the electron-molecule distance) and, hence, when combined with a nonzero angular momentum contribution, gives rise to a barrier for trapping an excess electron.

While the arrangement of water monomers in the $(H_2O)_4$ model considered in refs 75 and 105 is unrealizable experimentally, the model provides valuable insights into the characteristics required of an experimentally realizable, non-polar molecule or cluster likely to possess a low-energy non-valence temporary anion. Specifically, the system should possess a NVCB anion state belonging to the totally symmetric representation of the relevant point group. The natural orbital or Dyson orbital[106] associated with the excess electron in such anion states is largely s-like outside the molecular region. This suggests the possibility of excited p-like non-valence anion states, which, depending on the strength of the attraction, would be weakly bound or unbound. The p-like character is important, as this is associated with an angular momentum barrier that can contribute to the trapping of the excess electron. This consideration suggests that the rhombic $(NaCl)_2$ cluster is an ideal candidate for a non-valence temporary anion, as it has been predicted to have a bound non-valence anion state of Ag symmetry.[7,107] In the study of Anusiewicz et al.,[107] $(NaCl)_2$ was reported have a vertical electron binding energy (EBE) of 23 and 144 meV at the KT and coupled cluster singles and doubles with perturbative triples [CCSD(T)][108] levels of theory, respectively. (In the sign convention used in the present study, a positive EBE refers to a bound anion.) Similar results were reported by Sommerfeld et al.[7] who reported KT and EA-EOM-CCSD values of the EBE.

The lowest unoccupied molecular orbital (LUMO) from a HF calculation on the neutral $(NaCl)_2$ cluster at its equilibrium geometry is shown in Figure 4.1 from which it is seen that the LUMO is well described as the bonding combination of sp hybridized orbitals associated

with each Na atom, with the charge being localized outside the ring to minimize repulsion with the Cl^- ions. (The basis set and cluster geometry used for these calculations are described in section 4.3.) Since the A_g anion is only weakly bound, one might anticipate that the B_{2u} anion state resulting from the antibonding combination of the hybridized orbitals associated with the two Na atoms would lie energetically above the neutral cluster. In this study, we use EOM methods to characterize the B_{2u} anion state of rhombic $(NaCl)_2$ to determine if it is indeed temporary in nature at the equilibrium geometry of the neutral cluster. We note that the existence of excited state non-valence anions, whether bound or unbound, is relevant for understanding the capture of low-energy electrons, and possibly also the formation of vibrational Feshbach resonances.[79]

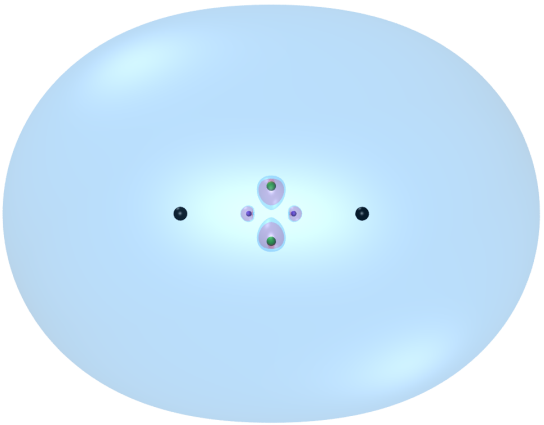

Figure 4.1: Lowest unoccupied molecular orbital from a Hartree-Fock calculation on neutral $(NaCl)_2$ using the aug-cc-pVTZ basis set on the atoms and two sets of 9s functions as described in the text and centered at the location of the two black spheres, on the same axis as the sodium atoms. The contour shown encloses 90% of the charge density.

4.3 Computational Details

The geometry of the rhombic form of $(NaCl)_2$ was optimized using the MP2 method[31] in conjunction with the aug-cc-pVTZ basis set[50,51] and using the frozen core (FC) approx-

imation. This geometry was used in a calculation of the harmonic frequencies at the same level of theory. Distortion along the totally symmetric breathing mode (q) was considered in order to follow the B_{2u} anion as it evolves from a bound state to a TA, with a value of $q = 0$ corresponding to the optimized geometry of the neutral cluster. The FC approximation was used in previous studies,[7,107] and the geometries considered in the current work are largely based on the geometry and definition of q given above. However, in the course of this work, it became apparent that correlating the 2s and 2p electrons in the sodium atoms had a significant effect on the optimized geometry of the neutral cluster and on the energies of the anion states relative to the neutral. As a result, we also optimized the geometry of the neutral cluster using the MP2 method, allowing correlation of the sodium 2s and 2p electrons using the aug-cc-pCVTZ basis[109] on the Na atoms. (Hereafter, calculations including electron correlation and correlating the Na L-shell electrons are referred to as correlated core.) The geometry of the neutral cluster optimized in the correlated core approximation is close to that obtained by displacing the FC structure to $q = -0.05233$. The normal mode relative displacements calculated in the FC and correlated core approximations are essentially identical.

The main computational approach used in this study to characterize the anion states of $(NaCl)_2$ is the EA-EOM-CCSD method, which has been found to accurately characterize both bound and unbound anion states provided sufficiently flexible basis sets are emplpyed.[6,8,75,92,110,111] In this approach, a CCSD calculation is carried out on the electronic ground state of the neutral molecule, and the resulting T1 and T2 amplitudes are used to carry out a similarity transform of the Hamiltonian which is then used to perform a one-particle (1p) plus two particle-one-hole (2p1h) configuration interaction (CI) calculation on the excess electron state. Calculations are also carried out using the EOM-CCSD(T)(a)* method[37] which accounts in an approximate manner for the contributions of triple excitations to the ground state of the neutral and of 3p2h excitations in the CI calculation of the anion. The EOM-CCSD(T)(a)* algorithm used is implemented for excitation energies but can be "tricked" into calculating electron affinities by starting from a closed shell configuration with two excess electrons in a "continuum" orbital.

The orbital depicted in Figure 4.1 was obtained from a HF calculation on the neutral molecule at q = 0 using the aug-cc-pVTZ basis set supplemented with two sets of diffuse s Gaussians located on the Na-Na axis but with their centers (shown as black spheres in Figure 4.1) displaced further than the Na atoms from the center of the ring. These supplemental sets contained nine even-tempered primitive Gaussians with the largest exponent being 0.25 and each successive exponent being smaller by a factor of $\sqrt{10}$. We note that the LUMO of $(NaCl)_2$ obtained from calculations employing supplemental diffuse s and p functions on the Na atoms has nearly the same EBE and charge distribution as that obtained with the basis set with the off-atom s functions. The use of off-atom basis functions proves beneficial in the procedure used to characterize the B_{2u} anion state at geometries at which it is unbound. The distance of the centers of the supplementary basis functions from the Na atoms was optimized to maximize the binding of the B_{2u} anion state for an expanded ring geometry with $q = 0.08$ for which the anion state is weakly bound in EA-EOM-CCSD calculations in the correlated core approximation. This resulted in a displacement of 5 Å of the centers of the diffuse sets from the Na atoms. We also checked that it remains close to optimal for $q = -0.07$ where the B_{2u} anion is temporary with the highest energy found in this study. This basis set gives a KT value of the vertical EBE (for forming the A_g anion) of 20 meV, 3 meV smaller than that reported by Anusiewicz et al.[107] Moreover, the EA-EOM-CCSD value of the EBE from our calculations (139 meV) employing this basis set and the FC approximation agrees closely with the EA-EOM-CCSD result of Sommerfeld et al.[7]

As noted above, we have also calculated the EBEs as a function of q, the extent of the displacement along the normal coordinate corresponding to the totally symmetric breathing mode of the neutral molecule. As q is varied, the location of the supplemental diffuse s functions relative to the sodium atoms was held fixed, displaced 5 Å from the Na atoms. The electronic structure calculations were carried out using CFOUR.[46]

In the Siegert picture,[14] temporary anions are characterized by a complex energy

$$E_{\text{res}} = E_{\text{r}} - \frac{i\Gamma}{2} \tag{4.1}$$

where E_{r} is the resonance position and Γ its width which is proportional to the reciprocal of the lifetime (atomic units have been assumed). Both E_{r} and Γ are geometry dependent.

For geometries at which the B_{2u} anion is unbound, the results from the EA-EOM-CCSD calculations were combined with the stabilization method[15] and analytic continuation[18] to determine the complex energies associated with the temporary anion states. Briefly, the exponents of the supplemental diffuse basis functions were multiplied by a scale factor, β, and the energies of the first seven eigenvalues corresponding to the electron attached states (relative to that of the neutral) are calculated for a series of β values ranging from 0.2 to 1.7.

A plot of the energies of the excess electron states (relative to the energy of the neutral molecule) vs β reveals avoided crossings that can be interpreted as resulting from the mixing of a diabatic discrete state corresponding to the anion (with detachment suppressed) with diabatic discretized representations of the continuum of the free electron plus the neutral molecule. Hereafter, the latter are referred to as DC levels. As is well documented in the literature, the resonance position and width can be extracted using data from the avoided crossing regions.[15,18,95,96,112] In the present study, we accomplish this by means of analytic continuation and locating the complex stationary point, $\beta*$, for which $dE/d\beta = 0$. In the case of a clear-cut avoided crossing between two levels, the analytic continuation can be carried out by fitting the data in the vicinity of an avoided crossing to the expression

$$P(\beta)E^2 + Q(\beta)E + R(\beta) = 0 \tag{4.2}$$

where

$$P(\beta) = 1 + p_1\beta + p_2\beta^2 + \ldots \tag{4.3a}$$

$$Q(\beta) = q_0 + q_1\beta + q_2\beta^2 + \ldots \tag{4.3b}$$

and

$$R(\beta) = r_0 + r_1\beta + r_2\beta^2 + \ldots \tag{4.3c}$$

The stationary point $\beta*$ is substituted back into the expression for the energy to obtain estimates of E_r and Γ. The use of a quadratic rather than a linear expression in E is to accommodate the branch-point structure associated with avoided crossings.[18,95,112]

For narrow resonances, for which $\Gamma/2 \ll E_r$, stabilization graphs generally display well-defined avoided crossings between the diabatic discrete state and the discretized continuum (DC) solutions as the scale parameter is varied. However, for resonances for which the value of $\Gamma/2$ approaches E_r in magnitude, the avoided crossings become less pronounced. For the geometries of $(NaCl)_2$ considered here, semiquantitative results for the B_{2u} anion can be obtained using the quadratic expression given by eq 4.2, with the P, Q, and R polynomials being, respectively, of order 3, 4, and 5, in β, and employing data from the two roots involved in an avoided crossing. However, to obtain better converged complex resonance energies, we employed a generalization of eq 4.2 to include terms of higher order in E. In our application of this approach to extract resonance parameters of the B_{2u} anion of $(NaCl)_2$, we included terms through E^3 for $q = 0.07$ and E^4 for smaller values of q and used data from three and four roots, respectively. We employ polynomials in eq 4.2 and its extensions of powers $n-m$, where m is the power of E in the expression for the energy and n is an integer ranging from 6 to 13. Typically, more data points were used than parameters in combination with least-squares fitting. In addition, for each geometry considered, several independent analytic continuation calculations using different sets of data points and different order polynomials in eq 4.3 were performed, each giving slightly different complex resonance energies, with the average of these results being reported for E_r and Γ.

4.4 Results and Discussion

4.4.1 Stabilization Calculations

The stabilization graph obtained from the EA-EOM-CCSD calculations on $(NaCl)_2$ using the correlated core approximation and at $q = 0$ is shown in Figure 4.2a. The figure also includes the energies of the DC levels obtained by solving for the eigenvalues of the one-electron system using the same basis set as that used for the EA-EOM-CCSD calculations but with the nuclear charges set equal to zero. The DC levels were calculated using Gaussian 16.[97] From inspection of the graph, it is seen that, for the energy range depicted, the EOM

calculations give one more energy level than there are DC levels. This is indicative of the presence of a TA resonance. It is also seen that the diabatic (i.e., unmixed) discrete state corresponding to the resonance falls near 9 meV. In order to obtain a more accurate value of E_r and to determine the width, we use the analytic continuation procedure described above, together with data from the second to fifth roots of the EA-EOM-CCSD calculations for scale factors ranging from 0.2 to 1.0. The resulting average E_r and Γ values are 8.95 and 7.28 meV, respectively.

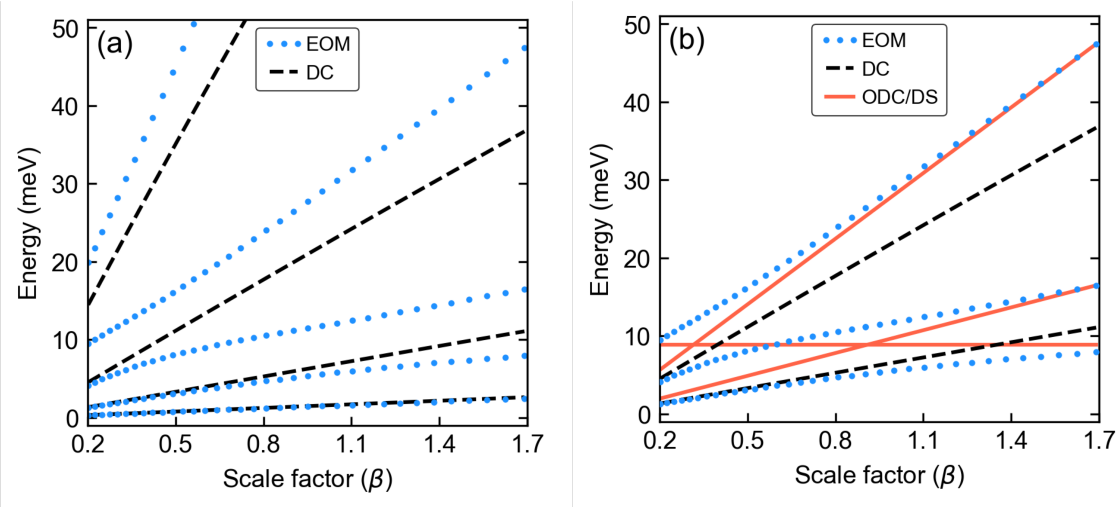

Figure 4.2: (a) Stabilization graph for $(NaCl)_2$ obtained from EA-EOM-CCSD calculations at $q = 0$ and using the correlated core approximation. The energies of the excess electron states from EOM-CCSD calculations and of the DC levels are shown as blue dotted lines and black dashed lines, respectively. (b) The energies of the excess electron states from EOM-CCSD calculations are shown as blue dotted lines. The energies of the DC levels are shown as black dashed lines and the unmixed discrete level by the horizontal red line, while estimates of the energies of the second and third DC levels orthogonalized to the discrete level are indicated by the sloped red line.

Figure 4.2b reproduces the portion of the stabilization graph involving the avoided crossings. In this figure, we also indicate the energy of the diabatic discrete state by a horizontal line. In addition, we have added lines to indicate the approximate energies of the DC levels when orthogonalized to the discrete level to give so-called orthogonalized DC (ODC) levels.

This helps make it more transparent that there are two avoided crossings occurring near β values of 0.3 and 0.9. Interestingly, the crossings of the discrete state and the relevant DC levels occur near larger β values (0.40 and 1.33, respectively). The shifts of the avoided crossings to lower β values than those that correspond to the crossings between the discrete level and the DC levels are a consequence of orthogonalization. If we treat the region near an avoided crossing as a two-level system, then the eigenvalue problem becomes

$$\begin{pmatrix} H_{11} - E & V - SE \\ V - SE & H_{22} - E \end{pmatrix} \begin{pmatrix} c_1 \\ c_2 \end{pmatrix} = \begin{pmatrix} 0 \\ 0 \end{pmatrix} \tag{4.4}$$

where H_{11} is the energy in the discrete state, H_{22} is the energy of the appropriate DC level, V is the coupling between the discrete state and the DC level, and S is the overlap of the associated wave functions. At $\beta = 1.3$, where the discrete level and the second DC level cross, one can use the energies of the diabatic and adiabatic levels to determine that $S = 0.52$ and $V = 1.86$ meV (at that β value).

Figure 4.3 plots, as a function of q, the energy of the B_{2u} anion state obtained from EA-EOM-CCSD calculations carried out with both the FC and correlated core approximations. (A value of $q = 0.1$ corresponds to an increase of the Na-Na distance by 0.118 Å and an increase of the Cl-Cl distance by 0.078 Å.) For q values at which the anion is unbound, the results were obtained using the stabilization procedure described above, and we plot both E_r and $\Gamma/2$. In both sets of calculations, the real part of the energy of the TA is seen to be a smooth continuation of the energy of the bound state, as q is decreased. The inclusion of correlation effects involving the Na core electrons increases the attraction of the electron for the cluster: the stabilization is ∼9 meV at $q = 0.15$, at which the anion is bound, and ∼3.5 meV at $q = 0$, at which the B_{2u} anion is unbound. (The smaller stabilization at $q = 0$ is consistent with the more extended charge distribution of the anion when it is temporary than when it is bound.) As a result, bothE_r and Γ are predicted to be smaller in the calculations correlating the core electrons of the Na atoms than in those carried out using the FC approximation at a given value of q. The resonance energy was also calculated at the geometry of the neutral cluster optimized at the MP2 level in the correlated core approximation, with the resulting values of E_r and $\Gamma/2$ being 14.40 and 8.94

meV, respectively. It should be noted that the geometry optimized at this level of theory is very close to that obtained in the FC approximation with q displaced to -0.05233, at which stabilization calculations making use of the correlated core approximation give values of E_r and $\Gamma/2$ (13.67 and 8.05 meV, respectively) that are within 1 meV of the resonance parameters obtained using the geometry optimized in the correlated core approximation.

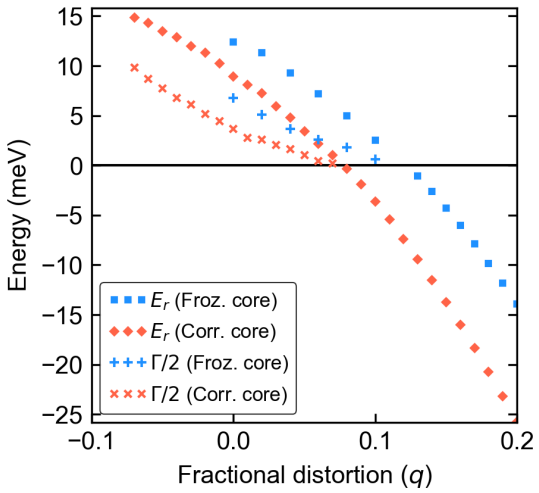

Figure 4.3: Resonance energy, E_r and $\Gamma/2$, from EA-EOM-CCSD stabilization calculations on the B_{2u} anion of $(NaCl)_2$ as a function of q, the distortion along the symmetric breathing normal coordinate. Results obtained in the frozen core (shown in blue) and correlated core (shown in red) approximations are reported. The figure also includes the negative of the EBE for q values for which the anion is bound.

While the use of the correlated core approximation impacts both E_r and Γ, when $\Gamma/2$ is plotted vs E_r for the q values for which the anion is predicted to be temporary, the results from the stabilization calculations with and without correlation of the Na core electrons are found to essentially fall on the same curve, as seen in Figure 4.4. This is consistent with the fact, discussed in detail later, that correlating the Na core electrons impacts the electron-cluster interaction potential only at short range and has a negligible impact on the barrier region which controls the width (for a given value of E_r).

Also shown in Figure 4.4 are least-squares fits of $\Gamma/2$ as a function of E_r for the core-correlated calculations using threshold laws[113] assuming either p-wave (dashed black line)

or f-wave (solid green line) character of the resonance. (Symmetry constrains the resonance to contain only odd l angular momentum terms.) The equations used in the fits are

$$\frac{\Gamma}{2}(l=1) = \frac{AE_{\mathrm{r}}^{3/2}}{1+BE_{\mathrm{r}}} \tag{4.5a}$$

$$\frac{\Gamma}{2}(l=3) = \frac{AE_{\mathrm{r}}^{7/2}}{225+45(BE_{\mathrm{r}})+6(BE_{\mathrm{r}})^2+(BE_{\mathrm{r}})^3} \tag{4.5b}$$

The fit based on eq 4.5a (with A = 0.172 and B = 0.037) is superior to that obtained assuming purely f-wave character (with A = 15.97 and B = 2.14). We note that, while the fit was based only on the data from the core-correlated calculations with q ranging from 0.07 to 0 (E_{r} ranging from approximately 1 to 9 meV), the best-fit curve was extended over the entire range of q values considered. The departure of the fit from the data from the smaller q values suggests that for these points the threshold formula is beginning to fail. At $q = 0$ in the correlated core approximation, the width Γ is already about 80 % as large as E_{r}, and the resonance cannot be considered narrow.

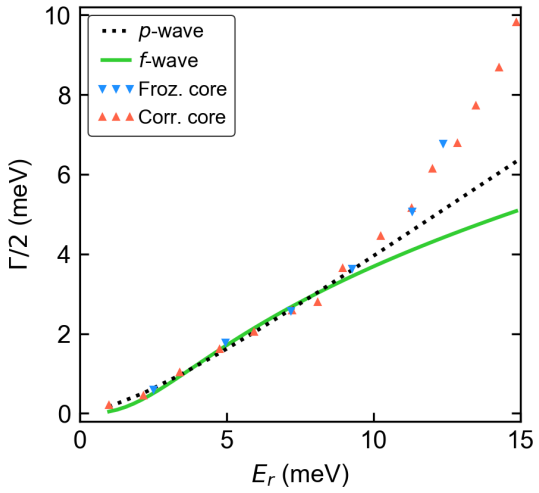

Figure 4.4: $\Gamma/2$ vs E_{r} from EA-EOM-CCSD/stabilization calculations on the B_{2u} anion of $(NaCl)_2$ with the results from the frozen core and correlated core approximations shown as blue triangles and red triangles, respectively. Also shown are fits based on eq 4.5, with the fit using the expression for a p-wave resonance shown as the black dotted line and that for an f-wave resonance shown as the solid green line.

4.4.2 Polarization and Effective Potentials for $e^- + (NaCl)_2$

In light of the finding that inclusion of correlation effects involving the core electrons of the Na atoms impacts the energies of the anion states, we find it instructive to examine the polarization potential of $(NaCl)_2$ calculated in the FC and correlated core approximations. Figure 4.5 plots, along the NaNa axis, the polarization potential of $(NaCl)_2$ calculated at the MP2 level in both the FC and correlated core approximations. As seen from this figure, the polarization potential is much more attractive in the correlated core approximation. These results were obtained by subtracting the MP2-level electrostatic potential from the change in the MP2 energy caused by a negative point charge at various locations along the NaNa axis. It should be noted that similar results are obtained in the HF approximation, which means that the increased attraction of the polarization potential close to the Na atoms is predominantly due to the inclusion of basis functions appropriate for describing polarization of the core electrons rather than to correlation of the core. However, it is important to note that, in the calculation of the EBEs of the anions, this is manifested in terms of correlation effects involving the diffuse excess electron and the tightly bound electrons of the Na cores.[114] Although both the A_g and B_{2u} anions have very extended charge distributions, the small amount of charge density of the excess electron near the Na cores results in a non-negligible stabilization of the anion when correlation effects between the excess electron and the core electrons are included.

As noted in the 4.2 Introduction, shape resonances can be viewed as resulting from the trapping of an excess electron in the effective potential describing the electron-molecule interaction. In light of this, it is instructive to consider the effective potential for a purely p-wave resonance of $(NaCl)_2$. Figure 4.6 plots the polarization, electrostatic, and angular momentum contributions to the effective potential obtained in the correlated core approximation at $q = 0$. The polarization and electrostatic contributions to the effective potential were obtained by applying the procedure of Boardman et al.[99] to the results of MP2 calculations of the electrostatic potential and of the energy of the cluster interacting with a negative point charge at various locations. The most striking aspect of the net effective potential is the large distance of the barrier from the center of the molecule: The maximum

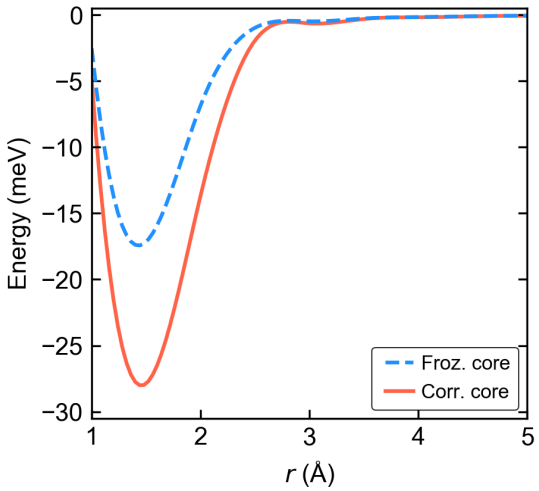

Figure 4.5: Polarization potential for the correlated core (solid red line) and frozen core (dashed blue line) approximations as a function of distance along the Na-Na axis (r, in angstroms).

of the barrier occurs near an electron-molecule distance of 14 Å at which the energy is 13.2 meV, about 4 meV above the value of E_r calculated for the B_{2u} resonance at $q = 0$. Polarization effects are negligible in the barrier region, and the barrier results from the interplay of the attractive electrostatic interaction and the repulsive angular momentum term. The distance of the barrier from the molecule is much greater than that found for valence shape resonances for which the barrier results from the interplay of the polarization and angular momentum contributions. We note that the effective potential shown in Figure 4.6 does not account for exchange between the excess electron and the electrons of the cluster or for orthogonality of the orbital occupied by the excess electron to the orbitals of the cluster of the same symmetry. Both of these effects are short-ranged and are not expected to impact the barrier region of the potential.

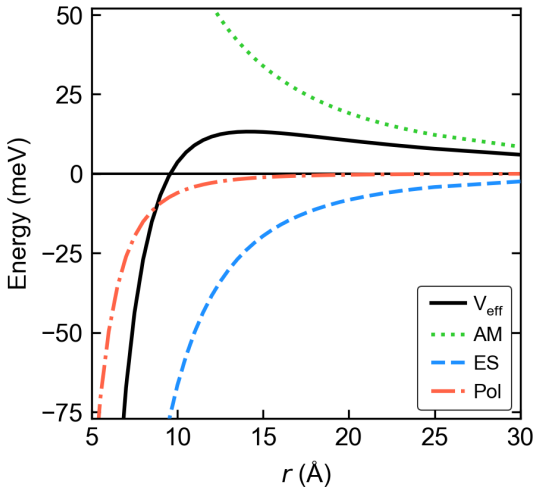

Figure 4.6: Effective radial potential, V_{eff} (solid black line), vs r, the distance from the center of the cluster, for p-wave scattering from the $(NaCl)_2$ cluster model with $q = 0$. The electrostatic contribution (ES) is shown as the dashed blue line, the polarization contribution (Pol) is shown as the red dash-dotted line, and the angular momentum contribution (AM) is shown as the green dotted line.

4.4.3 Potential Energy Curves

Figure 4.7 reports as a function of q the potential energy curves for the ground state of the neutral cluster as well as for the A_g and B_{2u} anion states. The total energy of the neutral molecule is from CCSD calculations, and the energies of the anion states are obtained by subtracting the EBEs from the EA-EOM-CCSD calculations from the energies of the neutral. These curves were generated allowing for core correlation. For q values at which the B_{2u} state lies higher in energy than the neutral cluster, the EBEs are associated with the negative of the real parts of the resonance energy from the stabilization calculations. The energies of both anion states display a q dependence similar to that of the neutral, consistent with the extra electron occupying a highly extended non-valence orbital. Whereas the A_g state is bound by approximately 150 meV over the entire range of q values considered, the energy of the B_{2u} state is very close to that of the neutral, being bound only for $q \gtrsim 0.08$.

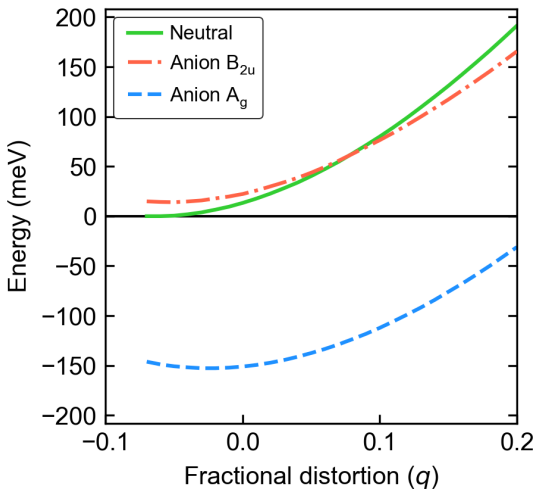

Figure 4.7: Relative energies of the A_g (dashed blue) and B_{2u} (dash-dotted red) anion states and of the ground state of the neutral $(NaCl)_2$ cluster (solid green) as a function of q, the fractional distortion along the symmetric breathing normal coordinate. The energy of the neutral ground state at its most stable geometry ($q = -0.06$) is taken as the zero of the energy scale. The energy of the neutral is from CCSD calculations and the energies of the anion states are from the EOM-CCSD calculations, all obtained using the correlated core approximation.

Based on the potential energy curves depicted in Figure 4.7, the B_{2u} anion of rhombic $(NaCl)_2$ should be detectable by IR absorption from the bound A_g anion state. However, it should be noted that Anusiewicz et al. found in their computational study that the ground state anion distorts from the rhombic to a C_{2v} structure. The energy lowering associated with this distortion was so small that these authors concluded that the structure averaged over the vibrational zero-point motion would still be D_{2h}. This distortion is presumably driven by the enhanced electron binding due to the accompanying dipole moment ($\sim$1.5 D in the calculations of Anusiewicz et al.). At the distorted structures, the excited state anion would acquire s-wave character which would act so as to shorten the anion lifetime and which could make its detection in IR absorption from the ground state anion more challenging.

Table 4.1 reports the EBE obtained using various theoretical methods of the A_g anion at $q = 0$. For the A_g state, the FC and correlated-core EBEs obtained using the EA-EOM-CCSD method are 139 and 164 meV, respectively. Thus, core correlation is more important for the A_g anion than for the B_{2u} temporary anion, consistent with the more diffuse charge distribution of the latter. Table 4.1 also includes EBEs calculated using the EOM-CCSD(T)(a)* method as well as with the ΔCCSD and ΔCCSD(T) methods. (The Δ methods involve calculating separately the energies of the ground neutral and the anion and are feasible only for anion states that demonstrate binding in the HF approximation.) The EOM-CCSD(T)(a)* and ΔCCSD(T) methods give EBEs that agree to within 1 meV of each other, with the EOM-CCSD(T)(a)* results being 148 and 176 meV in the FC and correlated core approximations, respectively. This shows that correlation of the Na core electrons is $\sim$4 meV more important in the EOM-CCSD(T)(a)* than in the EA-EOM-CCSD calculations and also that inclusion of higher order correlation effects absent in the EA-EOM-CCSD method lead to a 12 meV increase in the EBE of the A_g anion.

Table 4.1: Electron binding energy (meV) of the A_g anion state of $(NaCl)_2$ calculated at various levels of theory in the frozen core and correlated core approximations.

core	EOM-CCSD	EOM-CCSD(T)(a)*	ΔCCSD	ΔCCSD(T)
frozen	139	148	128	147
correlated	164	176	152	175

At $q = 0$, the EA-EOM-CCSD calculations predict the B_{2u} anion state to be unbound with respect to the neutral by 12.4 and 9.0 meV in the FC and correlated-core approximations, respectively. As we saw above, higher order correlation effects (not included in EOM-CCSD) stabilize the A_g anion state by about 12 meV, making it important to estimate their effect on the B_{2u} anion at q values that the EOM-CCSD calculations predict it to be a resonance. To this end, we also carried out EOM-CCSD(T)(a)* calculations to the B_{2u} anion at q values at which the anion is bound. We did such calculations at $q = 0.20$ and 0.15 and find that the use of EOM-CCSD(T)(a)* rather than EA-EOM-CCSD increases the EBEs at these q values by only 3.0 and 2.5 meV, respectively. Higher order correlation effects are expected to be even less important at q values at which the anion is metastable. Indeed, sta-

bilization calculations carried out using the EOM-CCSD(T)(a)* method at the geometry of the neutral cluster optimized at the MP2 level in the correlated core approximation showed that the resonance energy and width are impacted by less than 1 meV by the inclusion of higher order correlation effects.

4.5 Conclusion

In this study, we present the results of calculations that indicate that $(NaCl)_2$, at its equilibrium geometry, possesses both a bound non-valence anion of A_g symmetry and a non-valence temporary anion of B_{2u} symmetry. Inclusion of correlation of the Na core electrons is found to significantly impact the geometry of $(NaCl)_2$ and the energies of the A_g and B_{2u} anion states, although this is less important for the B_{2u} anion at geometries at which the anion is a resonance than those at which it is bound. Electron correlation effects recovered by the EOM-CCSD(T)(a)* method but lacking in EOM-CCSD are found to lead to an $\sim$12 meV increase of the EBE of the A_g anion (at $q = 0$) but have a smaller impact on the EBE of the B_{2u} anion. The B_{2u} temporary anion state of $(NaCl)_2$ in its rhombic structure should manifest itself both in low-energy electron scattering from the neutral cluster and in the IR photodetachment of the excess electron from the bound A_g anion. In the latter case, the resonant and direct detachment channels are expected to interfere, thereby modifying the Fano line shape.[115]

4.6 Acknowledgements

K.D.J. and A.K. acknowledge support from the National Science Foundation under grant CHE1762337. We also acknowledge the use of computational resources provided by the University of Pittsburgh's Center for Research Computing.

5.0 Analysis of the Contributions to the Kinetic and Potential Energies of an H Atom in the Presence of a Point Charge: The Molecular Virial Theorem Revisited

The text and figures in this chapter have been reprinted with permission from Kairalapova, A.; Jordan, K. D. Analysis of the Contributions to the Kinetic and Potential Energies of an H Atom in the Presence of a Point Charge: The Molecular Virial Theorem Revisited. *J. Phys. Chem. A* **2020**, *124*, 4534–4538, DOI: 10.1021/acs.jpca.0c02758. The author's contribution to the work included performing calculations, deriving equations, generating all figures, and editing/revising the manuscript.

5.1 Summary

The molecular virial theorem states that for a diatomic molecule or for an atom in the presence of a point charge, the changes in the average kinetic energy and average potential energy are equal to $\langle T\rangle = -U - R\,dU/dR$ and $\langle V\rangle = 2U + R\,dU/dR$, respectively, where U is the interaction energy and R is the internuclear separation or the atom-point charge separation. In this paper we directly evaluate the $\langle T\rangle$ and $\langle V\rangle$ expectation values of an H atom in the presence of a distant point charge, obtaining exact analytical expressions by use of Dalgarno–Lewis perturbation theory.

5.2 Introduction

For atoms as well as molecular systems at their equilibrium structures the virial theorem states that

$$\langle T\rangle = -\frac{1}{2}\langle V\rangle \tag{5.1}$$

where T and V denote the kinetic and potential energy operators, respectively. The virial theorem is necessarily obeyed for the exact wave function, whereas approximate wave functions can give average kinetic and potential energies that significantly deviate from obeying the virial theorem. The virial theorem was generalized to diatomic molecules at arbitrary internuclear separation by Slater[116] and subsequently by Hurley[117] to polyatomic molecules at arbitrary geometries to give the so-called molecular virial theorem. These generalizations assumed the validity of the Born–Oppenheimer[9] approximation. For diatomic molecules at an arbitrary bond length Slater obtained

$$\langle T \rangle = -E - R\frac{dE}{dR} \tag{5.2a}$$

$$\langle V \rangle = 2E + R\frac{dE}{dR} \tag{5.2b}$$

where E is the total energy and R is the internuclear separation. The changes in the average kinetic and potential energies due to the interaction are

$$\Delta \langle T \rangle = \langle T \rangle - \langle T \rangle_\infty = -U - R\frac{dU}{dR} \tag{5.3a}$$

$$\Delta \langle V \rangle = \langle V \rangle - \langle V \rangle_\infty = 2U + R\frac{dU}{dR} \tag{5.3b}$$

where $\langle T \rangle_\infty$ and $\langle V \rangle_\infty$ refer to the averages at infinite internuclear separation and U is the interaction energy. Thus for a neutral diatomic molecule at R values for which C_6 dispersion dominates

$$\Delta \langle T \rangle = 5U \tag{5.4a}$$

$$\Delta \langle V \rangle = -4U \tag{5.4b}$$

Interestingly, while a second-order perturbation theory treatment describes the long-range dispersion interaction purely in terms of the dipole–dipole coupling, the virial theorem indicates that the potential energy contribution is repulsive and that the net attraction is actually a consequence of the kinetic energy.

In general, one determines the average kinetic energy and potential energy contributions by fitting the interaction energies from electronic structure calculations as a function of R

and using eq 5.3 rather than by directly calculating expectation values of the T and V operators.

In order to obtain a better understanding of the origin of the attractive kinetic energy and repulsive potential energy contributions predicted by the virial theorem, it is useful to consider the simpler problems of an H atom in the field of a point charge, at a distance R from the atom, as well as in a uniform electric field, since exact, complete basis set results can be obtained for these cases. In the limit that only dipole polarization is important, the molecular virial theorem (eq 5.3) gives

$$\Delta \langle T \rangle = 3U \tag{5.5a}$$

$$\Delta \langle V \rangle = -2U \tag{5.5b}$$

For a positive point charge, $|e|$, this corresponds to the H_2^+ molecular ion with the neglect of charge delocalization, the long-range behavior of which has been the subject of numerous studies.[118–121] However, here our focus is on analyzing the field-induced shifts in the average kinetic and potential energies in terms of contributions to the wave function in the complete basis set limit and which are obtained by use of Dalgarno–Lewis perturbation theory.[118] Of course, the H atom in the presence of a uniform efield, has no bound states,[122] but for the calculations presented here autoionization is not an issue: for the complete basis set analytical results it is suppressed by the use of low-order perturbation theory, and for the finite basis set variational calculations it is suppressed by the limited spatial extent of the basis functions.

At large separation, R, of the point charge from the atom, the sign of the point charge is immaterial and

$$U = -\frac{\alpha}{2R^4} \tag{5.6}$$

where α is the dipole polarizability. In the complete basis set limit $\alpha = 4.5$ au and $U = -2.25R^{-4}$ au.[118] For the case of an atom in a uniform electric field, ε, the analog of the molecular virial theorem is

$$\Delta \langle T \rangle = -U + 2\varepsilon \frac{dU}{d\varepsilon} \tag{5.7a}$$

$$\Delta \langle V \rangle = 2U - 2\varepsilon \frac{dU}{d\varepsilon} \tag{5.7b}$$

where $U = -0.5\alpha\varepsilon^2$.

5.3 Theory

Although our primary interest is in delineating the various contributions to $\Delta \langle T \rangle$ and $\Delta \langle V \rangle$ as evaluated directly from the wave function, we find it instructive to first consider results obtained from finite basis set variational calculations. For these calculations we employ for the H atom a basis set comprised of the s and p portions of the aug-cc-pV6Z Gaussian-type orbital basis set.[50,51] This basis set (hereafter referred to as **A**) gives an energy of the ground state of the isolated H atom only 7×10^{-7} au above the exact value and a value of the dipole polarizability of 4.4928 au, in close agreement with the exact result of 4.5 au. We place the perturbing point charge, here taken to be $q = -|e|$, 10 Bohr from the H atom which results in an electric field of 0.01 au. The efield calculations were carried out on the H atom using this field strength. The finite-basis set calculations were carried out using the Gaussian 16 program.[97]

Table 5.1 reports the total energy, the $\langle V \rangle$ and $\langle T \rangle$ values, and the virial ratio of the isolated atom as well as of the atom in the presence of the point charge or the uniform electric field as obtained from the finite basis set calculations. For comparison the Table also reports exact results obtained in the complete basis set limit, calculated allowing only dipole polarization. (The procedure used to obtain the exact results is described below.) To facilitate analysis of the results, the Table also reports the changes in $\langle T \rangle$ and $\langle V \rangle$ caused by the perturbations.

From Table 5.1, it is seen that with basis set **A** the variational calculations on H atom in the presence of the point charge or the external uniform efield give $\langle V \rangle / \langle T \rangle$ ratios and $\Delta \langle T \rangle$ and $\Delta \langle V \rangle$ values very close to the exact results. The small discrepancies of the finite basis

set variational results from the exact results (described below) are due to the incompleteness of the basis set (in the s and p space) as well as to the recovery in the former of contributions other than dipole polarization. Specifically, at the values of R and field strength employed in the calculations, there is a small contribution from the γ hyperpolarizability, and in the point charge calculations there is also a more significant contribution from the B dipole–dipole–quadrupole hyperpolarizality. These higher-order contributions would cease to be important were R increased to, e.g., 20 Bohr and the external field decreased to 0.0025 au.

Table 5.1: Energies (au), virial ratios, $\langle V \rangle$, and $\langle T \rangle$ values (in au) of an H atom, both isolated and in the presence of a $-|e|$ point charge at $R = 10$ Bohr or a uniform electric field of strength 0.01 au.

system	basis	E_{tot}	$-\frac{\langle V \rangle}{\langle T \rangle}$	$\langle V \rangle$	$\langle T \rangle$	$\Delta \langle V \rangle$	$\Delta \langle T \rangle$
isolated[a]	CBS[b]	−0.5000000	2.000000	−1.0000000	0.5000000		
efield, pt. chg.	CBS[b]	−0.5002250	2.001802	−0.9995500	0.4993250	0.0004500	−0.0006750
isolated[a]	**A**, **B**	−0.4999993	2.000004	−0.9999966	0.4999973		
efield	**A**	−0.5002242	2.001811	−0.9995441	0.4993200	0.0004525	−0.0006774
efield	**B**	−0.5002238	2.000653	−1.0001211	0.4998973	−0.0001244	−0.0001001
pt. chg.	**A**	−0.5002218	2.001779	−0.9995554	0.4993337	0.0004412	−0.0006637
pt. chg.	**B**	−0.5002214	2.000640	−1.0001229	0.4999015	−0.0001263	−0.0000958

[a] Isolated H atom.
[b] Exact results in the complete s and p basis set (CBS) limit, allowing only for dipole polarization.

A clue as to the terms in the wave function responsible for the changes in $\langle V \rangle$ and $\langle T \rangle$ due to the point charge or external efield is provided by the following "experiment". We uncontracted the s functions in basis set **A**, and used the resulting set of primitive functions in a variational calculation of the energy of the isolated H atom. The s primitives were then contracted to a single function with the contraction coefficients being taken to correspond to those of the 1s orbital from the variational calculation. We now make a new basis set, designated **B**, by combining the single contracted s function with the six s functions of basis set **A**. Calculations with basis set **B** give the same energy and dipole polarizability of the isolated H atom as basis set **A**. However, they give much smaller in magnitude $\Delta \langle T \rangle$ and $\Delta \langle V \rangle$ values and an appreciably different virial ratio than obtained using basis set **A**. Thus a basis set with multiple s functions rather than the single contracted s function is important

in establishing the virial theorem result. Indeed, it has been noted in prior studies that the lowering of the kinetic energy of H_2^+ at large R is associated with a delocalization of the electron density.[121]

We now progress to a detailed analysis of the various contributions to the kinetic energy and potential energy resulting from the perturbation (point charge or uniform efield). The ground state wave function of the H atom in the presence of the point charge or efield may be expressed in terms of the orbitals of the unperturbed H atom as

$$\psi = |1\mathrm{s}\rangle + \sum_{n=2} c_n^{(p)} |n\mathrm{p}\rangle + \sum_{n\neq 1} c_n^{(s)} |n\mathrm{s}\rangle \tag{5.8}$$

where only s and p basis functions are included as we are focusing on dipole polarization. The coefficients in eq 5.8 are given by

$$c_n^{(p)} = \frac{\langle n\mathrm{p}|V'|1\mathrm{s}\rangle}{\epsilon_{1\mathrm{s}} - \epsilon_{n\mathrm{p}}} \tag{5.9}$$

and

$$c_n^{(s)} = \sum_{m=2} \frac{\langle n\mathrm{s}|V'|m\mathrm{p}\rangle\langle m\mathrm{p}|V'|1\mathrm{s}\rangle}{(\epsilon_{1\mathrm{s}} - \epsilon_{n\mathrm{s}})(\epsilon_{1\mathrm{s}} - \epsilon_{m\mathrm{p}})} \tag{5.10}$$

In eqs 5.9 and 5.10 and ensuing equations, V' denotes the external perturbation, and the orbitals and orbital energies are the exact results for the non-relativistic Schrödinger equation (the Hamiltonian of which is denoted by $H^{(0)}$) for the H atom. In addition, the sums also include the continuum contributions.

If we retain energy contributions through second-order in the perturbation, the energy lowering relative to that of an isolated H atom (i.e., $\langle 1\mathrm{s}|H^{(0)}|1\mathrm{s}\rangle$) is

$$\sum_{n=2} \left[c_n^{(p)^2} (\langle n\mathrm{p}|H^{(0)}|n\mathrm{p}\rangle - \langle 1\mathrm{s}|H^{(0)}|1\mathrm{s}\rangle) + 2c_n^{(p)} \langle n\mathrm{p}|V'|1\mathrm{s}\rangle \right] \tag{5.11}$$

which, upon the substitution,

$$\langle n\mathrm{p}|H^{(0)}|n\mathrm{p}\rangle - \langle 1\mathrm{s}|H^{(0)}|1\mathrm{s}\rangle = \epsilon_{n\mathrm{p}} - \epsilon_{1\mathrm{s}} \tag{5.12}$$

reduces to

$$\sum_{n=2} \frac{\langle 1\mathrm{s}|V'|n\mathrm{p}\rangle\langle n\mathrm{p}|V'|1\mathrm{s}\rangle}{\epsilon_{1\mathrm{s}} - \epsilon_{n\mathrm{p}}} \tag{5.13}$$

which is the standard second-order perturbation result. Dalgarno and Lewis[118] showed that for a perturbation of the form $D\,r\cos\theta$, where $D = q/R^2$ and ε for the point charge and uniform fields, respectively, one can find a function $f = D(r^2/2 + r)\cos\theta$ such that

$$\langle n\mathrm{p}|V'|1\mathrm{s}\rangle = \langle n\mathrm{p}|[H^{(0)}, f]|1\mathrm{s}\rangle = (\epsilon_{n\mathrm{p}} - \epsilon_{1\mathrm{s}})\langle n\mathrm{p}|f|1\mathrm{s}\rangle \tag{5.14}$$

allowing eq 5.13 to be rewritten as

$$-\sum_{n=2}\langle 1\mathrm{s}|V'|n\mathrm{p}\rangle\langle n\mathrm{p}|f|1\mathrm{s}\rangle = -\langle 1\mathrm{s}|V'f|1\mathrm{s}\rangle \tag{5.15}$$

Elimination of the the $\sum|n\mathrm{p}\rangle\langle n\mathrm{p}|$ summation in the left-hand side of eq 5.15 was accomplished by use of the identity operator, which for the H atom is

$$1 = |1\mathrm{s}\rangle\langle 1\mathrm{s}| + \sum_{n\neq 1}|n\mathrm{s}\rangle\langle n\mathrm{s}| + \sum_{n=2}|n\mathrm{p}\rangle\langle n\mathrm{p}| + \ldots \tag{5.16}$$

Specifically $\sum|n\mathrm{p}\rangle\langle n\mathrm{p}|$ was replaced by 1, as the other terms in the expansion do not result in non-zero integrals. The resulting integral on the right-hand side of eq 5.15 may be readily evaluated, giving $-2.25R^{-4}$ for the point charge perturbation and $-2.25\varepsilon^2$ au for the uniform efield perturbation.[118]

We now consider the contributions of the various terms in the wave function to the averages of the kinetic energy operator and the $-1/r$ portion of the potential energy operator, retaining terms that are second-order in the interaction. The relevant averages are given by

$$\Delta\left\langle\hat{A}\right\rangle = -\sum_{n=2}(c_n^{(p)})^2\langle 1\mathrm{s}|\hat{A}|1\mathrm{s}\rangle + \sum_{n,m=2}c_n^{(p)}c_m^{(p)}\langle n\mathrm{p}|\hat{A}|m\mathrm{p}\rangle + 2\sum_{n\neq 1}c_n^{(s)}\langle n\mathrm{s}|\hat{A}|1\mathrm{s}\rangle \tag{5.17}$$

where $\hat{A}$ denotes either the kinetic energy operator or $-1/r$. The first term on the right-hand side of eq 5.17 is a result of normalization, which may be evaluated as follows

$$-\sum_{n=2}\langle 1\mathrm{s}|f|n\mathrm{p}\rangle\langle n\mathrm{p}|f|1\mathrm{s}\rangle\langle 1\mathrm{s}|\hat{A}|1\mathrm{s}\rangle = -\langle 1\mathrm{s}|f^2|1\mathrm{s}\rangle\langle 1\mathrm{s}|\hat{A}|1\mathrm{s}\rangle \tag{5.18}$$

In accomplishing this simplification we made use of the fact that the $(c_n^{(p)})^2$ factor in eq 5.17 can be rewritten as $\langle 1\mathrm{s}|f|n\mathrm{p}\rangle\langle n\mathrm{p}|f|1\mathrm{s}\rangle$ by two applications of the Dalgarno–Lewis procedure again with $f = D(r^2/2 + r)\cos\theta$, and the replacement of $\sum|n\mathrm{p}\rangle\langle n\mathrm{p}|$ with 1 as discussed

above. The two integrals in the right-most term of eq 5.18, $\langle 1s|f^2|1s\rangle$ and $\langle 1s|\hat{A}|1s\rangle$, are readily evaluated with the results being presented in Table 5.2 below.

The second term on the right-hand side of eq 5.17 may be evaluated as

$$\sum_{n,m=2} \frac{\langle 1s|V'|np\rangle\langle np|\hat{A}|mp\rangle\langle mp|V'|1s\rangle}{(\epsilon_{1s}-\epsilon_{np})(\epsilon_{1s}-\epsilon_{mp})} = \sum_{n,m=2} \langle 1s|f|np\rangle\langle np|\hat{A}|mp\rangle\langle mp|f|1s\rangle = \langle 1s|f\hat{A}f|1s\rangle \tag{5.19}$$

In deriving this result, the Dalgarno–Lewis substitution was made twice and the identity operator was used twice to eliminate the summations. The values of this contribution for the two choices of $\hat{A}$ are summarized in Table 5.2.

Table 5.2: Contributions to $\Delta\langle T\rangle$ and $\Delta\langle V\rangle$ for an H atom perturbed by a point charge or a uniform efield evaluated in the complete basis set limit.

Contribution	$\Delta\langle T\rangle$ [a]	$\Delta\langle V\rangle$ [a]
$-\sum (c_n^{(p)})^2\langle 1s|\hat{A}|1s\rangle$	$-43/16$	$86/16$
$2\sum c_n^{(p)}\langle 1s|V'|np\rangle$		$-72/16$
$\sum\sum c_n^{(p)}c_m^{(p)}\langle np|\hat{A}|mp\rangle$	$27/16$	$-34/16$
$2\sum c_n^{(s)}\langle 1s|\hat{A}|ns\rangle$	$-92/16$	$92/16$
Total	$-27/4$	$18/4$

[a] The quantities reported are the coefficients of R^{-4} or ε^2.

The third contribution from eq 5.17 may be re-expressed as

$$2\sum_{\substack{n\neq 1,\\ m=2}} \frac{\langle 1s|V'|mp\rangle\langle mp|V'|ns\rangle\langle ns|\hat{A}|1s\rangle}{(\epsilon_{1s}-\epsilon_{mp})(\epsilon_{1s}-\epsilon_{ns})} = -2\sum_{n\neq 1} \frac{\langle 1s|fV'|ns\rangle\langle ns|\hat{A}|1s\rangle}{\epsilon_{1s}-\epsilon_{ns}}$$
$$= 2\sum_{n\neq 1} \langle 1s|fV'|ns\rangle\langle ns|g|1s\rangle \tag{5.20}$$

The first simplification made use of the Dalgarno–Lewis method and insertion of the identity operator to eliminate the sum over the p functions. The first simplification made use of the Dalgarno–Lewis method and insertion of the identity operator to eliminate the sum over the p functions. However, to deal with the sum over the ns ($n \neq 1$) functions required deriving functions g for which $\langle ns|[H^{(0)},g]|1s\rangle = \langle ns|\hat{A}|1s\rangle$ for $\hat{A}$ corresponding to the kinetic energy operator and $-1/r$. The g functions and their derivations are presented

in section 5.6 Supporting Information. Using the identity operator, the last term of eq 5.20 can be simplified as follows

$$2\sum_{n\neq 1}\langle 1\mathrm{s}|fV'|n\mathrm{s}\rangle\langle n\mathrm{s}|g|1\mathrm{s}\rangle = 2\langle 1\mathrm{s}|fV'g|1\mathrm{s}\rangle - 2\langle 1\mathrm{s}|fV'|1\mathrm{s}\rangle\langle 1\mathrm{s}|g|1\mathrm{s}\rangle \tag{5.21}$$

The integrals on the right-hand side of eq 5.21 are readily evaluated, and their contributions are included in Table 5.2.

As seen from eq 5.21 (and eq 5.40 of the section 5.6 Supporting Information), the contributions of the excited s levels to the average kinetic energy and average of $-1/r$ are proportional to D^2. However, if one considers the contribution of these terms to the total energy, they give a contribution proportional to D^4. In other words, the contribution is a consequence of the γ hyperpolarizability.

Table 5.2 reports the coefficients of the various contributions to $\Delta\langle T\rangle$ and $\Delta\langle V\rangle$. To obtain the energy contributions these need to be multiplied by R^{-4} and ε^2, in the case of the point charge and efield, respectively. Table 5.2 also includes the potential energy contribution from the second term of eq 5.11, which arises solely from the perturbation and does not involve matrix elements of the kinetic energy operator or $-1/r$.

Table 5.3: Contributions to $\Delta\langle T\rangle$ and $\Delta\langle V\rangle$ for an H atom perturbed by a point charge or a uniform efield evaluated in the complete basis set limit with the diagonal and off-diagonal $\langle n\mathrm{p}|\hat{A}|m\mathrm{p}\rangle$ contributions split apart.

Contribution	$\Delta\langle T\rangle$	$\Delta\langle V\rangle$
$\sum(c_n^{(p)})^2(\langle n\mathrm{p}\|\hat{A}\|n\mathrm{p}\rangle - \langle 1\mathrm{s}\|\hat{A}\|1\mathrm{s}\rangle)$	U	$-2U$
$2\sum c_n^{(p)}\langle 1\mathrm{s}\|V'\|n\mathrm{p}\rangle$		$2U$
$\sum\sum c_n^{(p)}c_m^{(p)}\langle n\mathrm{p}\|\hat{A}\|m\mathrm{p}\rangle$ (off-diag)	$-5/9U$	$5/9U$
$2\sum c_n^{(s)}\langle 1\mathrm{s}\|\hat{A}\|n\mathrm{s}\rangle$	$23/9U$	$-23/9U$
Total	$3U$	$-2U$

The sum of the various contributions to $\Delta\langle T\rangle$ and $\Delta\langle V\rangle$ agree exactly with the shifts predicted by the virial theorem (eq 5.6). We find it instructive to separate the diagonal and off-diagonal contributions from the terms with the $\langle n\mathrm{p}|\hat{A}|m\mathrm{p}\rangle$ factor and to combine

the diagonal $\langle n\mathrm{p}|\hat{A}|n\mathrm{p}\rangle$ contribution with that involving the $\langle 1\mathrm{s}|\hat{A}|1\mathrm{s}\rangle$ factor. The regrouped terms are reported in Table 5.3.

As required, for the terms involving diagonal matrix elements of $\hat{A}$, the $\Delta\langle V\rangle$ contribution is minus twice the $\Delta\langle T\rangle$ contribution, while for terms involving the off-diagonal $\langle n\mathrm{p}|\hat{A}|m\mathrm{p}\rangle$ elements, the $\Delta\langle V\rangle$ contribution is minus the $\Delta\langle T\rangle$ contribution. If the terms involving the non-diagonal $\langle 1\mathrm{s}|\hat{A}|n\mathrm{s}\rangle$ and $\langle n\mathrm{p}|\hat{A}|m\mathrm{p}\rangle$ matrix elements are grouped together, their net contributions to $\Delta\langle T\rangle$ and $\Delta\langle V\rangle$ are $2U$ and $-2U$, respectively.

The use of Dalgarno–Lewis perturbation theory together with the identity operator also allows us to express the wave function in eq 5.8 in a simple analytical form:

$$\psi = \left\{1 - D\left(\frac{r^2}{2} + r\right)\cos\theta + D^2\left[\left(\frac{r^4}{16} + \frac{3r^3}{8} + \frac{9r^2}{8}\right)\left(\cos^2\theta + \frac{1}{3}\right) - \frac{81}{16}\right]\right\}|1\mathrm{s}\rangle \quad (5.22)$$

where the second term accounts for the contribution from the p orbitals (i.e., the hybridization) and the third term results from the $|n\mathrm{s}\rangle$, $n \neq 1$, orbitals, which enter via mixing with the p orbitals. (The derivation of this contribution is given in the section 5.6 Supporting Information.) The term accounting for the admixture of the $|n\mathrm{s}\rangle$ levels is largely responsible for the lowering of the kinetic energy due to the external field, and is associated with an increase in the radial extent of the charge distribution of the H atom.

Figure 5.1 reports the change in charge density caused by the field-induced admixture of the $|n\mathrm{s}\rangle$, $n \neq 1$, states into the wave function. As seen from the figure for a field of $\varepsilon = 0.01$ au, the admixture with the ns orbitals results in a radial shift of $\sim$0.0005 $|e|$ from short r to $2 \sim 6.5$ Bohrs from the nucleus.

5.4 Conclusions

The molecular virial theorem predicts that the interaction of an atom with a distant point charge lowers the kinetic energy by $3|U|$ and raises the potential energy by $2|U|$, where $U = -0.5\alpha R^{-4}$. For the case of an H atom interacting with a point charge at large R, exact expressions can be obtained for the various contributions to the kinetic and potential energy changes by use of a procedure introduced by Dalgarno and Lewis. Although the exact

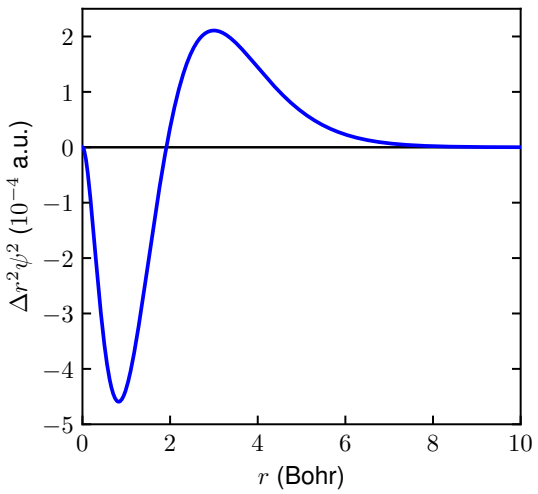

Figure 5.1: Change in $r^2\psi^2$ in going from the unperturbed 1s orbital to allowing for the field-induced admixture of excited ns orbitals, for an external uniform field of 0.01 au.

polarizability and energy at large R can be obtained using second order perturbation theory with a basis set with a single s function (provided it is the 1s eigenfunction of the isolated atom) and a complete set of p eigenfunctions, in order to accurately describe the kinetic and potential energy changes due to the interaction requires using a flexible set of s functions due to the importance of matrix elements of the form $\langle 1\mathrm{s}|\hat{A}|n\mathrm{s}\rangle$, as well as allowing mixing of the different p functions through the kinetic energy or $-1/r$ operators.

Although we have focused here on the contributions to the kinetic and potential energies of an H atom in an electric field, we note that the same strategy can be applied to evaluate the changes in the average kinetic and potential energies of two H atoms at large internuclear separation where dispersion interactions dominate.

5.5 Acknowledgements

This research was supported by the National Science Foundation, under Grant No. CHE1762337. The calculations were carried out on computers in the University of Pittsburgh's Center for Research Computing. We acknowledge useful discussions with Jack Simons and Stephen Slimak.

5.6 Supporting Information

5.6.1 Function g

In eq 5.17 of the text there are factors of the form $\langle n\mathrm{s}|\hat{A}|1\mathrm{s}\rangle\,/(\epsilon_{1\mathrm{s}} - \epsilon_{n\mathrm{s}})$. In order to eliminate the energy denominator, we need to identify a function g for which

$$(\epsilon_{n\mathrm{s}} - \epsilon_{1\mathrm{s}})\langle n\mathrm{s}|g|1\mathrm{s}\rangle = \langle n\mathrm{s}|\hat{A}|1\mathrm{s}\rangle \tag{5.23}$$

For an operator $\hat{A}$ for which $\langle 1\mathrm{s}|\hat{A}|1\mathrm{s}\rangle = 0$, g can be found by solving

$$[H^{(0)}, g]\,|1\mathrm{s}\rangle = \hat{A}\,|1\mathrm{s}\rangle \tag{5.24}$$

as was done in the original application of the Dalgarno-Lewis procedure[118] to the $D\,r\cos\theta$ operator. However, if the operator of interest has non-zero diagonal matrix elements, as do the kinetic energy and $-1/r$ operators of the H atom, then we need to use the more general equation[123]

$$[H^{(0)}, g]\,|1\mathrm{s}\rangle = (\hat{A} - \langle 1\mathrm{s}|\hat{A}|1\mathrm{s}\rangle)\,|1\mathrm{s}\rangle \tag{5.25}$$

We consider first the situation that $\hat{A} = -1/r$, for which $\langle 1\mathrm{s}|\hat{A}|1\mathrm{s}\rangle = -1$. For the H atom, in the case that $l = 0$, the radial Hamiltonian is

$$H^{(0)} = -\frac{1}{2}\frac{d^2}{dr^2} - \frac{1}{r}\frac{d}{dr} - \frac{1}{r} \tag{5.26}$$

Using this in eq 5.25 gives the differential equation

$$rg'' + 2g'(1 - r) + 2r - 2 = 0 \tag{5.27}$$

which has the solution

$$g = r + c_1 \left(-\frac{e^{2r}}{r} + 2Ei[2r] \right) + c_2 \tag{5.28}$$

The differential equation was solved using Mathematica.[124] We require

$$\langle 2\mathrm{s}|g|1\mathrm{s}\rangle = -\frac{\langle 2\mathrm{s}|-\frac{1}{r}|1\mathrm{s}\rangle}{\epsilon_{1\mathrm{s}} - \epsilon_{2\mathrm{s}}} \tag{5.29}$$

which is satisfied with the choice $c_1 = c_2 = 0$. Thus, for the $-1/r$ operator the appropriate function g is r. Since $\langle n\mathrm{s}|H^{(0)}|1\mathrm{s}\rangle = 0$ when $n \neq 1$, it follows that

$$\langle n\mathrm{s}|-\frac{1}{2}\frac{d^2}{dr^2} - \frac{1}{r}\frac{d}{dr}|1\mathrm{s}\rangle = -\langle n\mathrm{s}|-\frac{1}{r}|1\mathrm{s}\rangle \tag{5.30}$$

Thus, $-r$ is the appropriate choice for g when $\hat{A}$ is the kinetic energy operator. That $g = -r$ in this case can also be demonstrated using eq 5.25 with $\hat{A}$ chosen to be the kinetic energy operator.

5.6.2 Function h

The functional form of the wave function of the H atom in the presence of a field or a point charge with the terms through second order is given in eq 5.8 of the text. As follows from the main text, the $\sum c_n^{(p)} |n\mathrm{p}\rangle$ contribution is given by $-D(r^2/2 + r)\cos\theta\,|1\mathrm{s}\rangle$. It remains to find the analytical functional form of $c_n^{(s)}$ coefficient given by eq 5.10. $c_n^{(s)}$ can be simplified by applying the Dalgarno-Lewis procedure (eq 5.14) to eliminate the $\epsilon_{1\mathrm{s}} - \epsilon_{n\mathrm{p}}$ denominator to give

$$c_n^{(s)} = -\sum_{m=2} \frac{\langle n\mathrm{s}|V'|m\mathrm{p}\rangle\langle m\mathrm{p}|f|1\mathrm{s}\rangle}{\epsilon_{1\mathrm{s}} - \epsilon_{n\mathrm{s}}} \tag{5.31}$$

By application of the identity operator, this can be further simplified to

$$c_n^{(s)} = -\frac{\langle n\mathrm{s}|fV'|1\mathrm{s}\rangle}{\epsilon_{1\mathrm{s}} - \epsilon_{n\mathrm{s}}} \tag{5.32}$$

We find a function h to eliminate the energy denominator, accounting for non-zero diagonal matrix elements of the fV' operator

$$[H^{(0)}, h]\,|1\mathrm{s}\rangle = (fV' - \langle 1\mathrm{s}|fV'|1\mathrm{s}\rangle)\,|1\mathrm{s}\rangle \tag{5.33}$$

Both f and V' contain factors of $\cos\theta$ which leads to us try $h = D^2 b(\cos^2\theta + c)$, where b is a function of r and c is a constant. Evaluating the commutator, and then cancelling the D^2 factor and the $|1s\rangle$ function that appear on both sides of eq 5.33 gives the following differential equation

$$(\cos^2\theta + c)\left(-\frac{b''}{2} + b' - \frac{b'}{r}\right) + \frac{b}{r^2}(3\cos^2\theta - 1) = \left(\frac{r^3}{2} + r^2\right)\cos^2\theta - \frac{9}{4} \tag{5.34}$$

Integrating out the θ dependence gives the differential equation

$$\left(\frac{2}{3} + 2c\right)\left(-\frac{b''}{2} + b' - \frac{b'}{r}\right) = \frac{2}{3}\left(\frac{r^3}{2} + r^2\right) - \frac{9}{2} \tag{5.35}$$

which is solved with Mathematica[124] to give

$$b = \frac{r^4 + 6r^3 + 18r^2}{8(1+3c)} + c_1\left(-\frac{e^{2r}}{r} + 2Ei[2r]\right) + c_2 \tag{5.36}$$

To satisfy

$$\langle 2s|h|1s\rangle = -\frac{\langle 2s|fV'|1s\rangle}{\epsilon_{1s} - \epsilon_{2s}} \tag{5.37}$$

it is necessary to choose $c = 1/3$ and $c_1 = c_2 = 0$. It follows that

$$h = D^2\left(\frac{r^4}{16} + \frac{3r^3}{8} + \frac{9r^2}{8}\right)\left(\cos^2\theta + \frac{1}{3}\right) \tag{5.38}$$

Thus, $c_n^{(s)}$ is given by

$$c_n^{(s)} = \langle ns|h|1s\rangle \tag{5.39}$$

Using the identity operator, the contribution to the wave function from the sum over the $|ns\rangle$ states becomes

$$\begin{aligned}\sum_{n\neq 1} c_n^{(s)}|ns\rangle &= \sum_{n\neq 1}|ns\rangle\langle ns|h|1s\rangle = h|1s\rangle - \langle 1s|h|1s\rangle|1s\rangle \\ &= D^2\left[\left(\frac{r^4}{16} + \frac{3r^3}{8} + \frac{9r^2}{8}\right)\left(\cos^2\theta + \frac{1}{3}\right) - \frac{81}{16}\right]|1s\rangle\end{aligned} \tag{5.40}$$

where substitution of $\langle 1s|h|1s\rangle = 81D^2/16$ was made.

6.0 Summary

In this work it was illustrated that accounting for electron correlation effects is essential for describing weakly bound non-valence anion states of molecules and molecular clusters, as well as non-valence temporary anion shape resonances. These studies indicate that a highly polarizable system for which electrostatic interactions alone are not sufficiently attractive to bind an excess electron will possess non-valence correlation-bound anion states. The excess electron in such species is bound in a spatially diffuse orbital by long-range dispersion-like correlation interactions. The equation of motion coupled-cluster method was the main theoretical approach used in the present work. Other approaches that can characterize non-valence correlation-bound anions are second-order algebraic diagrammatic construction, orbital-optimized second-order Møller-Plesset perturbation theory, and Brueckner coupled-cluster methods. These methods allow for orbital relaxation in response to the dispersion type correlation between the excess electron and valence electrons of the molecule or cluster at hand. The accuracy of these methods depends on the nature of the molecule or cluster.

In calculations involving non-valence anions, a combination of electrostatic and correlation interactions is responsible for the binding of the excess electron. Molecules or clusters can also possess non-valence temporary anion shape resonances that are higher in energy than the neutral ground state. These shape resonances exist as a result of the excess electron being trapped by an angular momentum barrier. The resonances can be characterized by a complex energy which is determined as a function of the geometry. The model $(H_2O)_4$ cluster contains two dimers and the distance between them is varied. The asymmetric combination of the dipole-bound anion states of the dimers creates the temporary anion shape resonance. The resonance energy increases with decreasing distance between the dimers. The rhombic structure of $(NaCl)_2$ is distorted along the symmetric breathing mode. The antibonding combination of the orbitals of the sodium atoms result in the shape resonance. The resonance energy increases when the distortion reduces the distance between the sodium atoms.

EOM-CCSD calculations are computationally demanding, and, therefore, not applicable to large molecules or clusters. For treating larger systems, one will have to utilize one-electron model potentials with explicit treatment of polarization. Though not described here in detail, such potentials treat the neutral molecule classically and only describe its interaction with the excess electron quantum mechanically. However, to be successful, these models need to be parameterized based on high-level *ab initio* calculations, such as those presented in this thesis.

The last part of the thesis involves studies of the molecular virial theorem using an H atom interacting with a uniform electric field or with a point charge. Dalgarno-Lewis perturbation theory is used to find exact analytical expressions to the changes of the kinetic and potential energies. This approach can also be extended to treat, for example, two interacting H atoms at large separation to analyze dispersion interactions.

Bibliography

[1] Jordan, K. D.; Wang, F. Theory of dipole-bound anions. *Annu. Rev. Phys. Chem.* **2003**, *54*, 367–396.

[2] Fermi, E.; Teller, E. The capture of negative mesotrons in matter. *Phys. Rev.* **1947**, *72*, 399–408.

[3] Brown, W. B.; Roberts, R. E. On the critical binding of an electron by an electric dipole. *J. Chem. Phys.* **1967**, *46*, 2006–2007.

[4] Turner, J. E.; Anderson, V. E.; Fox, K. Ground-state energy eigenvalues and eigenfunctions for an electron in an electric-dipole field. *Phys. Rev.* **1968**, *174*, 81–89.

[5] Sevilla, M. D.; Besler, B.; Colson, A.-O. Ab initio molecular orbital calculations of DNA radical ions. 5. Scaling of calculated electron affinities and ionization potentials to experimental values. *J. Phys. Chem.* **1995**, *99*, 1060–1063.

[6] Voora, V. K.; Cederbaum, L. S.; Jordan, K. D. Existence of a correlation bound s-type anion state of C_{60}. *J. Phys. Chem. Lett.* **2013**, *4*, 849–853.

[7] Sommerfeld, T.; Bhattarai, B.; Vysotskiy, V.; Cederbaum, L. S. Correlation-bound anions of NaCl clusters. *J. Chem. Phys.* **2010**, *133*, 114301.

[8] Voora, V. K.; Jordan, K. D. Nonvalence correlation-bound anion state of C_6F_6: Doorway to low-energy electron capture. *J. Phys. Chem. A* **2014**, *118*, 7201–7205.

[9] Born, M.; Oppenheimer, R. Zur quantentheorie der molekeln. *Ann. Phys.* **1927**, *389*, 457–484.

[10] Čížek, J. On the correlation problem in atomic and molecular systems. Calculation of wavefunction components in Ursell-type expansion using quantum-field theoretical methods. *J. Chem. Phys.* **1966**, *45*, 4256–4266.

[11] Purvis, G. D.; Bartlett, R. J. A full coupled-cluster singles and doubles model: The inclusion of disconnected triples. *J. Chem. Phys.* **1982**, *76*, 1910–1918.

[12] Stanton, J. F.; Bartlett, R. J. The equation of motion coupled-cluster method. A systematic biorthogonal approach to molecular excitation energies, transition probabilities, and excited state properties. *J. Chem. Phys.* **1993**, *98*, 7029–7039.

[13] Schulz, G. J. Resonances in electron impact on diatomic molecules. *Rev. Mod. Phys.* **1973**, *45*, 423–486.

[14] Siegert, A. J. F. On the derivation of the dispersion formula for nuclear reactions. *Phys. Rev.* **1939**, *56*, 750–752.

[15] Hazi, A. U.; Taylor, H. S. Stabilization method of calculating resonance energies: Model problem. *Phys. Rev. A: At., Mol., Opt. Phys.* **1970**, *1*, 1109–1120.

[16] Jordan, K. D. Applications of analytic continuation in the construction of potential energy curves. *Int. J. Quantum Chem.* **1975**, *9*, 325–336.

[17] Falcetta, M. F.; Reilly, N. D.; Jordan, K. D. Stabilization calculations of the low-lying temporary anions states of Be, Mg, and Ca. *Chem. Phys.* **2017**, *482*, 239–243.

[18] Chao, J. S.-Y.; Falcetta, M. F.; Jordan, K. D. Application of the stabilization method to the N_2^- ($1^2\Pi_g$) and Mg^- (1^2P) temporary anion states. *J. Chem. Phys.* **1990**, *93*, 1125–1135.

[19] Simons, J.; Jordan, K. D. Ab initio electronic structure of anions. *Chem. Rev.* **1987**, *87*, 535–555.

[20] Bezchastnov, V. G.; Vysotskiy, V. P.; Cederbaum, L. S. Anions of Xenon clusters bound by long-range electron correlations. *Phys. Rev. Lett.* **2011**, *107*, 133401.

[21] Wang, F.; Jordan, K. D. Parallel-tempering Monte Carlo simulations of the finite temperature behavior of $(H_2O)_6^-$. *J. Chem. Phys.* **2003**, *119*, 11645–11653.

[22] Chipman, D. M. Theoretical study on the electron affinity of the water dimer. *J. Phys. Chem.* **1979**, *83*, 1657–1662.

[23] Wang, F.; Jordan, K. D. A Drude-model approach to dispersion interactions in dipole-bound anions. *J. Chem. Phys.* **2001**, *114*, 10717–10724.

[24] Sommerfeld, T. Multipole-bound states of succinonitrile and other dicarbonitriles. *J. Chem. Phys.* **2004**, *121*, 4097–4104.

[25] Voora, V. K.; Jordan, K. D. Nonvalence correlation-bound anion states of polycyclic aromatic hydrocarbons. *J. Phys. Chem. Lett.* **2015**, *6*, 3994–3997.

[26] Herbert, J. M. The quantum chemistry of loosely-bound electrons. *Rev. Comput. Chem.* **2015**, *28*, 391–517.

[27] Sommerfeld, T. Method for visualizing and quantifying the nonvalence character of excess electrons. *J. Chem. Theory Comput.* **2013**, *9*, 4866–4873.

[28] Janesko, B. G.; Scalmani, G.; Frisch, M. J. Quantifying solvated electrons' delocalization. *Phys. Chem. Chem. Phys.* **2015**, *17*, 18305–18317.

[29] Koopmans, T. Über die zuordnung von wellenfunctionen und eigenwerten zu den einzelnen elektronen eines atoms. *Physica* **1934**, *1*, 104–113.

[30] Pople, J. A.; Head-Gordon, M.; Raghavachari, K. Quadratic configuration interaction. A general technique for determining electron correlation energies. *J. Chem. Phys.* **1987**, *87*, 5968–5975.

[31] Møller, C.; Plesset, M. S. Note on an approximation treatment for many-electron systems. *Phys. Rev.* **1934**, *46*, 618–622.

[32] Schirmer, J.; Cederbaum, L. S.; Walter, O. New approach to the one-particle Green's function for finite Fermi systems. *Phys. Rev. A* **1983**, *28*, 1237–1259.

[33] Nooijen, M.; Snijders, J. G. Second order many-body perturbation approximations to the coupled cluster Green's function. *J. Chem. Phys.* **1995**, *102*, 1681–1688.

[34] Stanton, J. F.; Gauss, J. Perturbative treatment of the similarity transformed Hamiltonian in equation-of-motion coupled-cluster approximations. *J. Chem. Phys.* **1995**, *103*, 1064–1076.

[35] Nooijen, M.; Bartlett, R. J. Equation of motion coupled cluster method for electron attachment. *J. Chem. Phys.* **1995**, *102*, 3629–3647.

[36] Saeh, J. C.; Stanton, J. F. Application of an equation-of-motion coupled cluster method including higher-order corrections to potential energy surfaces of radicals. *J. Chem. Phys.* **1999**, *111*, 8275–8285.

[37] Matthews, D. A.; Stanton, J. F. A new approach to approximate equation-of-motion coupled cluster with triple excitations. *J. Chem. Phys.* **2016**, *145*, 124102.

[38] Bozkaya, U.; Turney, J. M.; Yamaguchi, Y.; Schaefer, H. F.; Sherrill, C. D. Quadratically convergent algorithm for orbital optimization in the orbital-optimized coupled-cluster doubles method and in orbital-optimized second-order Møller-Plesset perturbation theory. *J. Chem. Phys.* **2011**, *135*, 104103.

[39] Neese, F.; Schwabe, T.; Kossmann, S.; Schirmer, B.; Grimme, S. Assessment of orbital-optimized, spin-component scaled second-order many-body perturbation theory for thermochemistry and kinetics. *J. Chem. Theory Comput.* **2009**, *5*, 3060–3073.

[40] Handy, N. C.; Pople, J. A.; Head-Gordon, M.; Raghavachari, K.; Trucks, G. W. Size-consistent Brueckner theory limited to double substitutions. *Chem. Phys. Lett.* **1989**, *164*, 185–192.

[41] Hedin, L. New method for calculating the one-particle green's function with application to the electron-gas problem. *Phys. Rev.* **1965**, *139*, A796–A823.

[42] Becke, A. D. Density-functional thermochemistry. III. The role of exact exchange. *J. Chem. Phys.* **1993**, *98*, 5648–5652.

[43] Lee, C.; Yang, W.; Parr, R. G. Development of the Colle-Salvetti correlation-energy formula into a functional of the electron density. *Phys. Rev. B* **1988**, *37*, 785–789.

[44] Vosko, S. H.; Wilk, L.; Nusair, M. Accurate spin-dependent electron liquid correlation energies for local spin density calculations: a critical analysis. *Can. J. Phys.* **1980**, *58*, 1200–1211.

[45] Noga, J.; Bartlett, R. J. The full CCSDT model for molecular electronic structure. *J. Chem. Phys.* **1987**, *86*, 7041–7050.

[46] Stanton, J.; Gauss, J.; Cheng, L.; Harding, M.; Matthews, D.; Szalay, P. CFOUR, coupled-cluster techniques for computational chemistry. 2010.

[47] Turney, J. M. et al. Psi4: an open-source ab initio electronic structure program. *Wiley Interdiscip. Rev.: Comput. Mol. Sci.* **2012**, *2*, 556–565.

[48] Furche, F.; Ahlrichs, R.; Hättig, C.; Klopper, W.; Sierka, M.; Weigend, F. Turbomole. *Wiley Interdiscip. Rev.: Comput. Mol. Sci.* **2014**, *4*, 91–100.

[49] Voora, V. K.; Ding, J.; Sommerfeld, T.; Jordan, K. D. A self-consistent polarization potential model for describing excess electrons interacting with water clusters. *J. Phys. Chem. B* **2013**, *117*, 4365–4370.

[50] Dunning, T. H., Jr. Gaussian basis sets for use in correlated molecular calculations. I. The atoms boron through neon and hydrogen. *J. Chem. Phys.* **1989**, *90*, 1007–1023.

[51] Kendall, R. A.; Dunning, T. H., Jr.; Harrison, R. J. Electron affinities of the first-row atoms revisited. Systematic basis sets and wave functions. *J. Chem. Phys.* **1992**, *96*, 6796–6806.

[52] Vysotskiy, V. P.; Cederbaum, L. S.; Sommerfeld, T.; Voora, V. K.; Jordan, K. D. Benchmark calculations of the energies for binding excess electrons to water clusters. *J. Chem. Theory Comput.* **2012**, *8*, 893–900.

[53] Sanche, L.; Schulz, G. J. Electron transmission spectroscopy: Resonances in triatomic molecules and hydrocarbons. *J. Chem. Phys.* **1973**, *58*, 479–493.

[54] Sommerfeld, T. A fresh look at the $^2A_1$ CO_2^- potential energy surface. *J. Phys. B: At., Mol., Opt. Phys.* **2003**, *36*, L127–L133.

[55] Yoshioka, Y.; Schaefer, H. F.; Jordan, K. D. Theoretical investigation of the electron affinity of CO_2. *J. Chem. Phys.* **1981**, *75*, 1040–1041.

[56] Gutsev, G. L.; Bartlett, R. J.; Compton, R. N. Electron affinities of CO_2, OCS, and CS_2. *J. Chem. Phys.* **1998**, *108*, 6756–6762.

[57] Sommerfeld, T.; Meyer, H.-D.; Cederbaum, L. S. Potential energy surface of the CO_2^- anion. *Phys. Chem. Chem. Phys.* **2004**, *6*, 42–45.

[58] Vanroose, W.; McCurdy, C. W.; Rescigno, T. N. Interpretation of low-energy electron-CO_2 scattering. *Phys. Rev. A* **2002**, *66*, 032720.

[59] Harbach, P. H. P.; Wormit, M.; Dreuw, A. The third-order algebraic diagrammatic construction method (ADC(3)) for the polarization propagator for closed-shell molecules: Efficient implementation and benchmarking. *J. Chem. Phys.* **2014**, *141*, 064113.

[60] Widmark, P.; Malmqvist, P.; Roos, B. Density matrix averaged atomic natural orbital (ANO) basis sets for correlated molecular wave functions. *Theoret. Chim. Acta* **1990**, *77*, 291–306.

[61] Dunning, T. H. Gaussian basis functions for use in molecular calculations. III. Contraction of (10s6p) atomic basis sets for the first-row atoms. *J. Chem. Phys.* **1971**, *55*, 716–723.

[62] Vanroose, W.; Zhang, Z.; McCurdy, C. W.; Rescigno, T. N. Threshold vibrational excitation of CO_2 by slow electrons. *Phys. Rev. Lett.* **2004**, *92*, 053201.

[63] Compton, R. N.; Reinhardt, P. W.; Cooper, C. D. Collisional ionization between fast alkali atoms and selected hexafluoride molecules. *J. Chem. Phys.* **1978**, *68*, 2023–2036.

[64] Frisch, M. J.; Trucks, G. W.; Schlegel, H. B.; Scuseria, G. E.; Robb, M. A.; Cheeseman, J. R.; Scalmani, G.; Barone, V.; Mennucci, B.; Petersson, G. A., et al. Gaussian 09 Revision A.03. 2009; Gaussian Inc. Wallingford CT.

[65] Barone, V. Anharmonic vibrational properties by a fully automated second-order perturbative approach. *J. Chem. Phys.* **2005**, *122*, 014108.

[66] Chowdhury, S.; Kebarle, P. Electron affinities of di- and tetracyanoethylene and cyanobenzenes based on measurements of gas-phase electron-transfer equilibria. *J. Am. Chem. Soc.* **1986**, *108*, 5453–5459.

[67] Burrow, P. D.; Howard, A. E.; Johnston, A. R.; Jordan, K. D. Temporary anion states of hydrogen cyanide, methyl cyanide, and methylene dicyanide, selected cyanoethylenes, benzonitrile, and tetracyanoquinodimethane. *J. Phys. Chem.* **1992**, *96*, 7570–7578.

[68] Perdew, J. P.; Burke, K.; Ernzerhof, M. Generalized gradient approximation made simple. *Phys. Rev. Lett.* **1996**, *77*, 3865–3868.

[69] Voora, V. K.; Jordan, K. D. Nonvalence correlation-bound anion states of spherical fullerenes. *Nano Lett.* **2014**, *14*, 4602–4606.

[70] Echenique, P. M.; Pendry, J. B. The existence and detection of Rydberg states at surfaces. *J. Phys. C: Solid State Phys.* **1978**, *11*, 2065–2075.

[71] Echenique, P.; Uranga, M. Image potential states at surfaces. *Surf. Sci.* **1991**, *247*, 125–132.

[72] Silkin, V. M.; Zhao, J.; Guinea, F.; Chulkov, E. V.; Echenique, P. M.; Petek, H. Image potential states in graphene. *Phys. Rev. B* **2009**, *80*, 121408.

[73] Stampfli, P. Theory for the electron affinity of clusters of rare gas atoms and polar molecules. *Phys. Rep.* **1995**, *255*, 1–77.

[74] Desfrançois, C.; Abdoul-Carime, H.; Schermann, J.-P. Ground-state dipole-bound anions. *Int. J. Mod. Phys. B* **1996**, *10*, 1339–1395.

[75] Voora, V. K.; Kairalapova, A.; Sommerfeld, T.; Jordan, K. D. Theoretical approaches for treating non-valence correlation-bound anions. *J. Chem. Phys.* **2017**, *147*, 214114.

[76] Rogers, J. P.; Anstöter, C. S.; Verlet, J. R. R. Ultrafast dynamics of low-energy electron attachment via a non-valence correlation-bound state. *Nat. Chem.* **2018**, *10*, 341–346.

[77] Rogers, J. P.; Anstöter, C. S.; Verlet, J. R. R. Evidence of electron capture of an outgoing photoelectron wave by a nonvalence state in $(C_6F_6)n^-$. *J. Phys. Chem. Lett.* **2018**, *9*, 2504–2509.

[78] Sommerfeld, T. Coupling between dipole-bound and valence states: the nitromethane anion. *Phys. Chem. Chem. Phys.* **2002**, *4*, 2511–2516.

[79] Hotop, H.; Ruf, M.-W.; Allan, M.; Fabrikant, I. I. Resonance and threshold phenomena in low-energy electron collisions with molecules and clusters. *Adv. At., Mol., Opt. Phys.* **2003**, *49*, 85–216.

[80] Sommerfeld, T.; Dreux, K. M.; Joshi, R. Excess electrons bound to molecular systems with a vanishing dipole but large molecular quadrupole. *J. Phys. Chem. A* **2014**, *118*, 7320–7329.

[81] Desfrançois, C.; Bouteiller, Y.; Schermann, J. P.; Radisic, D.; Stokes, S. T.; Bowen, K. H.; Hammer, N. I.; Compton, R. N. Long-range electron binding to quadrupolar molecules. *Phys. Rev. Lett.* **2004**, *92*, 083003.

[82] Garrett, W. R. Quadrupole-bound anions: Efficacy of positive versus negative quadrupole moments. *J. Chem. Phys.* **2012**, *136*, 054116.

[83] Garrett, W. R. Critical electron binding to linear electric quadrupole systems. *J. Chem. Phys.* **2008**, *128*, 194309.

[84] Compton, R.; Dunning, F.; Nordlander, P. On the binding of electrons to CS_2: Possible role of quadrupole-bound states. *Chem. Phys. Lett.* **1996**, *253*, 8–12.

[85] Zhu, G.-Z.; Liu, Y.; Wang, L.-S. Observation of excited quadrupole-bound states in cold anions. *Phys. Rev. Lett.* **2017**, *119*, 023002.

[86] Abdoul-Carime, H.; Desfrançois, C. Electrons weakly bound to molecules by dipolar, quadrupolar or polarization forces. *Eur. Phys. J. D* **1998**, *2*, 149–156.

[87] Barsotti, S.; Sommerfeld, T.; Ruf, M.-W.; Hotop, H. High resolution study of cluster anion formation in low-energy electron collisions with OCS clusters. *Int. J. Mass Spectrom.* **2004**, *233*, 181–192.

[88] Jordan, K. D.; Burrow, P. D. Studies of the temporary anion states of unsaturated hydrocarbons by electron transmission spectroscopy. *Acc. Chem. Res.* **1978**, *11*, 341–348.

[89] Jagau, T.-C.; Dao, D. B.; Holtgrewe, N. S.; Krylov, A. I.; Mabbs, R. Same but different: Dipole-stabilized shape resonances in CuF^- and AgF^-. *J. Phys. Chem. Lett.* **2015**, *6*, 2786–2793.

[90] Skomorowski, W.; Gulania, S.; Krylov, A. I. Bound and continuum-embedded states of cyanopolyyne anions. *Phys. Chem. Chem. Phys.* **2018**, *20*, 4805–4817.

[91] Carelli, F.; Gianturco, F. A.; Wester, R.; Satta, M. Formation of cyanopolyyne anions in the interstellar medium: The possible role of permanent dipoles. *J. Chem. Phys.* **2014**, *141*, 054302.

[92] Jagau, T.-C.; Zuev, D.; Bravaya, K. B.; Epifanovsky, E.; Krylov, A. I. A fresh look at resonances and complex absorbing potentials: density matrix-based approach. *J. Phys. Chem. Lett.* **2014**, *5*, 310–315.

[93] Voora, V. K.; Ding, J.; Sommerfeld, T.; Jordan, K. D. A self-consistent polarization potential model for describing excess electrons interacting with water clusters. *J. Phys. Chem. B* **2013**, *117*, 4365–4370.

[94] Domcke, W. Analytic theory of resonances, virtual states and bound states ion electron-molecule scattering and related processes. *J. Phys. B: At. Mol. Phys.* **1981**, *14*, 4889–4922.

[95] McCurdy, C.; McNutt, J. On the possibility of analytically continuing stabilization graphs to determine resonance positions and widths accurately. *Chem. Phys. Lett.* **1983**, *94*, 306–310.

[96] Jordan, K.; Voora, V.; Simons, J. Negative electron affinities from conventional electronic structure methods. *Theor. Chem. Acc.* **2014**, *133*, 85–99.

[97] Frisch, M. J.; Trucks, G. W.; Schlegel, H. B.; Scuseria, G. E.; Robb, M. A.; Cheeseman, J. R.; Scalmani, G.; Barone, V.; Petersson, G. A.; Nakatsuji, H., et al. Gaussian 16 Revision C.01. 2016; Gaussian Inc. Wallingford CT.

[98] Falcetta, M. F.; Jordan, K. D. Assignments of the temporary anion states of the chloromethanes. *J. Chem. Phys.* **1990**, *94*, 5666–5669.

[99] Boardman, A. D.; Hill, A. D.; Sampanthar, S. Partial wave scattering by non-spherically symmetric potentials. I. General theory of elastic scattering. *Phys. Rev.* **1967**, *160*, 472–475.

[100] White, A. F.; McCurdy, C. W.; Head-Gordon, M. Restricted and unrestricted non-Hermitian Hartree-Fock: Theory, practical considerations, and applications to metastable molecular anions. *J. Chem. Phys.* **2015**, *143*, 074103.

[101] Jagau, T.-C.; Krylov, A. I. Characterizing metastable states beyond energies and lifetimes: Dyson orbitals and transition dipole moments. *J. Chem. Phys.* **2016**, *144*, 054113.

[102] Skomorowski, W.; Krylov, A. I. Real and imaginary excitons: Making sense of resonance wave functions by using reduced state and transition density matrices. *J. Phys. Chem. Lett.* **2018**, *9*, 4101–4108.

[103] Fossez, K.; Mao, X.; Nazarewicz, W.; Michel, N.; Garrett, W. R.; Płoszajczak, M. Resonant spectra of quadrupolar anions. *Phys. Rev. A* **2016**, *94*, 032511.

[104] Jordan, K. D.; Burrow, P. D. Temporary anion states of polyatomic hydrocarbons. *Chem. Rev.* **1987**, *87*, 557–588.

[105] Kairalapova, A.; Jordan, K. D.; Maienshein, D. N.; Fair, M. C.; Falcetta, M. F. Theoretical approaches for treating non-valence correlation-bound anions. *J. Phys. Chem. A* **2019**, *123*, 2719–2726.

[106] Oana, M. C.; Krylov, A. I. Dyson orbitals for ionization from the ground and electronically excited states within equation-of-motion coupled-cluster formalism: Theory, implementation, and examples. *J. Chem. Phys.* **2007**, *127*, 234106.

[107] Anusiewicz, I.; Skurski, P.; Simons, J. First evidence of rhombic $(NaCl)^-$. Ab Initio reexamination of the sodium chloride dimer anion. *J. Phys. Chem. A* **2002**, *106*, 10636–10644.

[108] Raghavachari, K.; W.Trucks, G.; A.Pople, J.; Head-Gordon, M. A fifth-order perturbation comparison of electron correlation theories. *Chem. Phys. Lett.* **1989**, *157*, 479–483.

[109] Prascher, B. P.; Woon, D. E.; Peterson, K. A.; Jr., T. H. D.; Wilson, A. K. Gaussian basis sets for use in correlated molecular calculations. VII. Valence, core-valence, and scalar relativistic basis sets for Li, Be, Na, and Mg. *Theor. Chem. Acc.* **2011**, *128*, 69–82.

[110] Falcetta, M. F.; DiFalco, L. A.; Ackerman, D. S.; Barlow, J. C.; Jordan, K. D. Assessment of various electronic structure methods for characterizing temporary anion states: Application to the ground state anions of N_2, C_2H_2, C_2H_4, and C_6H_6. *J. Phys. Chem. A* **2014**, *118*, 7489–7497.

[111] Bhaskaran-Nair, K.; Kowalski, K.; Jarrell, M.; Moreno, J.; Shelton, W. A. Equation of motion coupled cluster methods for electron attachment and ionization potential in polyacenes. *Chem. Phys. Lett.* **2015**, *641*, 146–152.

[112] Isaacson, A. D.; Truhlar, D. G. Single-root, real-basis-function method with correct branch-point structure for complex resonances energies. *Chem. Phys. Lett.* **1984**, *110*, 130–134.

[113] Blatt, J. M.; Weisskopf, V. F. *Theoretical Nuclear Physics*; Springer, 1952.

[114] Sommerfeld, T.; DeFusco, A.; Jordan, K. D. Model potential approaches for describing the interaction of excess electrons with water clusters: Incorporation of long-range correlation effects. *J. Phys. Chem. A* **2008**, *112*, 11021–11035.

[115] Fano, U. Effects of configuration interaction on intensities and phase shifts. *Phys. Rev.* **1961**, *124*, 1866–1878.

[116] Slater, J. C. The virial and molecular structure. *J. Chem. Phys.* **1933**, *1*, 687–691.

[117] Hurley, A. C. Virial theorem for polyatomic molecules. *J. Chem. Phys.* **1962**, *37*, 449–450.

[118] Dalgarno, A.; Lewis, J. T. The exact calculation of long-range forces between atoms by perturbation theory. *Proc. R. Soc. Lond. A* **1955**, *233*, 70–74.

[119] Robinson, P. D. Hypervirial theorems and perturbation theory in quantum mechanics. *Proc. R. Soc. Lond. A* **1965**, *283*, 229–237.

[120] Lyon, W. D.; Matcha, R. L.; Sanders, W. A.; Meath, W. J.; Hirschfelder, J. O. Perturbation treatment of the ground state of H_2^+. *J. Chem. Phys.* **1965**, *43*, 1095–1100.

[121] Winn, J. S. Implications of the virial theorem on the description of weak bonds. *J. Chem. Phys.* **1981**, *74*, 608–611.

[122] Jentschura, U. D. Resummation of the divergent perturbation series for a hydrogen atom in an electric field. *Phys. Rev. A* **2001**, *64*, 013403.

[123] Mavromatis, H. A. The Dalgarno-Lewis summation technique: Some comments and examples. *Am. J. Phys.* **1991**, *59*, 738–744.

[124] Wolfram Research, Inc., Mathematica, Version 12.0. 2019; Champaign, IL.